An Analysis of a PV/T RO System in the Arava Valley

A Major Qualifying Project
Submitted to the Faculty of Worcester Polytechnic Institute
in partial fulfillment of the requirements for the Degree in Bachelor of Science
in
Mechanical Engineering
Electrical and Computer Engineering

Authored by

_____
Elizabeth Bliss

_____
Jonathan Friedman

_____
Tyler Golemo

_____
Aaron Pepin

Project Advisors:
Professor Isa Bar-On
Professor Alexander Emanuel

WPI

Dead-Sea & Arava Science Center
מרכז מדע ים המלח והערבה
Under the Auspices of Ben-Gurion University of the Negev
בחסות אוניברסיטת בן גוריון בנגב

Acknowledgements

We like to thank some individuals for their help in the completion of this project. First, Our advisors, Professor Isa Bar-On and Professor Alexander Emanuel for providing helpful insight throughout the course of our project. Our supervisors at the Arava and Dead Sea Science Center, Dr. Alex Gusarov and Dr. Tareq Abuhamed for their incredible resourcefulness and constant availability. The entire staff of the Arava Institute and members of Kibbutz Ketura for welcoming us into their home and their office space. To Nir Menahem, for his guidance and for introducing us to the system. Finally, to Charles Granit for constant moral support and motivation.

Authorship

1 Abstract
Primary Author: Group

2 Introduction
Primary Author: Tyler Golemo and Aaron Pepin

3 Background
3.1 PV Systems
Primary Author: Elizabeth Bliss

3.2 PV/T Systems
Primary Author: Elizabeth Bliss
Secondary Author: Aaron Pepin

3.3 Reverse Osmosis Systems
Primary Author: Jonathan Friedman

3.4 PV/T RO Systems
Primary Author: Jonathan Friedman

3.5 Potential applications
Primary Author: Jonathan Friedman

4 Methodology
4.1 Experiments
5.1.1 RO
Primary Author: Tyler Golemo
Secondary Author: Aaron Pepin

4.1.2 Baseline PV Panel Performance Data
Primary Author: Elizabeth Bliss

4.1.3 Effect of PV Panel Coverage on Power Output
Primary Author: Elizabeth Bliss

4.1.4 Effect of Localized Cooling and Heating on PV Panel Power Output
Primary Author: Elizabeth Bliss

4.1.5 PV/T
Primary Author: Aaron Pepin

4.2 PV/T RO Component Analysis
Primary Author: Jonathan Friedman
Secondary Author: Aaron Pepin

5 Calculations, Modeling, and Simulation
5.1 Heat Transfer Calculations
Primary Author: Jonathan Friedman and Aaron Pepin

5.1.1 MATLAB Program
Primary Author: Jonathan Friedman

5.1.2 Output Heat Flux
Primary Author: Jonathan Friedman
Secondary Author: Aaron Pepin

5.2 ANSYS-Fluent Simulation
Primary Author: Aaron Pepin

6 Results
6.1 Experiments
6.1.1 Effect of Temperature on RO Processes
Primary Author: Tyler Golemo
Secondary Author: Aaron Pepin

6.1.2 Baseline PV Panel Performance Data
Primary Author: Elizabeth Bliss

6.1.3 Effect of PV Panel Coverage on Power Output
Primary Author: Elizabeth Bliss

6.1.4 Effect of Localized Cooling and Heating on PV Panel Power Output
Primary Author: Elizabeth Bliss

6.1.5 PV/T
Primary Author: Aaron Pepin

7 Component System Design
7.1 RO Membranes
7.1.1 Type of Membrane
7.1.2 Membrane Setup
Primary Author: Tyler Golemo

7.2 RO Pump System
7.2.1 Energy Recovery Devices
7.2.2 Clark Pump
7.2.3 Pumps
Primary Author: Jonathan Friedman

7.3 PV/T Heating System
7.3.1 Material Selection

7.3.2 Conduit Design
Primary Author: Aaron Pepin

7.4 Electrical Systems
7.4.1 Power Management
7.4.2 Battery
Primary Author: Elizabeth Bliss

7.4.3 Novel Breaker System
Primary Author: Elizabeth Bliss
Secondary Author: Jonathan Friedman

7.5 PV System
Primary Author: Elizabeth Bliss

7.6 Integrated System Design
Primary Author: Group

8 Conclusions
Primary Author: Group

Table of Contents

Table of Figures

Table of Tables

1 Abstract

Potable water resources are scarce in the Arava Valley and reverse osmosis (RO) systems purify available water. Photovoltaics(PV) can be used to provide power for small-scale RO systems. PV panels operate more efficiently at lower temperatures; RO is more energy efficient with preheated feedwater. The system under investigation combines these two effects through a thermal transfer system mounted to a PV panel. Experiments were completed on the existing system and component analysis was completed and energy efficiency improvements were proposed.

2 Introduction

Since its founding in 1996, the Arava Institute has had a significant impact on the Arava Valley region. The institute was founded in Kibbutz Ketura, a community 60 kilometers north of Eilat, and a hub for cooperative environmental leadership in the Middle East. The goal of the institute is to advance cross-border environmental cooperation in the face of political conflict and conduct research into a variety of environmental studies. The institute hosts students and interns from a variety of geographical backgrounds, and encourages dialogue on the unique disputes of the region. Students of the Institute attend classes and earn undergraduate or masters credit through Ben Gurion University.

In collaboration with researchers from the Arava and Dead Sea Science Center, this project focuses on the desalination of water utilizing a reverse osmosis (RO) membrane in conjunction with a photovoltaic/thermal (PV/T) system. The Arava Valley is an ideal location for this research because it experiences an average yearly solar irradiance of 2100 to 2300 kWh/m^2[1] and the groundwater has high concentrations of salt[2]. This results in a great interest in research into desalination and solar technologies.

Reverse osmosis is most typically run on large scales since this allows for a very high percentage of feedwater to be converted into purified water. Large scale industrial RO plants have recovery rates generally ranging from 50-85%[3]. In contrast, small-scale RO systems have recovery rates between 5-15%[4] and are used for personal home use, boats, and remote area applications. This study seeks to improve the energy efficiency of a small-scale RO system with the addition of a PV/T system.

A small-scale photovoltaic/thermal reverse osmosis system has been installed at the Arava Institute for the past year. Previous studies have focused on the recovery rate of the RO system and the factors which influence this efficiency. This project looks to build on those results and provide suggestions for more energy efficient options for each area of the system.

Over the course of the project, the following objectives were completed:

- Analysis of the existing experimental PV/T system developed at the Arava and Dead Sea Science Center.
- Completion of RO, PV/T, and electrical experiments to characterize the existing systems.
- Research and analysis of alternative and additional components for the PV/T RO system

[1] "Solar resource maps for Israel and Surrounding Regions." (n.d.). Retrieved February 23, 2017, from http://solargis.com/products/maps-and-gis-data/free/download/israel-and-surrounding-regions

2 Yechieli, Y. (n.d.). "Evolution of brackish groundater in a typical arid region: Northern Arava Rift Valley, southern Israel." Retrieved February 23, 2017, from http://www.sciencedirect.com/science/article/pii/088329279290026Y

[3] "What is Reverse Osmosis?", *Puretec Industrial Water*, 23 Feb. 2017, puretecwater.com/reverse-osmosis/what-is-reverse-osmosis

[4] "About Reverse Osmosis Systems", *APS Water*, 23 Feb. 2017, www.apswater.com/article/39/About+Reverse+Osmosis+Systems

RO experiments were completed to observe the effect of temperature variation on permeate (the product of an RO membrane) characteristics. Studies were completed on the ability of a thermal system to transfer heat from a photovoltaic panel to a working fluid. Finally, the effects on power output caused by temperature gradients and shading of a PV panel were evaluated. The PV/T RO system was divided into five component systems which were individually analyzed for potential energy efficiency improvements. The final system design includes an RO system, an optimized power management and protection system powered by photovoltaics, and a thermal system designed to heat water from the back of the photovoltaic panel.

3 Background

3.1 Reverse Osmosis Systems

Reverse osmosis (RO) is used to take "dirty" water (water with concentrations of unwanted solutes such as salt or dirt) and purify it for safe uses. The fluid is pressurized to overcome the osmotic pressure of a fluid is overcome and dissolved solids are separated from the water. Since RO opposes the natural tendency for water to flow from high concentration to low concentration of solute, the process is energy intensive. The feedwater (the water to be purified by the process) must be pressurized by a pump and then pushed through the membrane; the pumps require almost all of the energy in the system.

Reverse osmosis is most typically run on large scales since this allows for a very high percentage of feedwater to be converted into purified water. The ratio of input feedwater to clean output water is known as the "recovery rate". Large scale industrial RO plants have recovery rates generally ranging from 50-85%[5]. Industrial RO plants can achieve these higher recovery rates with multiple pass systems, multi-stage systems, and reject water recovery. Since rejected brine remain highly pressurized, energy recovery systems are common to recuperate energy expenses, transferring the pressure from the outlet water to the inlet feedwater.

In contrast, small-scale RO systems have recovery rates between 5-15%[6] and are used for personal home use, boats, and remote area applications. These systems are typically simpler, usually having a pump, membrane, and an optional energy recovery system. A simplified schematic for the small-scale RO system studied in this paper is shown in Figure 1.

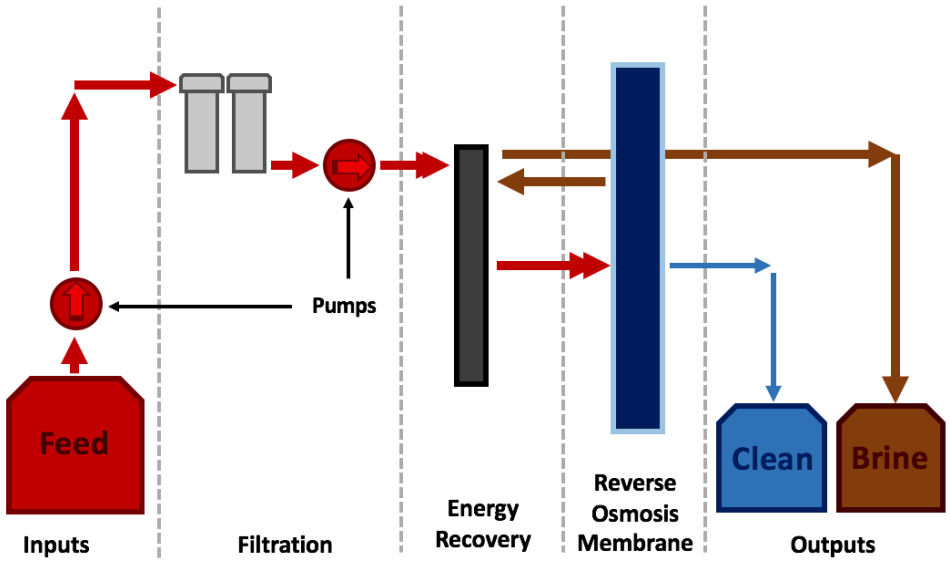

Figure 1: A Graphical Representation of a Small-Scale RO Process

[5] "What is Reverse Osmosis?", *Puretec Industrial Water*, 23 Feb. 2017, puretecwater.com/reverse-osmosis/what-is-reverse-osmosis

[6] "About Reverse Osmosis Systems", *APS Water*, 23 Feb. 2017, www.apswater.com/article/39/About+Reverse+Osmosis+Systems

3.2 PV Systems

PV technology transforms sunlight into electrical energy for both standalone uses and connection to the grid. Photons from the sunlight strike the PV cell and create a flow of electrons, or electricity. The first row of cells are typically connected in series with each other to create a string and increase voltage. The strings are connected in parallel to create a full panel and increase current[7]. From here, entire PV panels can be configured in parallel and series combinations to create the needed power for the application. PV systems produce a direct current (DC) voltage, which is convenient for many small-scale applications. In comparison to a wall outlet where a conversion from alternating current (AC) to DC voltage would be needed, solar panels do not need this conversion. For connection to the grid, this complicates the system slightly as the voltage needs to be inverted to AC voltage.

PV systems are increasingly appealing to small communities who cannot or do not want to be connected to the grid, and other applications where the power source may need to be moved frequently. In terms of small-scale, PV panels are used in many devices such as phone chargers, calculators, and LED street signs. With regards to large scale, PV panel fields are being built all over the world to be connected to the grid with the hopes of replacing coal and oil powered plants.

The largest issue facing PV systems is efficiency. The average efficiency of PV systems is 15-20%, even in full sunlight[8]. Small environmental changes such as a decrease in irradiance and increase in temperature have a large effect on the electrical output of the PV panel. Studies have shown that covering even a fraction of a panel, due to a shadow or a cloud, will reduce the power output of the panel significantly[9]. Under such conditions, some solar cells being blocked, which creates an open circuit for the entire string because the cells are connected in series. This means the panels need to be built in a large, open space where there are few possible obstructions. In warm climates such as the Arava Valley, overheating of the panel can have a similar effect[10], thus there has been an increased interest in cooling systems.

3.3 PV/T Systems

Photovoltaic Thermal (PV/T) systems consist of a PV panel and a thermofluid cooling system. Air, water, or another working fluid flows behind the panel to remove the excess heat. Pulling excess heat away from the PV panels increases their electrical efficiency, and heats the working fluid allowing for a higher thermal efficiency of the system. A simplified schematic for the integration with an RO system is shown in Figure 2. The efficiency is affected by the choice of working fluid, flow rate, input fluid temperature and surface area in contact with the fluid. All

---

[7] "Module Circuit Design." *PVEducation.org*. www.pveducation.org/pvcdrom/modules/module-circuit-design

[8] "Solar Performance and Efficiency." *Energy.gov.* 20 August 2013. energy.gov/eere/energybasics/articles/solar-performance-and-efficiency

[9] Sathyanarayana P. et al. "Effect of Shading on the Performance of Solar PV Panel." *SDM Institute of Technology.* Scientific and Academic Publishing. 2015. article.sapub.org/10.5923.c.ep.201501.01.html#Ref

[10] Moharram, K.A. et al. "Enhancing the performance of photovoltaic panels by water cooling." Ain Shams Engineering Journal. Vol 4. Issue 4. Pgs 869-877. Science Direct. December 2013. www.sciencedirect.com/science/article/pii/S2090447913000403

these were considered in the design of the PV/T system. This leads to a wide variety of designs being considered in the pursuit of optimizing this technology. More recent designs also include considerations for achieving purely turbulent flow to increase the effectiveness of the heat transfer to the fluid[11].

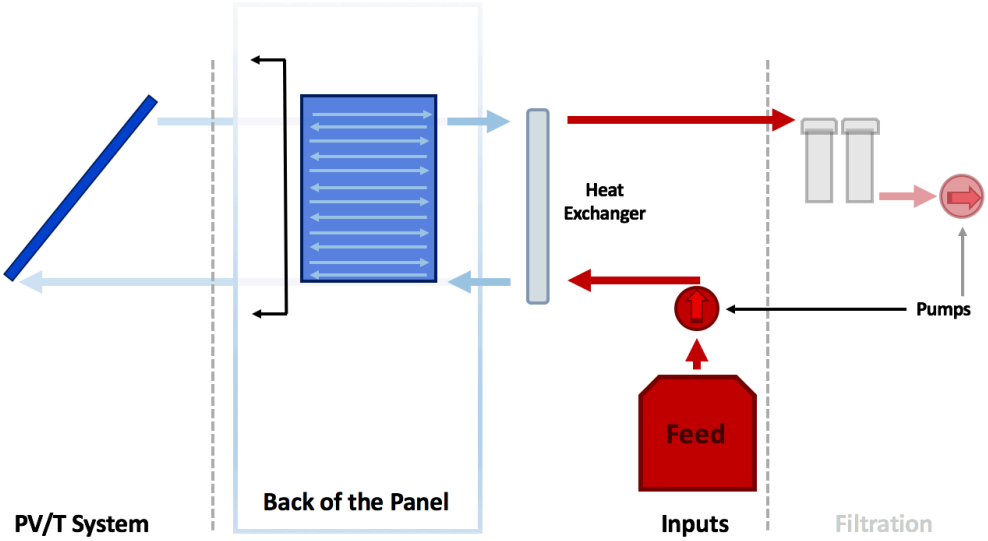

Figure 2: Graphical Representation of a PV/T System used to Heat Feedwater

3.4 PV/T RO Systems

As previously mentioned, thermofluid cooling systems have been added to photovoltaic panels to increase their power output by decreasing operating temperatures. For the RO processes, it has been found that membranes operate most efficiently in specific temperature ranges, typically around 35-55°C[12]. Preheating the feedwater to the target temperature range for the membrane can reduce energy consumption of the RO process, a critical issue for small-scale applications. By combining the thermofluid cooling systems for PV panels with the goal of preheating feedwater for RO processes, the system will have synergistic energy saving effects. A simplified scheme of the PV/T RO system is shown below in Figure 3.

[11] Subramanian, R. Shankar. "Heat transfer to or from a fluid flowing through a tube." web2. clarkson. edu/.../subramanian/.../Convective% 20Heat% 20Transfer (2008).

[12] Thomson, Murray, Marcos S. Miranda, and David Infield. "A small-scale seawater reverse-osmosis system with excellent energy efficiency over a wide operating range." *Desalination* 153.1-3 (2003): 229-236.

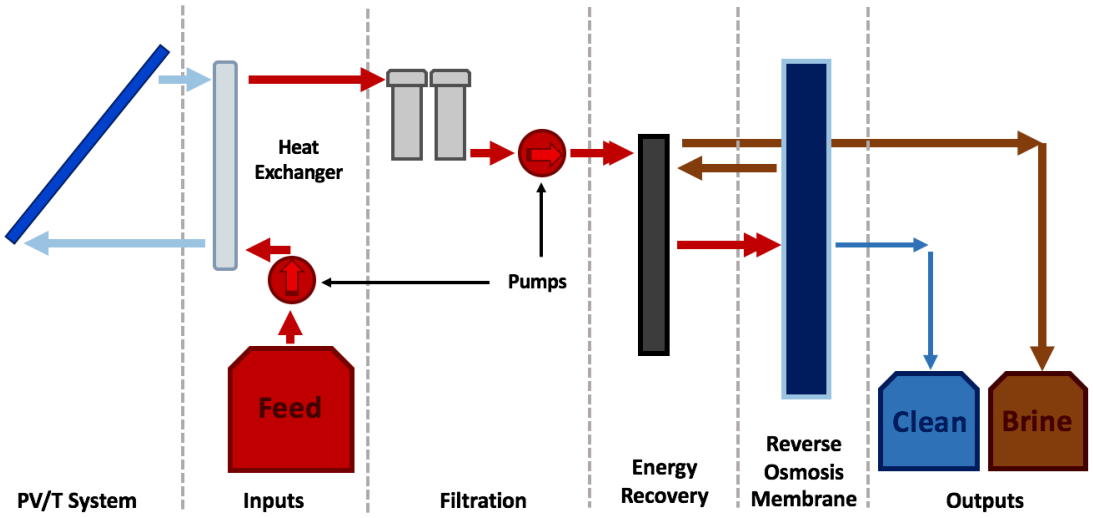

Figure 3: A Graphical Representation of the Combined PV/T RO System as Studied in this Paper

While there are two goals of the PV/T system, to heat the working fluid, and to cool the PV panel, the primary goal in this study is the heating of the working fluid. This is because there is a greater potential increase in relative efficiency for the RO membrane than the PV panel due to a temperature decrease. This is shown below in Figure 4[13].

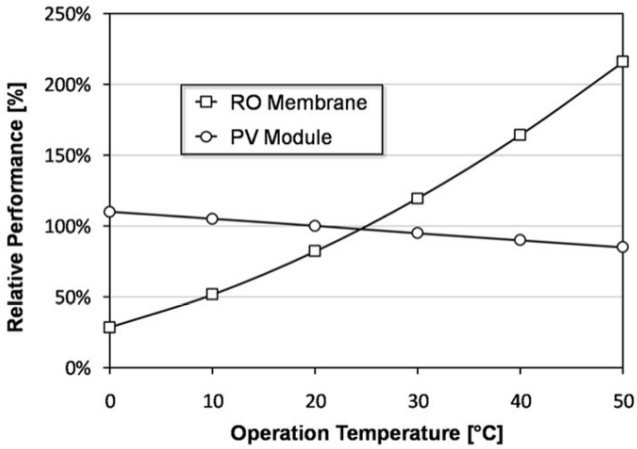

Figure 4: Relative Efficiencies of RO Process and PV Panels Based on Temperature

3.5 Potential Applications

Several possible applications exist for PV/T RO systems. The primary benefits of a joint PV/T RO system include increased mobility, off-grid functionality, and better joint energy efficiencies. Some local candidates include: water desalination for unrecognized Bedouin villages, any small Jordanian community such as Rahma, communities in the Gaza strip, and water purification for rural medical clinics.

[13] Alex Gusarov, e-mail message to authors, 18 January 2017.

4 Methodology

The first of the experiments were completed using a Treatment small-scale RO system modified for scientific experimentation, a full schematic of which is shown in Figure 5. The second and third experiments were focused on the study of independent PV systems, and used multiple PV panels available at the Arava and Dead Sea Science Center. The final experiment was a study of a novel PV/T system which was previously developed at the Arava and Dead Sea Science Center as well as a commercially produced PV/T system manufactured by Millennium Solar.

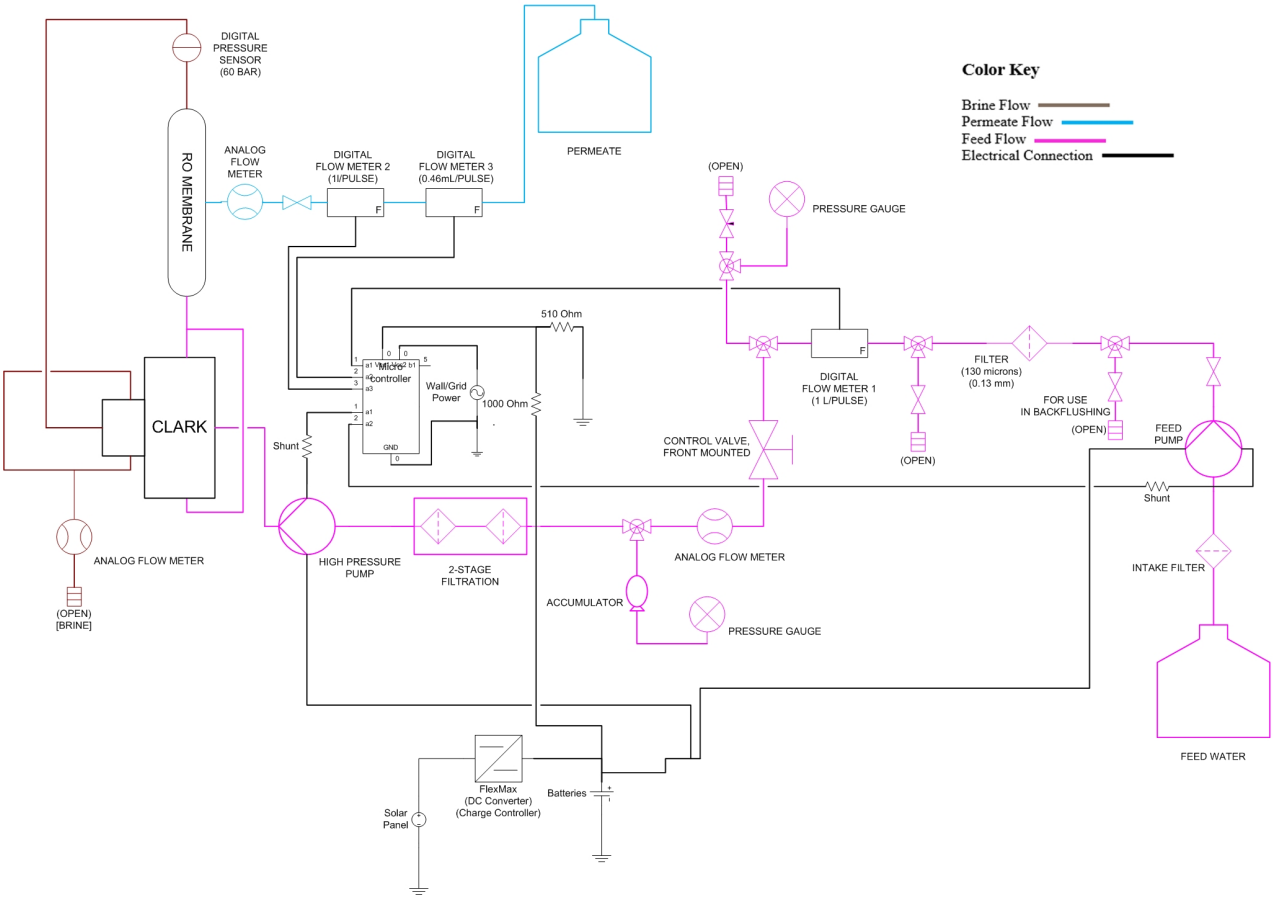

Figure 5: RO System Electrical and Mechanical Schematic

4.1 Experiments

4.1.1 Effect of Temperature on RO Processes

These three experiments were completed to determine the effects of feedwater temperature on the Reverse Osmosis (RO) process. Specifically, the tests look into temperature's effect on operation pressure needed, salt content, and production rate of the permeate. The RO system was operated with feedwater at temperatures of 15, 25, and 30 degrees C. Data was recorded on the feedwater flow rate, pressure, and temperature, permeate flow rate, brine flow rate, and the pressure difference between the feedwater and high pressure pumps.

As detailed above in Figure 5, the RO system centers on a singular DOW SW30-2540 membrane. The feedwater flows from its source tank through a Flojet Versijet R8600344 feedwater pump, through a 130 micron filter, an analog flow meter (1L/pulse), and a two stage filtration system before reaching the unlabeled high pressure pump. Next, the water will go through the Clark pump energy recovery system before going through the membrane. From here, the brine exits through a WIKA A-10 12719324 (60 bar max) digital pressure sensor before returning to the Clark pump to pressurize the incoming feedwater then exiting to the feedwater tank. The permeate exits through two digital flow meters (1L/pulse and .46mL/pulse) and is returned into the feedwater tank. Normally, the permeate and brine exit into separate tanks for use and disposal respectively but were combined in order to keep the feedwater at a standard salt content. Data was recorded from the various sensors by the Outback MATE3 microcontroller. Other changes for experimentation included adding an Extech Instrument 900W switching module power supply to control voltage and measure amperage used by the system and preheating of the water was done with two water heaters. Temperature of the feedwater was measured using two K type thermocouples, one in the feedwater tank and the other after the feedwater pump. The first is connected to a Tenmars TM-747D 4 channel datalogger while the second displays on the front of the Treatment system.

Once everything was set up, the system was turned on and run for 30 minutes to stabilize salt rejection. To begin experimentation, samples were taken of the feedwater, permeate, and brine. These were then measured to check the salt content in parts per thousand and millisiemens after heating/cooling the samples to 20-25°C. Data was also recorded from the three flow meters on the front of the system along with the current and voltage from the power source. This was repeated every ten minutes until thirty minutes had passed. The water was then heated to the next testing point and the process was repeated. The full experimental procedure is included in Appendix A: Experimental Procedure for Effect of Temperature on RO Processes Experiment and an image of the system is shown below in Figure 6.

Figure 6: Effect of Temperature on RO Processes Experiment Set Up

4.1.2 Baseline PV Panel Performance Data

The baseline PV panel data collection was conducted over two days to include variations due to changes in weather conditions. Every hour, the temperatures of the front and back of the panel were measured in 3 different places, top, middle, and bottom. The temperature of the junction box was also measured. The power output was recorded using the SolarEdge PV power output monitoring system for each time the temperatures were taken. The data was collected over two days to get a better idea of what weather conditions could occur. The data was taken every hour during regular working hours of 9:00 to 16:00.

Figure 7: Measurement Points for Baseline PV Temperature and Power Data Collection

4.1.3 Effect of PV Panel Coverage on Power Output

This experiment tested the photovoltaic (PV) panels with and without partial panel coverage simulated by putting a towel on the panel. For all conditions, the power produced by the panel was measured with an EKO MP-170 I-V Checker to determine the electrical efficiency. To measure irradiance for each test performed, weather data was collected from the Arava Institute Weather Station.

The panels were taken outside and put in sunlight. A measurement was taken with the I-V checker with the panel uncovered and the time was recorded. Part of the panel was covered with a towel and the panel was allowed to adjust for two minutes. A measurement was taken again with the I-V checker for each different test. At the end of all of the tests, the ambient sunlight, air temperature, and wind speed were recorded from the Arava Institute Weather Station. A photo from the experiment is shown in Figure 8 below. The full experimental procedure is included in Appendix B: Experimental Procedure for Effect of PV Panel Coverage on Power Output Experiment.

Figure 8: Effect of PV Panel Coverage on Power Output - Top Half Covering

4.1.4 Effect of Localized Cooling and Heating on PV Panel Power Output

These experiments tested the photovoltaic (PV) panels when there was a temperature gradient due to localized heating or cooling. Two PV panels were used, one as a control panel and one as a test panel, as shown in Figure 9. To do this, ice packs and a space heater were used to simulate cold and hot spots on the test panel. For all conditions, the power output of the system was measured with an EKO MP-170 I-V checker, front face temperatures were taken with a Mastech MS6520A infrared (IR) thermometer, and thermal images of the panels were taken with a UFPA thermal camera. Weather data was taken from the Arava Institute Weather Station.

The panels were taken outside and put in sunlight. A measurement was taken with the I-V checker with the panel at current temperatures and the time was recorded. The IR thermometer was used to measure the temperature of the panel on the front in several different places where the ice packs or space heater were applied. The thermal camera was used to take a thermal photo of the panel. Ice packs or a space heater were added to the back of the panel and the temperature of panel was left to adjust for 15 minutes. The power output, temperatures, and thermal images were taken for each different test with ice packs, space heater, or both. The ice packs or space heater were removed and the panel was left to adjust for 15 minutes. The power output, temperatures, and thermal images were taken again before performing another test. At the end of all of the tests, the ambient sunlight, air temperature, and wind speed were recorded from the Arava Institute Weather Station. The full experimental procedure is included in Appendix C: Experimental Procedure for Effect of Localized Cooling and Heating on PV Panel Power Output Experiment.

Figure 9: Effect of Localized Cooling and Heating on PV Panel Power Output - Set Up

4.1.5 PV/T

This experiment determined the amount of heat gained by the working fluid in a PV/T system as well as the effect of cooling PV panels on electrical output. Three different solar panels were studied. A SUNTECH STP250-20/Wd acted as the control and the remaining two panels had thermal cooling systems. One PV/T was a commercially available product manufactured by Millennium Solar while the other was a novel panel designed by the Arava and Dead Sea Science Center. Water was circulated through the PV/T systems using MRC WB-100 cooling baths, and the temperatures were measured with T-type thermocouples and a Tenmars TM-747d RS232 12 –channel datalogger. Regular thermal measurements were taken with a UFPA thermal camera and a MASTECH MS6520A IR Thermometer. Finally, power output was measured with a SolarEdge PV power output monitoring system.

Additionally, the experiment served as a calibration method for the team's existing simulations. This manifested as a comparison to the results from the heat transfer calculations, panel temperature model, and the fluid flow simulation.

A day before the experiment began, all three panels, the SUNTECH, Millennium Solar, and the novel PV/T system, were connected to the SolarEdge PV power output monitoring system. A 1 liter pitcher was used to determine the initial flowrates of the MRC WB-100 cooling baths, both with and without being attached to the PV/T systems. The baths were turned on and the pitcher was held under the output, and an additional person tracked the amount of time it took to fill. This was completed twice and then averaged. After this, thermocouples were inserted into the sides of the tubes which carried the input and output water to the cooling baths. These were held in place and the tubes were resealed with a combination of hot glue and duct tape. The cooling baths were then connected to the two PV/T systems, and the output flowrates from the PV/T systems were measured with the same 1 L pitcher as previously used. This measurement was again repeated twice for each bath, and the results were averaged. The Tenmars TM-747d RS232 12-channel datalogger was then attached to the four T-type thermocouples and set to record data every 30 seconds. The cooling baths were then turned on, and the refrigeration settings set to 25°C. The experiment was started at 11:00 am and temperature data collection started at 10:55.

Every 10 minutes thermal images were taken of the front and back of each of the panels. Additionally, every 10 minutes thermometer readings were taken with the IR thermometer on the front and the back of the panel at the locations shown below in Figure 10 and Figure 11 below, respectively. All readings were continued for two hours of system operation.

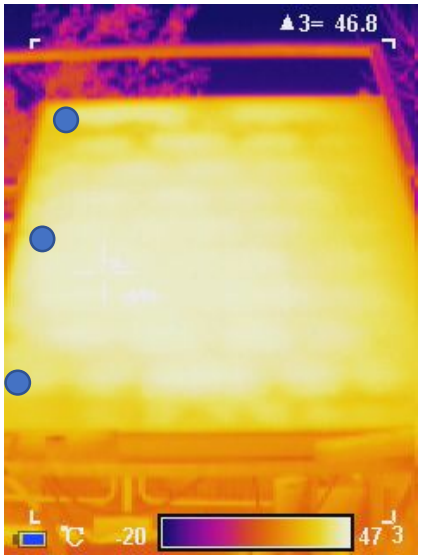

Figure 10: Measurement Points for Front of PV Panels

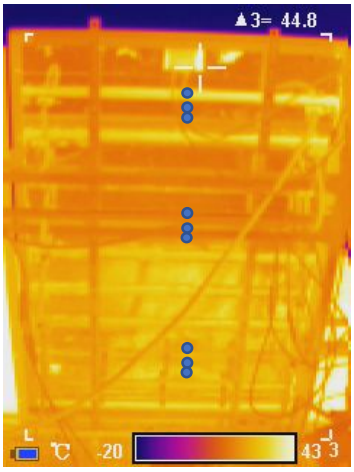

Figure 11: Measurement Points for Back of Novel PV/T System

4.2 PV/T RO Component Analysis

To complete a proper analysis, the PV/T RO system was divided up into five main component categories. The categories were: RO Membranes, Pump Systems, Fluid Heating Systems, Electrical Systems, and the PV Panels. These component groups were then broken up into subgroups to be analyzed for possible improvements and design considerations. Each of these divisions are shown below in Figure 12.

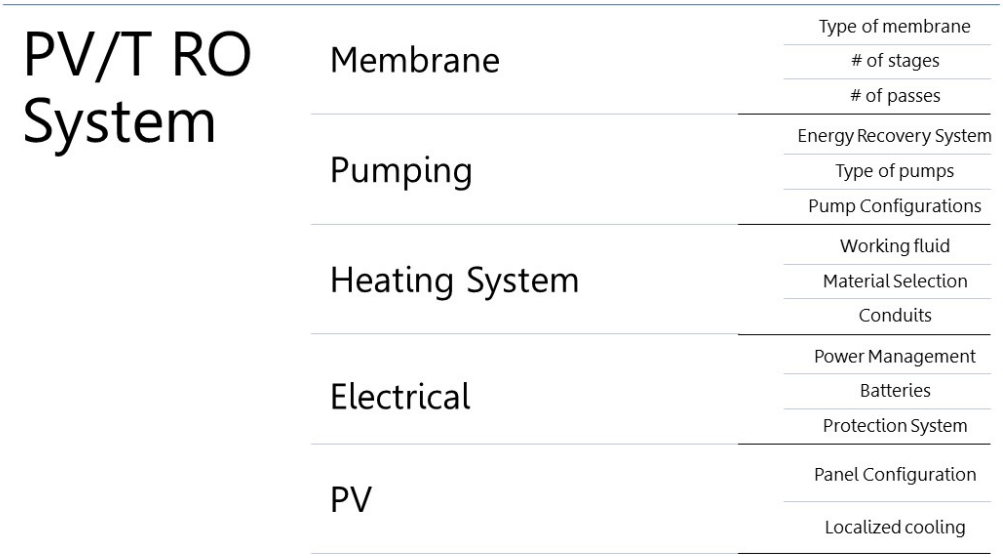

Figure 12: Component System Breakdown

The main goal of each category was a comprehensive quantification of the design parameters needed to select the ideal component for a variety of applications. The order in which this was considered is shown in the flow diagram in Figure 13. The results of these studies are discussed later in the paper, and recommendations based on different scale applications are proposed.

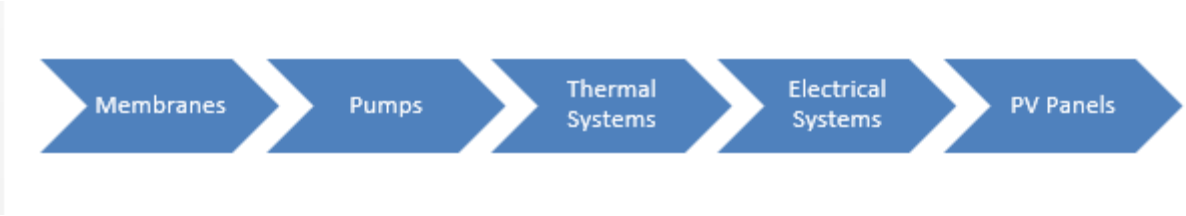

Figure 13: Flow Diagram of Component System Analysis

5 Calculations, Modeling, and Simulation

Manual calculations, a panel temperature model written in MATLAB, and a fluid flow simulation completed in ANSYS-Fluent were used to study the heat transfer that occurred through the PV/T system. The manual calculations studied the non-steady state heat transfer that occurred in the panel due to the incident solar irradiance over a set time period. This was then incorporated into the panel temperature model which output both the average temperature within the PV panel as well as the heat flux coming out of the back of the panel. The model completes these calculations for a PV panel without any kind of thermal transfer system. The fluid flow simulation then uses these parameters to predict the amount of heat that a working fluid would gain from moving through a thermal system on the back of the simulated panel. In Section 6 Results, these results were compared to the experimental results obtained over the course of the project.

5.1 Heat Transfer Calculations

Calculations were completed to analyze the heat transfer occurring throughout the PV/T panel. The aim of these calculations was to determine the current effectiveness of the novel PV/T design. These calculations had the input parameters of solar radiation, ambient temperature, water temperature, and water flowrate. The outputs of this analysis were the temperature of the photovoltaic panel, as well as the average output temperature of the water.

The heat transfer calculations encompassed non-steady state radiation, convection, and conduction. The calculations related to the heat transfer due to solar radiation are broken up into the shortwave and longwave sections of the radiation spectrum. The shortwave calculations are primarily dependent on the incident solar irradiance, whereas the longwave calculations are based on the Stefan-Boltzmann law. The forced convection across the front face of the panel was based on a forced convective heat transfer coefficient that was calibrated for this particular application with experimental data collected over the course of the project. Since an established correlation between the coefficient and wind speed was not readily available, this assumption is the primary potential limitation on the accuracy of the model. Finally, using the material properties for each of the six layers of the PV panel, shown in Figure 14, an overall conductive heat flux through the panel was established to define the heat loss to the solid module.

Table 1
Photovoltaic layer properties.

Layer	Thickness t, (m)	Thermal conductivity k, (W/m°K)	Density ρ, (kg/m^3)	Specific heat Capacity c, (J/kg°C)
1. Glass	0.003 [11]	1.8 [4]	3000 [5]	500 [5]
2. ARC	100×10^{-9} [13]	32 [14]	2400 [14]	691 [14]
3. PV Cells	225×10^{-6} [11]	148 [12]	2330 [5]	677 [5]
4. EVA	500×10^{-6} [9,12]	0.35 [12]	960 [17]	2090 [17]
5. Rear contact	10×10^{-6} [15]	237 [16]	2700 [16]	900 [16]
6. Tedlar	0.0001 [12]	0.2 [12]	1200 [5]	1250 [5]

Figure 14: Photovoltaic Panel Material Layers

The first analysis was completed for a PV panel, with no thermal system included. The calculations began with the incident solar radiation, and then took into effect forced convection on the front of the panel due to wind, free convection off the rear of the panel due to convection currents, conduction through the six material layers of the panel, and the power generation of the panel. The primary methodology for these calculations was taken from A.D Jones and C.P. Underwood from the University of Northumbria in 2001[14]. These calculations are shown in Equation 1.

$$C_{module}\frac{dT_{module}}{dt} = \sigma * A * \left(\varepsilon_{sky}(T_{ambient} - \delta T)^4 - \varepsilon_{module}{T_{module}}^4\right) + \alpha * \Phi * A - \frac{C_{FF} * E * \ln(k_1 E)}{T_{module}} - \left(h_{c,forced} + h_{c,free}\right) * A * (T_{module} - T_{ambient}) \quad [1]$$

$$C_{module} = Module\ Heat\ Capacity\ \left(\frac{J}{K}\right)$$

$$\sigma = Stefan\ Boltmann\ Constant\ \left(\frac{W}{m^2K^4}\right)$$

$$A = Area\ of\ Surface\ (m^2)$$

$$\varepsilon = Emissivity\ of\ sky\ dome, ground, PV\ module$$

$$T = Temperature\ (K)$$

$$\delta T = 20\ K\ for\ clear\ sky\ conditions$$

$$\alpha = Absorptivity\ of\ Cell\ Surface$$

$$\Phi = Total\ Incident\ Irradiance\ on\ Module\ Surface\ \left(\frac{W}{m^2}\right)$$

$$C_{FF} = Fill\ Factor\ Model\ Constant\ (1.22\ Km^2 for\ PV\ applications)$$

$$E = Incident\ Irradiance\ \left(\frac{W}{m^2}\right)$$

$$k_1 = 10^6\left(\frac{m^2}{W}\right)$$

$$h_c = Convection\ Coefficient\ \ (subscripts\ for\ forced\ and\ free)\left(\frac{W}{m^2K}\right)$$

5.1.1 Panel Temperature Model

PV panel temperature was calculated from equation 1. using MATLAB. The panel temperature is calculated as a function of solar irradiance, ambient air temperature, and initial panel temperature. The model uses input data collected from the Arava Institute weather station. The ode45 package is used to solve the differential equation 1 for a time span of 10 minutes. Every 10 calculated minutes, the model updates the ordinary differential equation (ODE) inputs to the next set of input parameters, and carries over the latest calculated panel temperature to be used for the next iteration of calculations. The program prompts the user to select the Excel file

[14] Jones, A. D., and C. P. Underwood. "A thermal model for photovoltaic systems." *Solar energy* 70.4 (2001): 349-359.

provided from the weather station, the date for which to use data for the calculation, the starting time, and elapsed time to calculate. The program also offers users the option to export the calculated panel temperatures to a CSV file, as well as the hourly averages for ease of use in other simulations or calculations. Finally, the model outputs a graph with two datasets on it: the calculated panel temperature (measured on the left hand axis) and the incoming solar irradiance (right hand axis). A sample graph output is shown below in Figure 15. The program requires a guess of the panels initial temperature. The effect of this assumption can be seen in the graph between 0 hours elapsed and about 0.25 hours elapsed as a dip in the calculated panel temperature. The solar irradiance data is graphed on top of the simulated panel temperature to show that incoming radiation and panel temperature are heavily correlated. The code for the program is available in Appendix E.

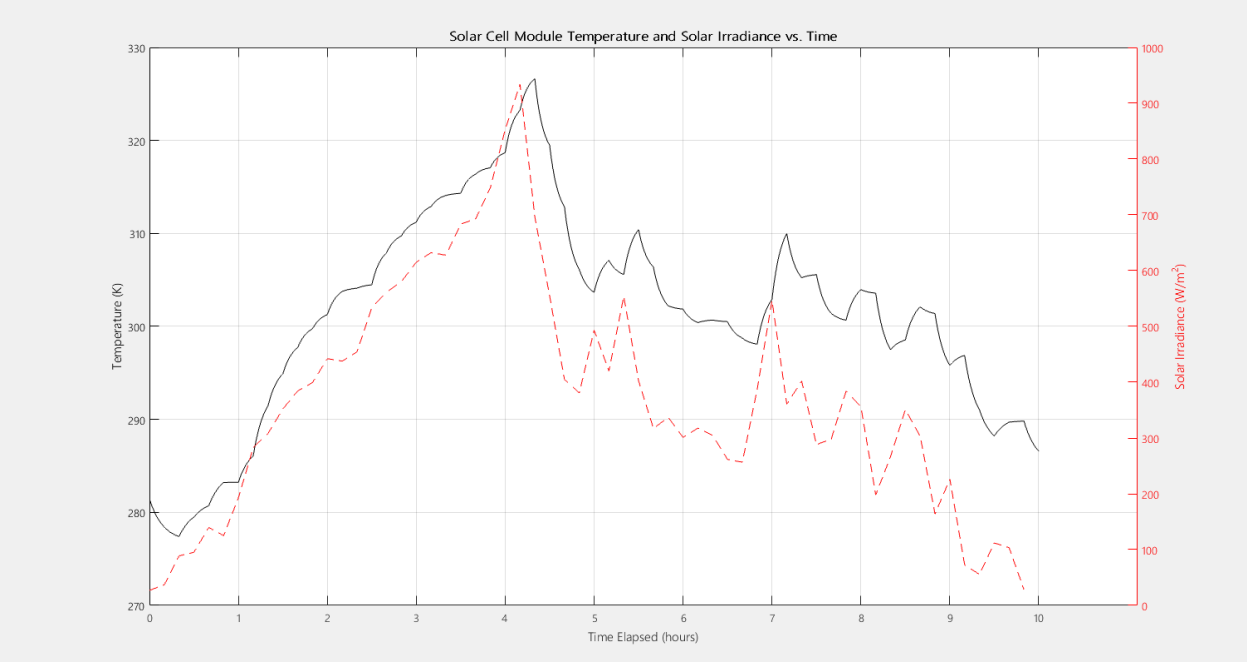

Figure 15: Sample MATLAB Output Graph of 31 January 2017

5.1.2 Output Heat Flux

Heat transfer calculations were completed to determine the different potential heat flux values coming out of the back of the PV panel. This was important to calculate in addition to the average panel temperature because it was the primary input for the ANSYS fluid flow simulation and specifically occurs at the back of the panel instead of being an average across the entire thickness.

In equation 2., the heat flux out of the back of the panel is calculated by subtracting the losses to reflection, the irradiance used for power generation, losses to convection, and the heat flux through the panel from the incoming irradiance. Figure 16 is a graphical representation of the variables used in this equation.

$$Irradiance - Reflected - Power\ Gen. - Convection - q_{panel} = q_{back\ of\ panel} \quad [2]$$

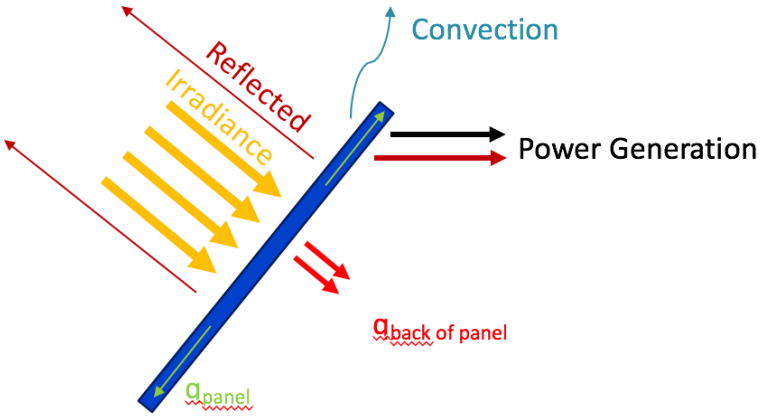

Figure 16: A Graphical Representation of the Factors Considered in the Heat Transfer Calculations

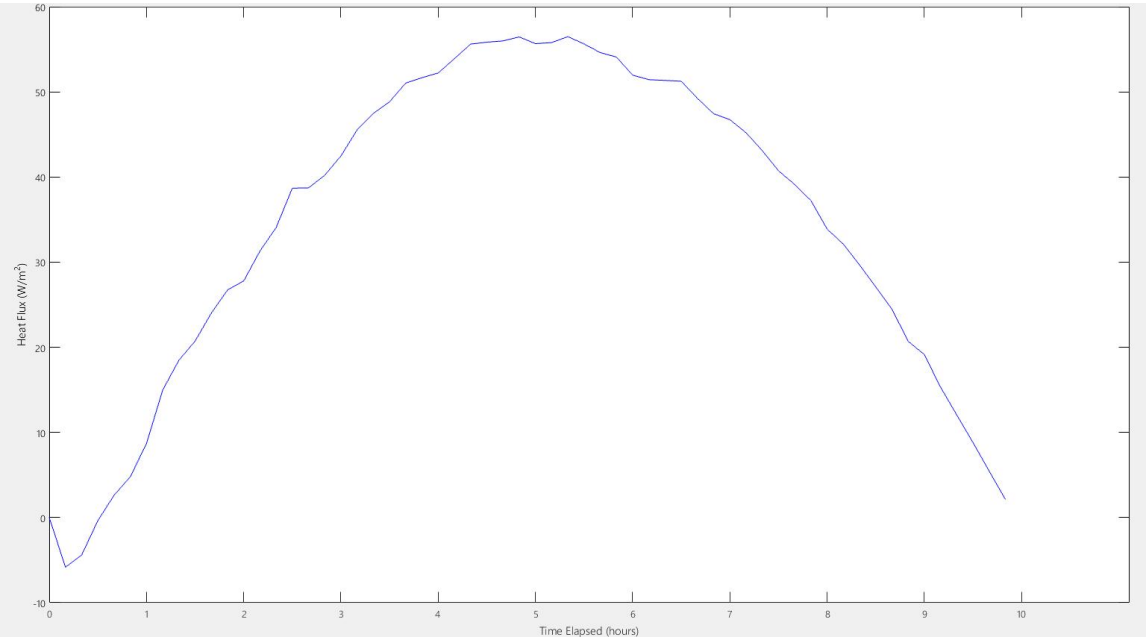

Figure 17: MATLAB Graph of Output Heat Flux for 10 February 2017

From this calculation, and for the situation described, the total heat flux out of the back of the panel was determined to have a maximum of 55 W/m^2 on 10 February 2017 as shown in Figure 17. From here, the next consideration was the amount of area where heat was actually transferred to the working fluid, which in these calculations was treated as pure water. An assumption was made that all of the heat flux is transferred to the working fluid, this assumes perfect insulation on the back of the PV/T system. Even with these assumptions, this maximum value was believed to be too low, as explored further in 6.1.5 PV/T

5.2 Fluid Flow Simulation

Using SolidWorks and ANSYS-Fluent, a solid model was created and then modified to simulate the amount of heat that was transferred from the back of the panel into the water running through conduits. The SolidWorks model, shown in Figure 18, exhibited the following changes in comparison to the novel PV/T system, shown in Figure 19.

- The solid model utilized a smooth transition from the square conduit to the round tubing instead of the sharp transition that exists in the actual system
- The material for the polyurethane tubing was simulated in the Fluent solver instead of as an additional solid model
- The aluminum plate and the aluminum conduit were merged into one solid instead of as two separate solids in contact

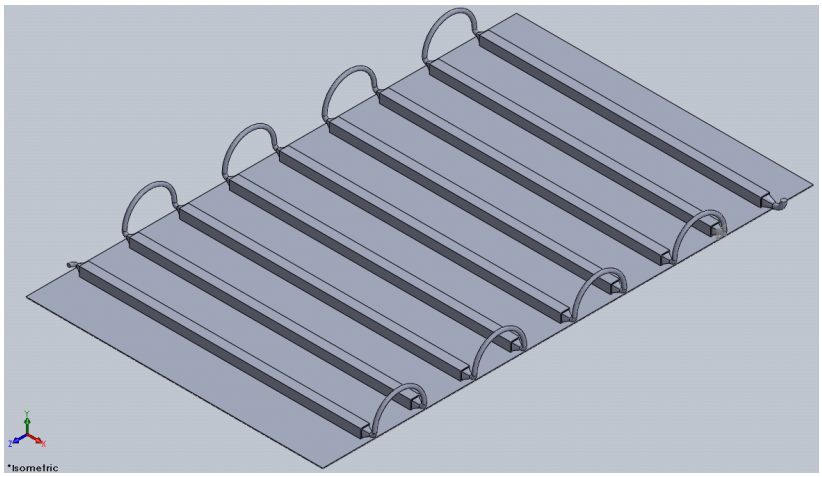

Figure 18: SolidWorks Model of Novel PV/T System

Figure 19: Novel PV/T System

The solid model was then modified for analysis in the ANSYS-Fluent software. A uniform heat flux was assumed to be coming from the back of the panel with a value calculated using the MATLAB code described in Section 5 Calculations, Modeling, and Simulation above. This analysis allowed for a representation of a temperature distribution across the aluminum plate on the back of the novel PV/T system, as well as the amount of heat that was transferred to the fluid, as shown in Figure 20. This temperature gradient could cause a temperature gradient on the front face of the PV panel, detrimentally affecting the power output of the PV system. [15]

Depending on the frequency and the placement of the conduits on the back of the panel, this temperature gradient would be more or less exaggerated. More conduits would result in a more uniform distribution, whereas fewer conduits would exhibit a more distinct gradient. An exaggerated temperature gradient would limit the efficiency increases gained by the panel cooling to the hottest part of the PV panel. Depending on the specific panel and its temperature coefficient to power output, this temperature gradient could have a more pronounced effect[16].

In Figure 20 the working fluid was considered to be water with 1% salt content by mass. The input flowrate for the water was set to .16 kg/s and the input irradiance to the PV/T system was set as 55 W/m^2 going into the aluminum plate.

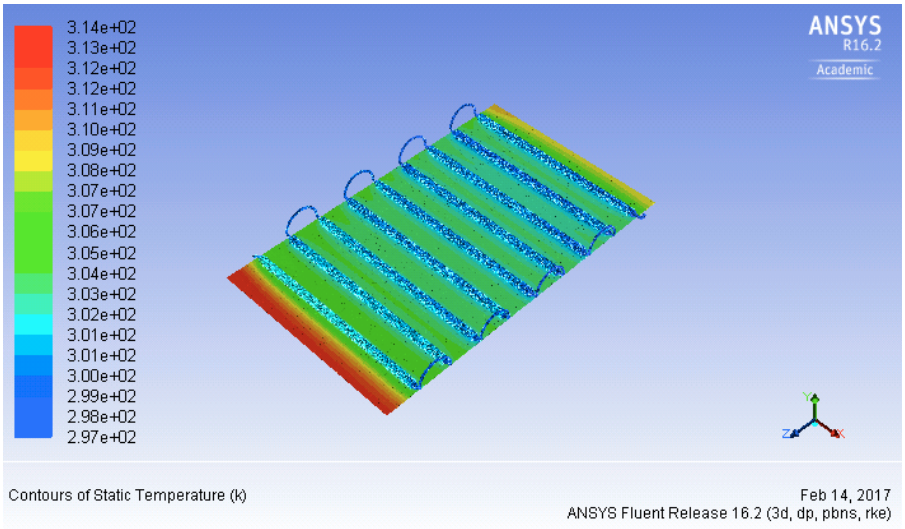

Figure 20: Output of Fluid Flow Simulation

Analysis of this simulation result shows that over the 8.46 m of aluminum conduit present in the novel PV/T system, a temperature gain of .25°C was achieved. While maintaining the input heat flux, salt content, and solid model, the input flowrate was changed to .02 kg/s which resulted in a temperature gain of 1.2°C. This simulation was a first order assessment of the effectiveness of the PV/T system studied. The results were compared with experimental data, as shown in Section 4.1.5 PV/T. Further simulations would benefit from considering different experimental methods of obtaining value for an input heat flux to improve the accuracy of the simulation.

[15] Schuss, Christian, et al. "Detecting Defects in Photovoltaic Cells and Panels and Evaluating the Impact on Output Performances." *IEEE Transactions on Instrumentation and Measurement* 65.5 (2016): 1108-1119.
[16] Schuss, Christian, et al. "Detecting Defects in Photovoltaic Cells and Panels and Evaluating the Impact on Output Performances." *IEEE Transactions on Instrumentation and Measurement* 65.5 (2016): 1108-1119.

6 Results

Four experiments were completed over the course of the project to gather data on different characteristics of the PV/T RO system. The first observed the effect that the temperature of the input feedwater to the RO system had on the pressure of the fluid going through the RO membrane and the output permeate quality. In the second two experiments, the effect of partial covering and temperature gradients on the PV panel electrical efficiency were studied. Baseline PV panel efficiencies were measured to compare to these experiments. In the final experiment, the amount of heat transferred from a PV panel to a working fluid running through a thermal transfer system was observed. This value was then compared to the results of the calculations in the previous Section 5 Calculations, Modeling, and Simulation.

6.1 Experiments

6.1.1 Effect of Temperature on RO Processes

Temperatures of 16, 25, and 35°C were used in testing how temperature effects the quality of the permeate as well as the pressure needed for the RO membrane. A complete set of data can be found in Appendix F: Data Collection from Effect of Temperature on RO Processes Experiment.

Figure 21 below shows the pressure of the brine exiting the membrane in comparison to time. In ideal circumstances this should be indicative of the pressure throughout the RO membrane. A clear step down in pressure is seen for each of the three temperatures tested, as was confirmed in other studies[17]. The power consumption of the pumps is directly related to the pressure seen in the RO membrane. This correlation is further explored by comparing the pump power consumption to the system pressure in Figure 18. Higher pressures result in a higher average power consumption. These findings are further explored in Section 7.2 RO Pump System.

[17] "Factors Affecting RO Membrane Performance", *Water Treatment Guide*, 23 Feb. 2017, www.watertreatmentguide.com/factors_affecting_membrane_performance.htm

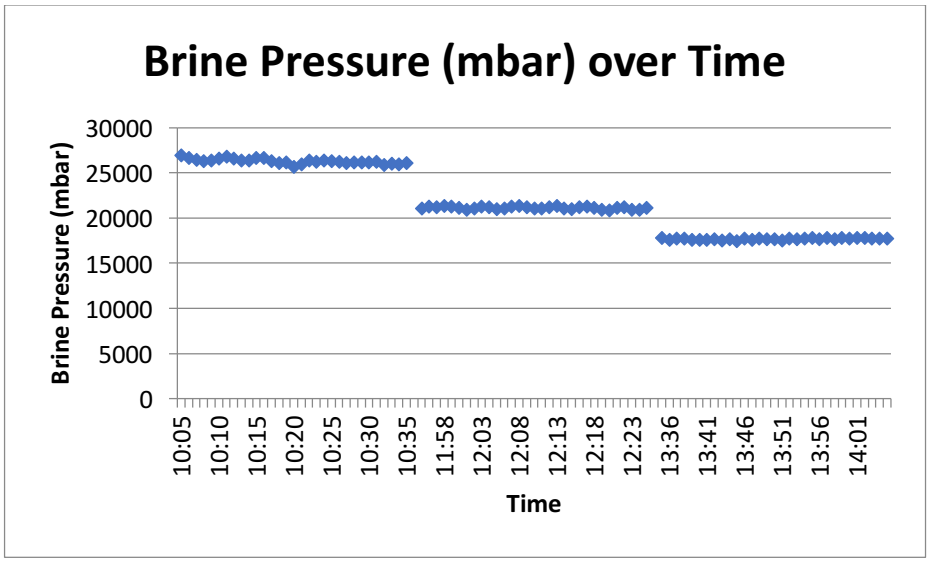

Figure 21: Measured Brine Pressure over Time

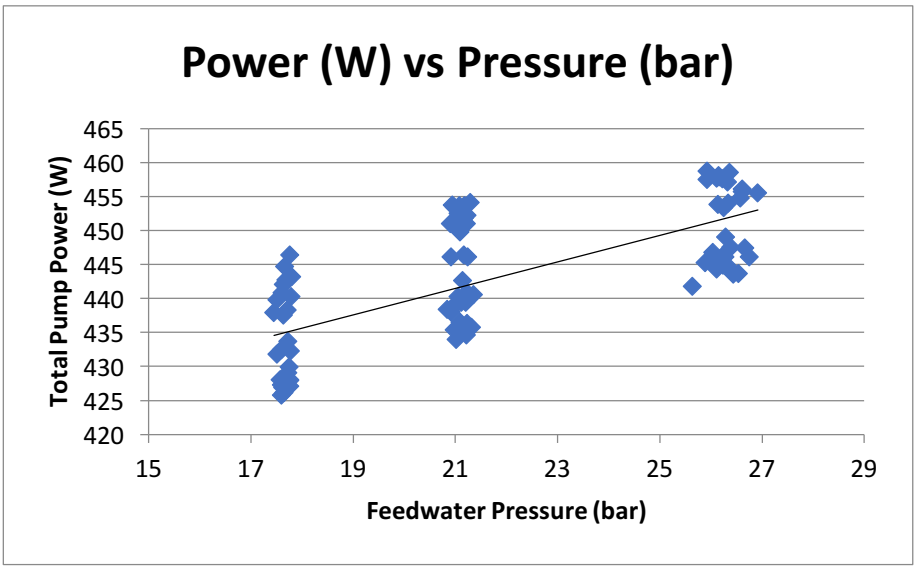

Figure 22: Power Needed for RO Pumps versus RO Membrane Pressure

However, some of the present trends are disputed in some of literature. For example, the salt content in the permeate rose with temperature. This can be seen below in Figure 23. Sources have been found in support and against this finding. Due to the limited amount of data collected, this experiment was determined to be inconclusive.

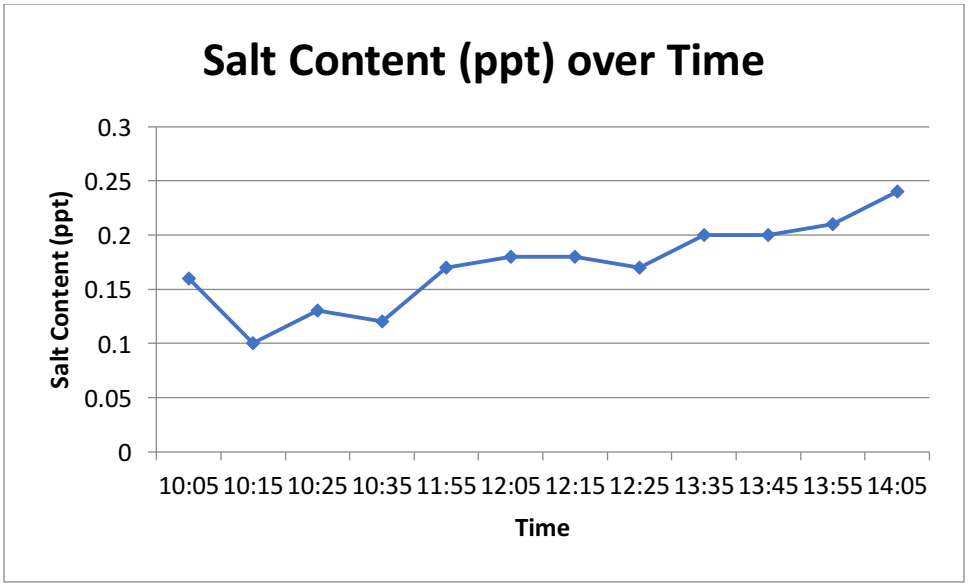

Figure 23: Permeate Salinity in ppt over Time

6.1.2 Baseline PV Panel Performance Data

The baseline temperature and power data for an average winter day was collected. The data was used to experimentally confirm the forced heat transfer coefficient used in the panel temperature model. The collected data is shown in Table 1 and Table 2 below.

Table 1: PV Panel Baseline Performance Data for 31 January

31Jan2017	Front			Back							
Time	Top	Middle	Bottom	Top	Middle	Bottom	Junction Box	Irradiance (W/m^2)	Air Temp (C)	Wind Speed (m/s)	Power Out (W)
10:00	41.0	41.8	40.1	43.2	43.7	43.1	33.3	615.1	16.68	0.683	187.15
11:03	47.1	48.2	47.1	45.5	46.6	46.5	39.8	853	18.35	1.319	242.09
12:01	28.1	28.0	26.9	31.3	31.2	31.1	27.1	493.1	16.52	2.001	89.38
12:58	26.1	25.0	25.0	26.5	26.5	25.4	25.1	301.1	17.15	0.961	65.43
14:02	33.2	33.5	32.5	33.5	34.5	31.7	28.9	546.5	18.22	2.714	191.48
15:04	22.6	22.8	22.6	26.5	26.4	25.1	24.4	356.2	18.2	3.67	28.82
15:55	23.3	24.6	23.2	25.1	26.2	25.1	21.0	226.3	18.08	2.989	12.73

Table 2: PV Panel Baseline Performance Data for 2 February

2Feb2017	Front			Back							
Time	Top	Middle	Bottom	Top	Middle	Bottom	Junction Box	Irradiance (W/m^2)	Air Temp (C)	Wind Speed (m/s)	Power Out (W)
8:58	31.1	32.2	29.9	29.9	30.3	31.1	22.0	487.4	12.68	0.796	144.7
9:59	40.2	40.4	38.1	40.4	40.5	40.1	28.0	676.7	15.02	2.595	198.37
11:01	36.7	41.8	41.7	36.9	40.2	41.7	26.1	768	16.72	4.224	217.18
11:55	38.1	41.8	41.7	40.9	42.9	44.0	27.2	806	17.98	2.942	224.93
12:54	39.3	43.6	43.4	37.6	39.9	41.2	29.7	768.6	17.92	4.374	217.54
14:22	32.0	37.3	36.2	35.1	36.2	38.6	26.9	598.4	19.29	3.177	176.63
14:59	30.1	32.3	32.3	30.2	30.4	31.3	22.0	473.2	18.74	3.554	85.42
15:54	24.2	26.7	25.6	24.8	25.9	24.1	21.4	210.8	16.44	3.434	11.67

This data shows the correlation between panel temperature, output power, and solar irradiance. The weather for 31 January was cloudy, and that can be seen by the drop in all three variables from 11:00 to 13:00. The weather for 2 February was a clear, sunny day, and the power output, irradiance, and panel temperature all follow a bell curve pattern when graphed against time, as shown in Figure 24 below.

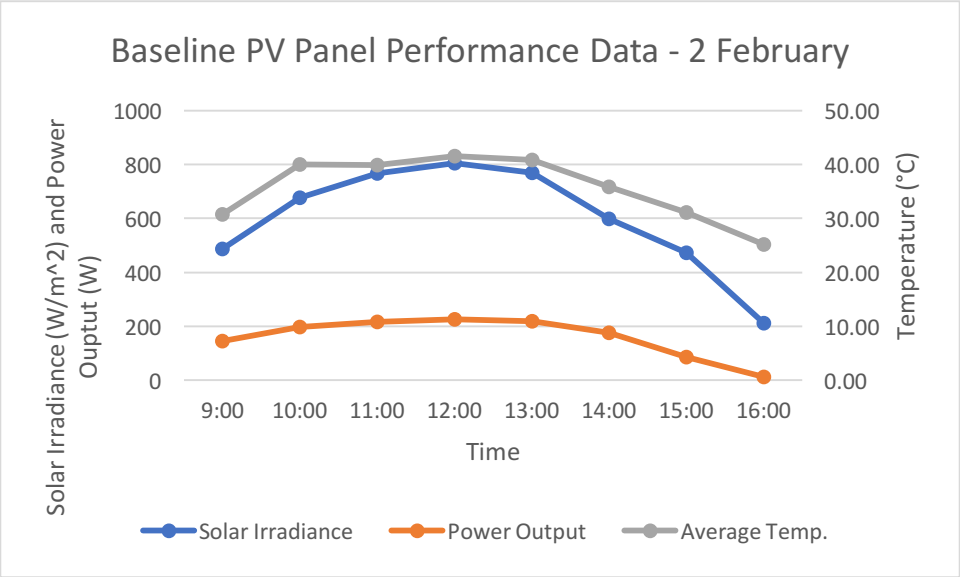

Figure 24: Baseline PV Panel Performance Data - 2 February

6.1.3 Effect of PV Panel Coverage on Power Output

This experiment was completed to test the decrease in efficiency of the solar panel when partially covered. The relevant data and calculations for the experiment can be found in Table 3 below. The weather data was taken from the Arava Institute weather station. To calculate the

input power of the panel, the area of the PV panel was measured and multiplied by the average radiation. Then, output power was divided by input power to get efficiency. The calculated efficiency is more accurate than the measured efficiency from the I-V checker due to having more accurate weather data. A table with full data and calculations can be found in Appendix G: Data Collection from Effect of PV Panel Coverage on Power Output Experiment.

Figure 25: Effect of PV Panel Coverage on Power Output Experiment - Top Half Covering

Table 3: Effect of PV Panel Coverage on Power Output Experiment Data

Covering	Pm (W)	Efficiency (Calc) (%)
none (full sun)	117.85	18.99
top half	1.01	0.15
bottom half	1.07	0.16
left half	1.29	0.17
left column	0.21	0.025
top row	1.28	0.15
bottom left corner	28.98	4.65
bottom half, top left corner	0.85	0.14
top left corner	30.91	4.96
none (full sun)	128.78	25.92
None (cloudy)	58.20	11.71

A baseline efficiency of 18.99% can be seen in the first test in the table where there is no covering. As expected, covering of the panel or covering due to clouds cause the panel efficiency to decrease. The lowest efficiency was 0.14% when the bottom half of the panel and the top left corner were covered. Similarly, when half of the panel was covered whether it was top, bottom, or left, the panel efficiency decreased to an average of 0.16%. When only the top left corner of the panel was covered, the efficiency decreased to 4.96%. Although there were complications with the weather measurements, the data still shows a general trend that supports covering a panel decreases the power output significantly. While this test may not be completely accurate in representing the exact decrease in power output, it does confirm that even small obstructions on the panel can have a large impact due to the wiring of the panel as discussed in Section 3.1 Reverse Osmosis Systems

6.1.4 Effect of Localized Cooling and Heating on PV Panel Power Output

This experiment was conducted to determine the effects that localized cooling and heating had on the electrical and thermal efficiency. All relevant thermal images can be found in Appendix H: Thermal Images from Effect of Localized Cooling and Heating on PV Panel Power Output Experiment. The relevant data and calculations for the experiment can be found in Table 4 below. To calculate the input power on the panel, the area of the PV panel was measured and multiplied by the average radiation. Then, output power was divided by input power to get efficiency, as shown in Equation 3 below. The calculated efficiency is more accurate than the measured efficiency from the I-V checker due to having more accurate weather data. In the panel temperature column, JB is the junction box, M is the middle of the panel, B is the bottom, T is the top, and R is the right side. A table with full data and calculations can be found in Appendix I: Data collection from Effect of Localized Cooling and Heating on PV Panel Power Output Experiment.

$$\frac{P_m}{P_{in}} * 100 = efficiency\ (100\%) \quad [3]$$

Figure 26: Effect of Localized Cooling and Heating on PV Panel Power Output Experiment - Set Up

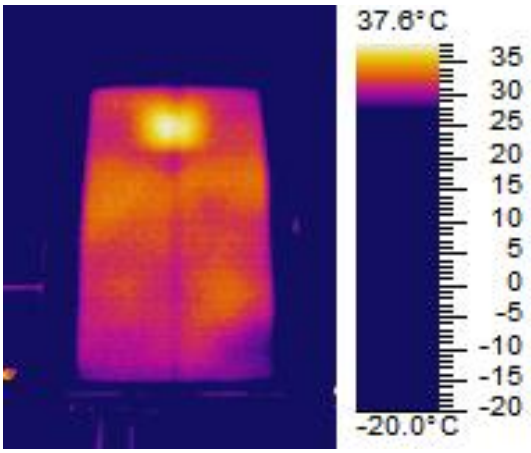

Figure 27: Effect of Localized Cooling and Heating on PV Panel Power Output Experiment - Thermal Image

Table 4: Effect of Localized Cooling and Heating on PV Panel Power Output Experiment Data

Panel	Heat/Cool	Configuration	Pm (W)	Panel Temp.	Efficiency (Calc) (%)
left	none	none	4.64	JB - 45.9 M - 44.5 B - 42.9	Avg = 4.56
right	none	none	5.09	JB - 48.9 M - 44.3 B - 42.2	Avg = 4.29
right	cool	bottom right	5.16	JB - 39.3 M - 33.7 B - 28.5	3.66
right	cool	bottom row	15.97	JB - 44.4 M - 41.1 B - 39.1	9.77
right	cool	right side	4.83	JB - 46.1 M - 42.3 R - 40.6	2.76
right	heat	top half	3.43	JB - 52.2 T - 47.6 B - 46.2	2.33
right	both	top half heat, bottom row cool	3.11	JB - 48.6 M - 46.3 B - 42.1	2.47

The test panel had an average efficiency of 4.29% when unchanged. As expected, when a change of temperature on only part of the panel is present due to heating or cooling, power output and efficiency decrease. The lowest efficiency was 2.33% when the top half of the panel was heated with the space heater. The test where the bottom row of the panel was cooled with ice packs

showed an increase of efficiency to 9.77%. This test is suspected to be an abnormality. This could be due to a sudden weather change that was not detected by the weather station, or a fault in the equipment. The decrease in efficiency for all the other tests shows that any irregularity in panel temperature will cause a decrease in panel efficiency, whether it is heating or cooling.

6.1.5 PV/T

This experiment was run with three solar panels, the Millennium PV/T system, the novel PV/T system developed by the Arava and Dead Sea Science Center, and a SUNTECH STP250-20/Wd panel as a control. Before the experiment was initiated, the flowrates out of the cooling baths and the flowrates out of the thermal systems were measured. The results of this are shown in Table 5, the Millennium PV/T system was attached to cooling bath 1 and the novel PV/T system to cooling bath 2.

Table 5: Cooling Bath Flow Rates

	Output Trial 1 (sec/L)	Output Trial 2 (sec/L)	Output Flow rate (L/min)	Output Flowrate with PV/T System Trial 1 (sec/L)	Output Flowrate with PV/T System Trial 2 (sec/L)	Thermal System Output Flowrate (L/min)
Cooling Bath 1	5.6	5.93	10.4	8.28	8.5	7.15
Cooling Bath 2	6.26	6.51	9.4	11.04	10.93	5.46

Both panels were fed similar initial flowrates, with both cooling bath units rated for 9 L/min. In the final column, the difference in the flow resistance provided by the two thermal systems is quantified. Faster flowrates through a PV/T system cause a higher rate of heat transfer to the working fluid[18], an idea which will be explored more with the results in this section.

A preliminary study was run using the same three panels over the course of 1 hour the day before the actual test. As can be seen in Figure 28, each of the PV/T systems displayed a relatively uniform temperature gradient horizontally across the panel and the top of the panel appeared to experience higher rates of cooling. This was taken into account in developing the final methodology for the actual experiment.

[18] F. P. Incropera, D. P. DeWitt, T. L. Bergman, and A. S. Lavine, "Fundamentals of Heat and Mass Transfer", 6th ed. (Wiley, 2007).

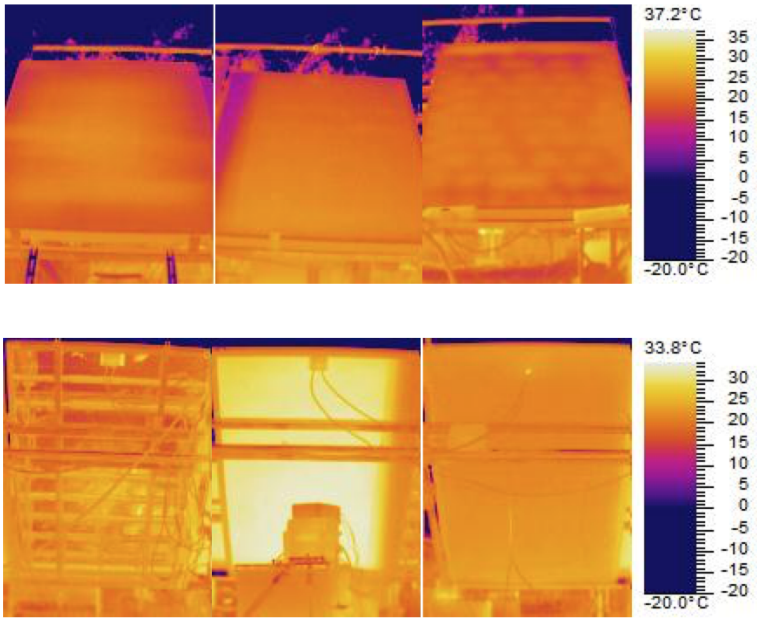

Figure 28: Trial PV/T Experiment Thermal Images

Thermocouples were installed in the input and output piping on the cooling baths. These were recorded by the data logger every 30 seconds. While all the data collected is included in Appendix L: Data collection from Thermocouples from the PV/T Experiment, Figure 29 shows the input and output temperatures for the cooling bath attached to the Novel PV/T system.

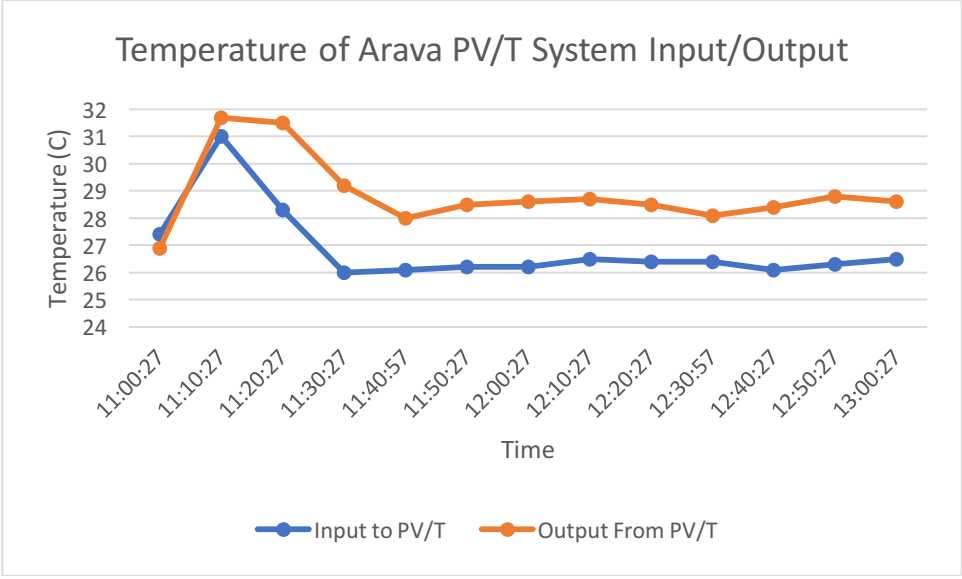

Figure 29: Temperature of Arava PV/T System Input/Output

As the graph showed, at the flowrate of .09 kg/s, the Novel PV/T system was able to raise the fluid temperature by 2°C. In contrast, The ANSYS results showed that at a flowrate of .16 kg/s and at .02 kg/s, the same length of conduit would produce a temperature increase of .25 and 1.2°C respectively. This experimental to simulation correlation requires further study. The

temperature of the output water would only increase with proper insulation on the back of the system, higher ambient temperatures, or higher irradiance values.

The data from the thermocouples on the Millennium panel shows that the water was cooled as a result of being run through the thermal system. This result is unexpected, and may have been due to a broken thermocouple.

Thermal images of the front and back of each of the three panels were taken and analyzed. Figure 30 shows the initial (left) and final(right) thermal pictures from the front of the SUNTECH control panel. Each pair of images were scaled to ensure that they were comparable. These images are helpful for visualizing hot spots and temperature gradients, however, are not accurate representations of the exact surface temperature of the panel.

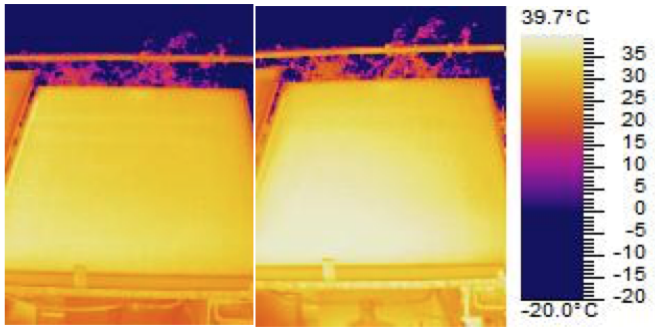

Figure 30: Front Face of PV Control

Figure 31 shows the initial and final thermal pictures from the front of the Millennium panel.

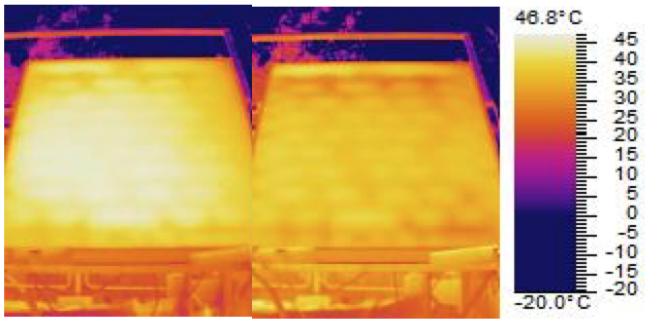

Figure 31: Front Face of Millennium PV/T Panel

As can be seen in these images, the millennium system was effective at creating near uniform cooling across the entire surface of the panel. Although this test was only run for two hours, it is believed that the entire panel would continue cooling uniformly over a prolonged period of operation.

Figure 32 shows the initial and final thermal pictures from the front of the novel panel.

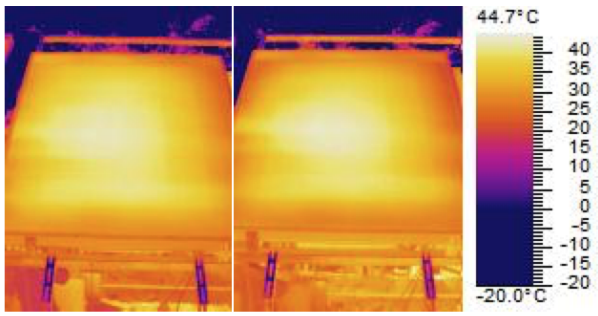

Figure 32: Front Face of Novel PV/T System

In these thermal images, it is possible to see a large hotspot in the middle of the PV panel. This is believed to be a result of bending of the PV panel due to the method through which the thermal system was held to the back. This bending causes the middle of the PV panel to pull away from the thermal system, creating an insulating air gap. This could be fixed through an alternative method of securing the thermal system to the back of the PV panel.

The thermal images of the back of each of the panels are compared as one image below, with more images included in Appendix K. From left to right Figure 33 shows the novel panel, PV panel, and the Millennium panel. The images on the top are the initial and the bottom row are the final.

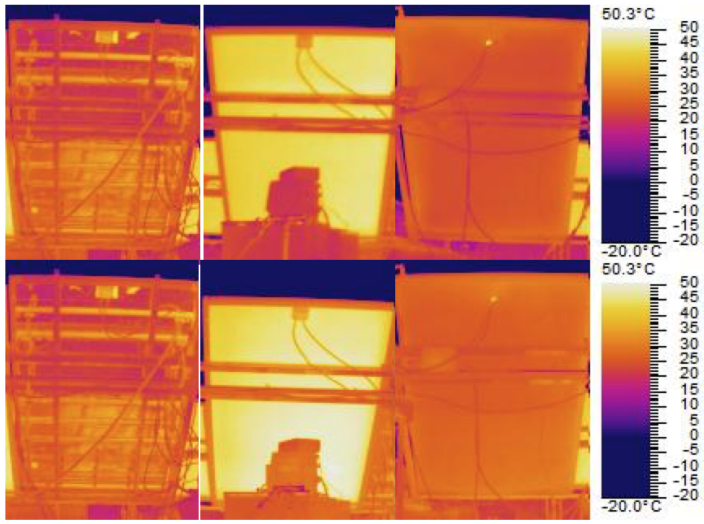

Figure 33: Initial and Final Thermal Images of the Back of the Panels

The temperature of the front of the panels were recorded at the top, middle, and bottom of each panel along the left edge every ten minutes as shown in Figure 34. The average temperature from each of the panels at 10 minute intervals are shown in Figure 35 below and the full data set can be seen in Appendix J: Data Collection from the front of the PV panels from the PV/T Experiment.

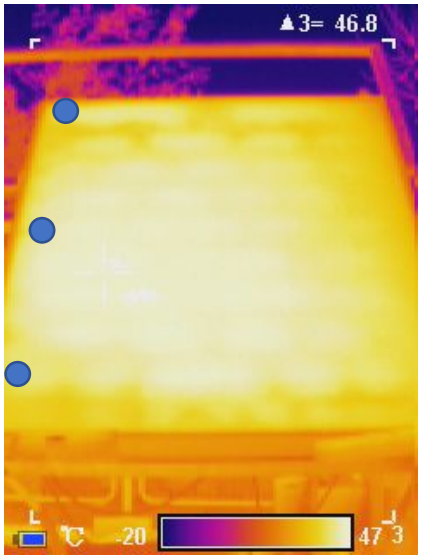

Figure 34: Location of IR Thermometer Data Collections

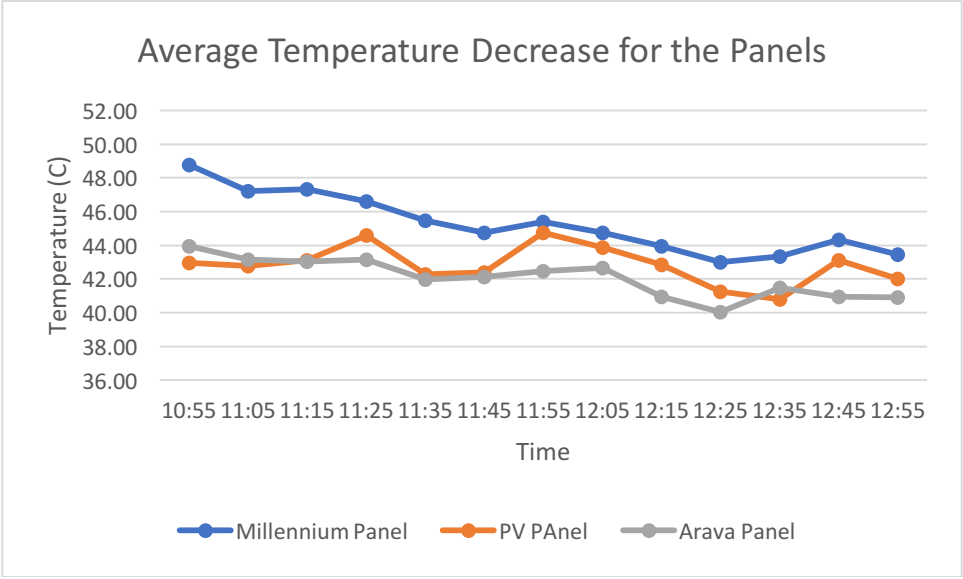

Figure 35: Average Temperature Decrease for the Panels

Figure 35 shows that the novel PV/T system was more effective at cooling the panel than the Millennium PV/T system. Although the cooling bath feeding the Millennium panel took longer to get to the target temperature of 25°C, both panels reached this goal at 12:20, and the novel PV/T maintained a cooler front surface temperature. The Millennium panel took longer to cool due to the insulation on the back of the panel as part of the thermal system.

To study the behavior of the novel thermal system, temperatures were recorded with the IR thermometer at the top, middle, and bottom of three of the aluminum plate. Three vertical locations in each area were measured as shown in Figure 36. These data show a trend of the cooling panel over time, but also the inconsistency of the temperatures produced on the aluminum plate between the fluid conduits in the novel PV/T system. This is likely caused by the separation between the PV and thermal systems as discussed above. The results from this data

collection is included in Appendix M: Data Collection from the Back of the Novel PV/T from the PV/T Experiment.

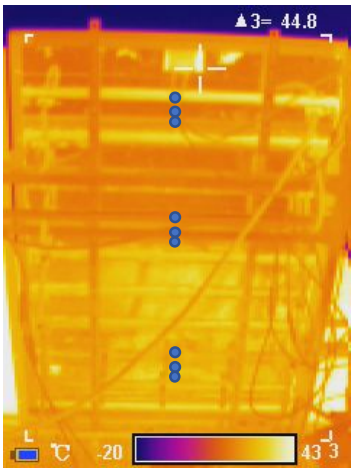

Figure 36: Data Collection Points for the Back of the Novel PV/T System

Finally, the power output for each panel, ambient temperature and the solar irradiance were retrieved from the Arava Institute weather station and SolarEdge monitoring system to which the panels were connected. While the novel PV/T panel was developed using a Millennium PV panel, the two systems are not directly comparable. The Millennium panel was operating with thermal insulation on the back, while the novel PV/T was not insulated, leaving the thermal system open to heat loss due to convection to the air. Figure 37 shows each of the panels power outputs as a function of time, while Figure 38 shows the power output of each panel for the different irradiance values experienced during the experiment.

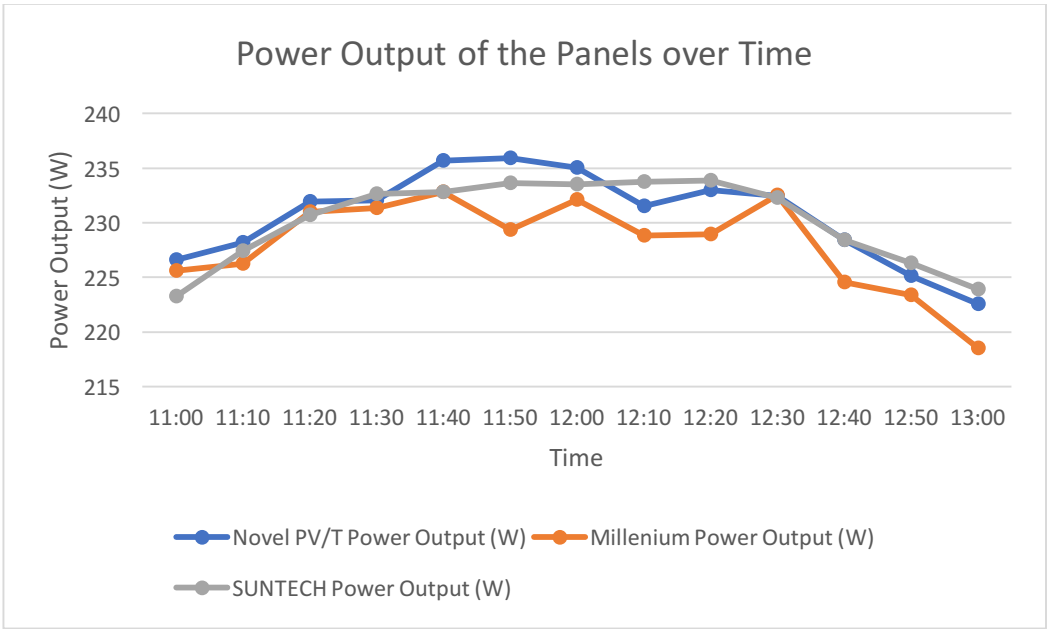

Figure 37: A Graph of the Power Output of the Three Panels versus Time elapsed in the Experiment

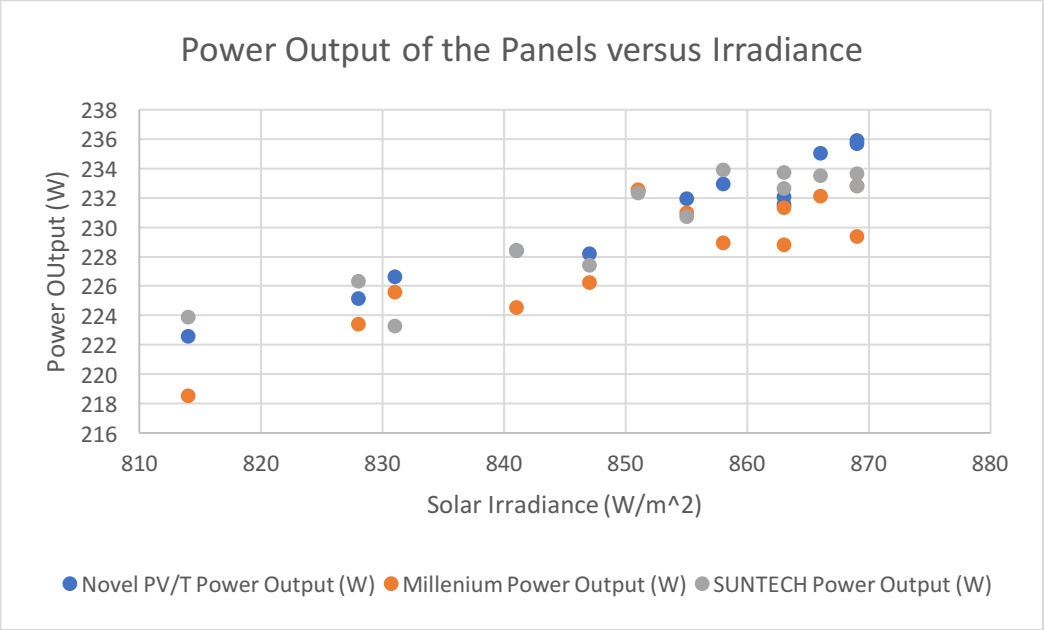

Figure 38: A Graph of the Power Output of all Three Panels Versus the Incoming Solar Irradiance

The differences in power output were small enough (<2%) to not be indicative of any systematic improvements caused by the water cooling. This was in part a result of the relatively low ambient temperatures, which did not provide as much resistance to the cooling, or bring the PV panel to an operating temperature that would decrease efficiency[19].

[19] "STP255-20/Wd, STP250-20/Wd, STP245-20/Wd" *Suntech Power* Feb 23, 2017, http://www.elektropartners.nl/local_resources/file/zonnepanelen/STP250.pdf

7 Component System Design

This section describes research which was completed in exploration of improvements in energy efficiency for each of the five identified component systems. Each component system was broken up into sub areas of study to quantify the potential efficiency increases for the resulting PV/T RO system.

7.1 RO Membranes

This section explores different types of RO membranes manufactured by various companies, as well as multiple configurations in which they could be used.

7.1.1 Type of Membrane

When considering a RO system based on permeate output, the first component that needs to be decided on is the membrane setup itself. The membrane for a system is chosen based the salinity of the feedwater along with the required output. As the salinity of the water increases, so does the pressure needed to overcome the osmotic pressure. Currently, a 2.5 inch diameter by 40 inch long membrane manufactured by DOW is in use in the existing RO system. This membrane and a variety of others for consideration are shown in Table 6 below.

Table 6: Membrane Operating Specifications

Description	Company	Part No.	Op Pressure (PSI)	Liters/ Day	PSI per liter	Recovery rate (%)	Stabilized rejection (%)
Current Membrane[20]	Dow	DOW SW30-2540	800	2649.8	0.3019	10	99.4
Seawater SWC Series[21]	Hydronautics	SWC-2540	800	1968.4	0.4064	10	99.4
Extra Low Energy use for Brackish[22]	Applied Membranes Inc	M-B2540AXLE	100	3217.6	0.03107	10	99
Standard Brackish High Flow[23]	Applied Membranes Inc	M-B2540AHF	225	4012.5	0.05607	15	99
Extra Low Energy[24]	Applied Membranes Inc	M-T2540AXLE	100	3217.6	0.03107	15	99
High Flow[25]	Applied Membranes Inc	M-T2540AHF	225	4012.5	0.05607	15	99.5

The brackish reclaimed water at the Arava Institute has a salt percentage of 0.1%(experimentally determined), so additional salt has been added for testing as necessary to simulate more brackish conditions. Testing was never conducted above 2% salt content, so a brackish water membrane would be the most suitable choice for this application. Newer technology present in the extra low energy membranes allow for a 55% reduction in pressure needed for operation [citation needed]. Using these membranes requires less pumping power, therefore using less energy. Table 7 below shows a variety of sizes of Applied Membranes Inc. extra low energy brackish water membranes and their corresponding outputs to be chosen based on the needs of any given application.

[20] "DOW FILMTEC Membranes." *DOW*. Retrieved 23 February, 2017, from msdssearch.dow.com/PublishedLiteratureDOWCOM/dh_082d/0901b8038082d595.pdf?filepath=liquidseps/pdfs/noreg/609-00377.pdf&fromPage=GetDoc

[21] "Hydronautics Seawater SWC Series Membranes." *Applied Membranes Inc.* Retrieved February 23, 2017, from www.appliedmembranes.com/hydranautics-seawater-swc-series-membranes.html

[22] "Extra-Low Energy Brackish RO Membrane Elements." *Applied Membranes Inc*. Retrieved February 23, 2017, from http://www.appliedmembranes.com/extra-low-energy-brackish-ro-membrane-elements.html

[23] "Brackish Water (FRP Wrapped) Membranes." *Applied Membranes Inc.* Retrieved February 23, 2017, from http://www.appliedmembranes.com/brackish-water-frp-wrapped-membranes.html

[24] "Extra-Low Energy (XLE) RO Membranes." *Applied Membranes Inc.* Retrieved February 23, 2017, from http://www.appliedmembranes.com/extra-low-energy-xle-ro-membranes.html

[25] "Commercial/Industrial Thin Film Reverse Osmosis Membranes." *Applied Membranes Inc.* Retrieved February 23, 2017, from http://www.appliedmembranes.com/commercial-industrial-thin-film-reverse-osmosis-membranes.html

Table 7: Membrane Model Numbers and Specs.

Model No.[26]	Dimensions (Dia " x Length")	Liters/Day
M-B2514AXLE	2.5 x 14	719.23
M-B2521AXLE	2.5 x 21	1381.7
M-B2540AXLE	2.5 x 40	3217.6
M-B4014AXLE	4.0 x 14	2044.1
M-B4021AXLE	4.0 x 21	3880.1
M-B4040AXLE	4.0 x 40	9842.1

7.1.2 Membrane Setup

A reverse osmosis system can be fully functional with a single membrane, but there are options for multiple stages and passes. As seen in Figure 39 below, a stage occurs when the brine output of one membrane is put through a second. This allows for additional water recovery, albeit at a much lower percentage than the first stage due to the higher salt content[27].

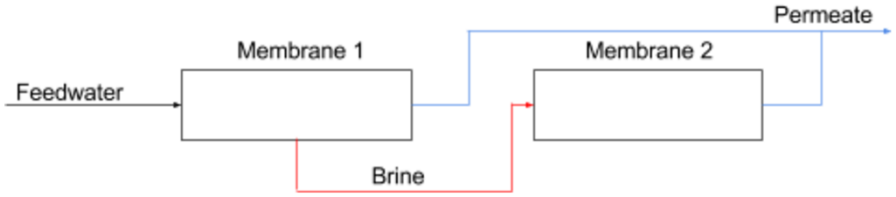

Figure 39: RO Membranes Arranged in Two Stages

Figure 40 shows a two pass system. Passes take permeate out of one membrane and put it through another for further purification.

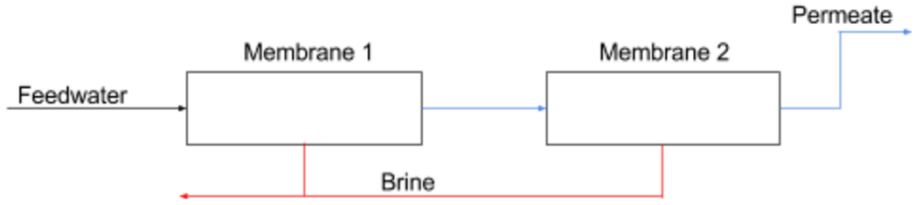

Figure 40: RO Membranes Arranged as a Two Pass System

[26] "Extra-Low Energy Brackish RO Membrane Elements." *Applied Membranes Inc*. Retrieved February 23, 2017, from http://www.appliedmembranes.com/extra-low-energy-brackish-ro-membrane-elements.html
[27] "Basics of Reverse Osmosis." (n.d.). Retrieved February 23, 2017, from http://puretecwater.com/downloads/basics-of-reverse-osmosis.pdf

Table 8: Pros and Cons of RO Membrane Configurations

Parameter	Pros	Cons
Multiple Stages	Higher water output	Added cost of second membrane
Multiple Passes	Better purification of water	Lowered recovery rate

Table 8 above shows the pros and cons of multiple stages and passes. As the table states, adding a second membrane can be costly. In the case of multiple stages, it is more efficient to use a membrane with a higher daily output to satisfy the needs of the application. Multiple passes are not practical in small-scale systems because the benefits of further purifying the water are outweighed by the reduction in permeate output. For example, if two 10% recovery membranes are used, only 1% of the initial feedwater will exit as permeate.

7.2 RO Pump System

This section explores the potential options for the pumping section of the RO system. This includes different types and configurations of pumps, as well as energy recovery devices.

7.2.1 Energy Recovery Devices

When looking at the pump configuration for the RO system, the concept of energy recovery devices must be assessed first to determine system requirements. During the RO process, a large amount of energy is used to pressurize the water to be run through the membrane[28]. The rejected brine stream that comes out after the membrane filtration remains highly pressurized, typically within 1-2 bar of the input feedwater stream[29]. For a single pass, single stage system set-up like the Arava system, the rejected brine stream is no longer needed for the RO process. In order to save on energy consumption, the rejected brine stream is typically run through an energy recovery device to transfer the pressure from the stream to the incoming feedwater stream destined for the RO membrane. This pressure transfer is accomplished through different mechanisms based on the type of energy recovery device used.

The first energy recovery device, called a Pelton wheel, used the pressurized output stream to run a water wheel, coupled with a shaft that would pressurize the incoming water on the other end[30]. Since then, more technologies have been developed to more efficiently transfer pressure between the streams. Three of these modern recovery devices were considered for use on this system: Spectra Watermakers Clark Pump, Energy Recovery Inc.'s Pressure Exchanger, and the Advanced Turbo Turbocharger also offered by Energy Recovery Inc.

---

[28] Lachish, Uri "Optimizing the Efficiency of Reverse Osmosis Seawater Desalination" 22 Feb. 2017, http://urila.tripod.com/Seawater.htm

[29] "DOW FILMTEC™ Membranes DOW FILMTEC Seawater RO Elements for Marine Systems", *DOW*, 22 Feb. 2017, http://msdssearch.dow.com/PublishedLiteratureDOWCOM/dh_082d/0901b8038082d595.pdf?filepath=liquidseps/pdfs/noreg/609-00377.pdf&fromPage=GetDoc

[30] Contreras, Alfredo S. B. "An energy recovery device for small-scale seawater reverse osmosis desalination" Loughborough University, 2009

Using energy recovery devices has become the standard practice in industrial scale seawater reverse osmosis (SWRO) due to its significant energy and capital savings. Within the small-scale RO industry, energy recovery devices are not always used due to their capital costs and the change in focus away from maximum efficiencies that are seen on the industrial scale. This is compounded by the fact that almost all energy recovery devices are large in size to accommodate industrial scale RO, a factor that makes them generally unsuitable for small-scale RO.

The Advanced Turbo Turbocharger and the Pressure Exchanger are not suggested for use with this system due to their physical size being much too large, and for the fact that they are designed to handle flows at a starting rate of 190 L/minute, which is 19 times the target flow rate[31].

7.2.2 Clark Pump

Initially designed to be used aboard long journey seafaring vessels, the Clark pump energy recovery device has a suitable size for this application. Unlike the other two recovery devices considered, the Clark pump's operation is purely mechanical, meaning it runs completely on input streams, requiring no additional external motors or power sources as shown in Figure 41[32].

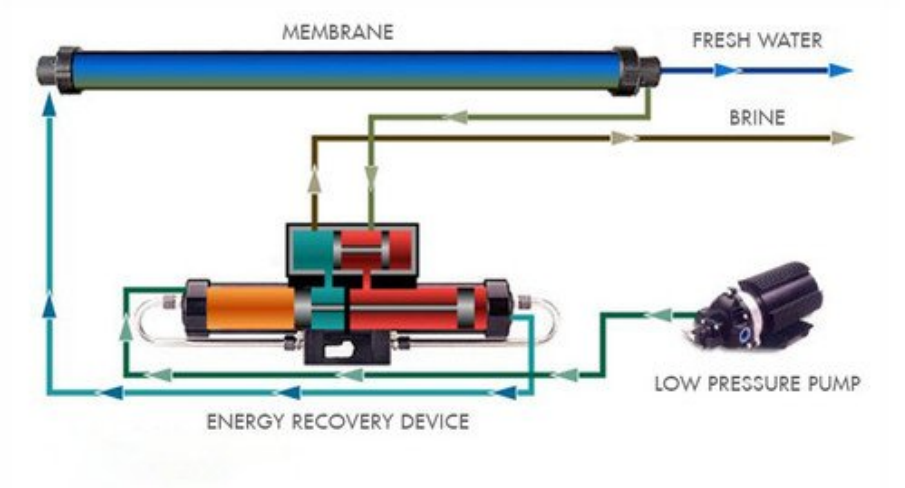

Figure 41: Graphic of the Operation of a Clark Pump Energy Recovery Device[33]

Below Equations 4-12 are calculations using the Clark pump to determine the system's target characteristics, in particular what pressure is needed to be supplied to the Clark pump as an input. Target characteristics are calculated for four different kinds of fluids: seawater, highly brackish water, brackish water, and lightly brackish water.

[31] "Desalination Products Catalog", *Energy Recovery Inc*., 22 Feb. 2017, http://www.energyrecovery.com/wp-content/uploads/2014/12/0916_ER_desalProducts_brochure_interactive_v3.pdf
[32] Miranda & Thomson, "Theory, Testing and Modelling of a Clark pump", 17 Sept. 2000, Centre for Renewable Energy Systems Technology, Angela Marmont Renewable Energy Laboratory, Loughborough University of Technology, Leicestershire, UK
[33] "Our Technology." *Spectra Watermakers*, 22 Feb. 2017. https://www.spectrawatermakers.com/us/us/explore/our-technology

The final output pressure from the pumping system for seawater is 55 bar, highly brackish is 40 bar, brackish water is 15 bar, and lightly brackish is 7 bar[34]. These requirements are derived from common operating pressures for RO membranes designed to desalinate these kinds of fluids. Brackish water represents a wide range of salinities, 0.5% to 3.5%[35], so a wide range of pressures was selected. The selected flow rate for the system is 10 L/minute of feedwater. Assumptions made in these calculations include, no pipe losses, P_HP=Membrane Spec, P_t=10% constant, and P_c=(P_HP-2 bar) for a 'properly functioning membrane'.

$$P_1 + \frac{1}{2}\rho {V_1}^2 + \rho g h = P_2 + \frac{1}{2}\rho {V_2}^2 + \rho g h \quad [4]$$

$$P_1 = \frac{1}{2}\rho {V_{exit}}^2 \quad [5]$$

$$\rho_{1\%\ salt\ @\ 35C} = 1000\frac{kg}{m^3} \quad [6]$$

$$Q_{exit} = 9\frac{L}{Min} \quad [7]$$

$$\frac{9\ L}{Min} X \frac{.001\ m^3}{1\ L}\ X \frac{1\ Min}{60\ s} = Q_{exit} = 1.5e-4\frac{m^3}{s} \quad [8]$$

$$Q = AV => V_{exit} = \frac{Q_{exit}}{A_{pipe}} = (1.5e-4\frac{m^3}{s})/(\pi\left(\frac{13\ mm}{2}\right)^2 = 1.13\frac{m}{s}$$

$$P_1 = \frac{1}{2} * 1000\frac{kg}{m^3} * \left(1.13\frac{m}{s}\right)^2 = 638.45\ Pa\ (psig) \quad [9]$$

$$P_1 = 102\ kPa = 14.8\ psi = 1.02\ bar = P_{exit} \quad [10]$$

$$P_F = P_{HP} + (1 - P_t)(P_t - P_c) \quad [11]$$

$$P_F = 55\ bar + (1 - .1)(1.02\ bar - 53\ bar) \quad [12]$$

$$P_{F-seawater} = 8.2\ bar$$

$$P_{F-40\ bar\ brackish} = 6.718\ bar$$

$$P_{F-15\ bar\ brackish} = 4.22\ bar$$

$$P_{F-7\ bar\ brackish} = 3.42\ bar$$

[34] Lachish, Uri "Optimizing the Efficiency of Reverse Osmosis Seawater Desalination" 22 Feb. 2017, http://urila.tripod.com/Seawater.htm

[35] "Estuaries", *National Oceanic and Atmospheric Administration*, 22 Feb 2017, http://oceanservice.noaa.gov/education/kits/estuaries/estuaries01_whatis.html

Some experimentally obtained information was used in this calculation, such as using water density and flow rate from one of the RO experiments to calculate exit flow velocity and pressure. Using a Clark pump in this scenario reduces required input pressure from 55 bar down to 8.2 bar, as seen in Table 9, an 85.1% reduction. This substantial reduction in required pressure translates to significant energy savings.

Table 9: Target Pressures for Pumping Systems

Flow Rate = 10 L/minute				
Water Salinity	Input Pressure (bar)	Input Pressure (psi)	Head (m)	Head (ft)
Seawater	8.22	118.93	83.84	275.00
Highly Brackish	6.72	97.47	68.54	224.82
Brackish	4.22	61.21	43.04	141.18
Lightly Brackish	3.42	49.60	34.88	114.42

7.2.3 Pumps

There are two main classification of pumps, centrifugal and positive displacement. Centrifugal pumps deliver a constant head[36], and can deliver very high flow rates[37]. Positive Displacement pumps deliver a constant flow rate[38] and can typically deliver high pressures[39]. Detailed in Table 10 below, three different kinds of pumps within centrifugal and positive displacement were considered to meet the needs of the system. Below is a table of information comparing these types against each other with some typical characteristics. Since the system is solar powered and there are no inverters in the system, only pumps that are available in DC powered configurations were considered for ease of integration.

[36]"Centrifugal Pumps", *EngineeringToolbox*, 22 Feb. 2017, www.engineeringtoolbox.com/centrifugal-pumps-d_54.html
[37] "Pump Types Guide - Find the right pump for the job", *PumpScout*, 22. Feb 2017, www.pumpscout.com/articles-scout-guide/pump-types-guide-aid100.html
[38] "Positive Displacement Pumps", *EngineeringToolbox*, 22 Feb. 2017, http://www.engineeringtoolbox.com/positive-displacement-pumps-d_414.html
[39] "When to use a Positive Displacement Pump", *Pump School*, 23 Feb. 2017, www.pumpschool.com/intro/pd%20vs%20centrif.pdf

Table 10: Pump Characteristics by Type

Pump Type	Classification	Relative Price Range	Typical Single Pump Output Pressure	Typical Single Pump Flow Rate	Typical Single Pump Power Consumption	Main Advantage(s)
Diaphragm	Positive Displacement	Low	60-130 psi	3-10 L/minute	10-30 W	Inexpensive, very common,many DC powered options, compact
End Suction[40]	Centrifugal	Medium	7-60 psi	35-500 L/minute	80-1500 W	High flow rates, relative low power consumption for flow rate
Plunger[41]	Positive Displacement	High	100-900 psi	6-10 L/minute	200-1500 W	High pressure

From this, as seen in Table 11 below, diaphragm pumps were selected for further investigation due to their low cost, low power consumption, high availability, pressure output, and their conservative flow rates. For comparison, a plunger pump is also considered for the sole purpose of being able to operate SWRO with no energy recovery device. This option is meant to illustrate the effectiveness of using low pressure pumps in conjunction with energy recovery devices as opposed to no energy recovery device.

[40] "GT IRRI-GATOR Self-Priming Centrifugal Pumps - 60 HZ", Goulds Water Technology, 23 Feb. 2017, documentlibrary.xylemappliedwater.com/wp-content/blogs.dir/22/files/2012/07/BGT-R3.pdf
[41] "SIJ 2.4-900P-180 BT", *Sun Pumps Inc.*, 23 Feb. 2017, www.sunpumps.com/Products/SIJ%202.4-900P-180%20BT

Table 11: Characteristics of DC Pumps Used in Schemes

Name	Voltage	Power Consumption	Max Flow Rate	Max Pressure
Ultra Quiet[42]	12 V	19 W	13.33 L/minute	0.49 bar
FL-3308[43]	12 V	70 W	6 L/minute	9 bar
Solar Well[44]	12 V	96 W	8 L/minute	6.875 bar
Plunger	180 V	1493 W	9.6 L/minute	62 bar

All of the below pump schemes were developed to meet the needs of SWRO with a Clark pump for energy recovery. In theory designing a system for SWRO demonstrates the upper bound of what is required since it is the most energy intensive RO fluid. If lower salinity fluids are being used for RO, then measures can be added to these proposed schemes to reach the required pressures.

Pump scheme #1 is the current systems pump set-up, which employs pre-configured pumps in series[45]. When put in series, pumps will add pressure head and should have matching flow rates for best performance; pumps in parallel will add flow rates together and should have matching pressure heads for best performance[46].

Scheme #2 consists of two FL-3308 pumps in parallel. The unique trait of the FL-3308 pump (out of all DC diaphragm pumps considered), is that a single pump can produce the required pressure for SWRO. This means that the pumps can be run in parallel, unlike the other schematics which primarily utilized pumps in series. A single pump does not have the required flow rate, so two are used to obtain the necessary flow rate. Since this scheme employs two low cost pumps, there is a low degree of complexity and a low cost for repairs or replacements.

Scheme #3 uses a Solar Well pump as a primary pump to produce the majority of flow and pressure requirements, and supplements the Solar Well pump with several Ultra Quiet pumps. The Solar Well pump is placed in parallel with one Ultra Quiet; these pumps are then placed in

[42] "Ultra Quiet Mini DC 12V Lift 5M 800L/H Brushless Motor Submersible Water Pump." *eBay*, 19 Feb. 2017, www.ebay.com/itm/Ultra-Quiet-Mini-DC-12V-Lift-5M-800L-H-Brushless-Motor-Submersible-Water-Pump-/121988963251

[43] "130PSI 6L/Min Water High Pressure Diaphragm Self Priming Pump DC12V 70W FL-3308", *eBay*, 23 Feb. 2017, www.ebay.com/itm/130PSI-6L-Min-Water-High-Pressure-Diaphragm-Self-Priming-Pump-DC12V-70W-FL-3308/131861277842?_trksid=p2047675.c100005.m1851&_trkparms=aid%3D222007%26algo%3DSIC.MBE%26ao%3D2%26asc%3D41395%26meid%3De013ff18c0564ae29d55952427780f53%26pid%3D100005%26rk%3D6%26rkt%3D6%26mehot%3Dpp%26sd%3D131556382165

[44] "12V Submersible Deep DC Solar Well Water Pump, Solar, battery, alternate energy", eBay, 23 Feb. 2017, www.ebay.com/itm/12V-Submersible-Deep-DC-Solar-Well-Water-Pump-Solar-battery-alternate-energy-/191776770021

[45] "Reverse Osmosis System Manual PROFILTER-SW-65", *Treatment CFS Ltd*, 23 Feb. 2017

[46] "Pumps in Parallel or Serial", *EngineeringToolbox*, 22 Feb. 2017, www.engineeringtoolbox.com/pumps-parallel-serial-d_636.html

series with three Ultra Quiets. Due to its relative complexity, a block diagram schematic of scheme #3 has been included below in Figure 42 for clarity.

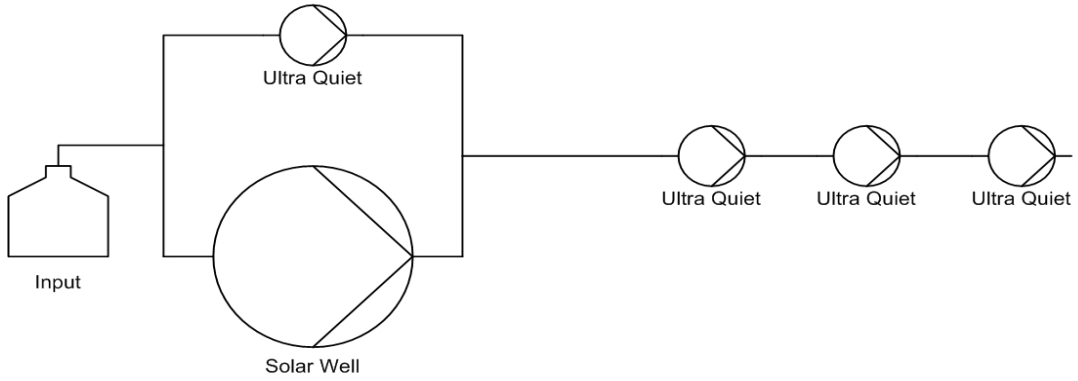

Figure 42: Scheme 3 Schematic

Scheme #4 has 17 Ultra Quiet pumps in series. Due to the number of required pumps, this scheme has a high probability of part failure, which would impact uptime for the RO system. While the probability for part failure is high, the cost of repair or replacement is low.

Scheme #5 is a single plunger pump running without an energy recovery device. This pump is costly, and requires several times more power than any of the other proposed schemes, and would require several times more solar panels to simply generate a high enough voltage to run this pump. Each of these schemes are detailed in Table 12 below.

Table 12: Possible DC Pump Configurations

Scheme #	# of pumps	Approximate Total Cost	Total Power Consumption	Required Voltage	Main Advantage(s)
1 (current system)	2	$800[47]	400 W	24 V	Pre-configured
2	2	$50	140 W	12 V	Very cheap, simple configuration, low power consumption
3	5	$175	172 W	12 V	Primary pump is submersible, low power consumption
4	17	$300	323 W	12 V	Inexpensive pumps
5	1	$2000[48]	200 - 1500 W[49]	120 - 180 V	Single pump, no ERD required

[47] "Flojet R8600344A Pump - 22.7 l/m", *Spraytech*, 23 Feb 2017, www.spraytech.uk.com/flojet-r8600344a-pump---227-lm-635-p.asp
[48] "SAVIOR Sunray SOLFLO-SIJ 2.4-900P-180 BT Brush Type Plunger Pump", *Amazon*, 23 Feb. 2017, www.amazon.com/SAVIOR-SOLFLO-SIJ-2-4-900P-180-BT-Plunger/dp/B0171EQTZ2
[49] "Sunpumps High Pressure Plunger Pump Model SIJ 2.4-900P-180 BT", *Sun Pumps*, 23 Feb. 2017, www.sunpumps.com/Photo/589?d=2/19/20175:17:15AM

7.3 PV/T Heating System

There are two options for the type of working fluid with the existing PV/T RO system. The current iteration of the system is setup to have freshwater mixed with an anti-corrosion agent circulated through the PV/T system. This then is channeled through a titanium shell and tube heat exchanger to transfer the heat to the feedwater for the RO process. While this system makes the design parameters of the PV/T system looser, it does add additional inefficiencies and heat losses to the overall PV/T RO system.

The other option is to design a PV/T system that would be able to handle the potential corrosivity of the brackish feedwater, and transfer the heat from the back of the panel directly to the RO feedwater. This system has the potential to be much more efficient but requires additional material selection consideration. The following sections show some possibilities for material selection for such a system, including both pure metals and metal alloys.

7.3.1 Material Selection

The primary factors considered in this analysis are thermal conductivity (W/m-K), density (g/cm^3), thermal expansion coefficients (per °C), and price. The following sections break down each of these factors, ranked in order of priority.

1. Thermal Conductivity
2. Density
3. Price
4. Thermal Expansion Coefficient

The first three categories are quantified in Table 13 with the thermal expansion coefficient studied later. As a final consideration, the corrosion resistance of the chosen materials is also studied. For the current design analysis, it is assumed that the working fluid will be distilled water, or regular water with an anti-corrosion additive. An additional case is then studied where the salt water for the desalination system is run directly through the PV/T system, and therefore, corrosion resistance is a consideration of higher priority.

Table 13: Material Properties Under Consideration

Material	Thermal Conductivity[50] (W/m*K)	Price/lb[51]	Density (g/cm^3)
Aluminum	205	$0.83/lb	2.7
Silver	406	$286.72/lb	10.5
Copper	385	$2.66/lb	8.96
Iron	79.5	$0.03-0.04/lb	8
Titanium	19-23	$1.58/lb	4.5
Nickel	90	$4.74/lb	8.9

Thermal Conductivity
Thermal conductivity of the material chosen is critical to the operation of the PV/T system. This is particularly important in the pursuit of a small-scale system where the amount of available PV panels would likely be limited. The amount of surface area needed for the heat transfer, and therefore the length of the conduit necessary is directly affected by the material's ability to conduct heat to the working fluid. For comparison purposes, polyethylene has a thermal conductivity of 0.33 W/m-K, less than 1/100 than the materials in the table even though it is one of the higher thermally conductive plastics.

In the commercial design produced by Millennium Solar, copper was the metal used, while in the novel PV/T constructed at the Arava and Dead Sea Science Center, Aluminum was the metal chosen for the system.

Density
The density of the material selected determines the weight of the PV/T system which will be added onto the back of the regular PV panel. Materials with a high density risk bending, or breaking the PV panels. Additionally, heavier PV/T systems will limit the mobility of the PV/T RO system, mobility being a particular benefit for small-scale systems. Depending on the amount of material used for the particular PV/T design, weight can become critical. In this category copper and iron both greatly outweigh titanium and aluminum.

Price
Although important for the economic feasibility of any product, price plays a particular role in this analysis since PV/T technology is currently widely viewed as optional for RO systems. It is important to note that the price of materials is constantly in fluctuation and varies based on the region where the system would be produced. nsideration of higher priority.

[50] "Thermal conductivity." *HyperPhysics*. N.p., n.d. Web. 22 Feb. 2017. http://hyperphysics.phy-astr.gsu.edu/hbase/Tables/thrcn.html.
[51] "InvestmentMine." *Metals Pricing*. N.p., 22 Feb. 2017. Web. 22 Feb. 2017. <http://www.infomine.com/investment/metal-prices/>.

Table 13 is to provide pricing context, not exact prices.

Through this consideration, iron is shown to be the most cost effective, however, it has lower thermal conductivity than two of its competitors, aluminum and copper.

Thermal Expansion Coefficient

The thermal expansion coefficient refers to the amount of volume distortion or growth that can be expected per degree Celsius of temperature increase. This factor was given the lowest priority because in the applications of a small-scale PV/T RO system, it would likely not develop into a serious issue. However, at the time of this analysis, no studies were found that directly pertained to this material property. If the PV/T system were to experience significant expansion or shape deformation, then it has the potential to cause damage to the PV panel that it is bonded to. This could lead to air gaps between certain sections of panel and PV/T system, allowing for an insulating layer to adversely affect the heat transfer from the panel to the working fluid. The thermal expansion coefficients for the materials are displayed below in Figure 43.

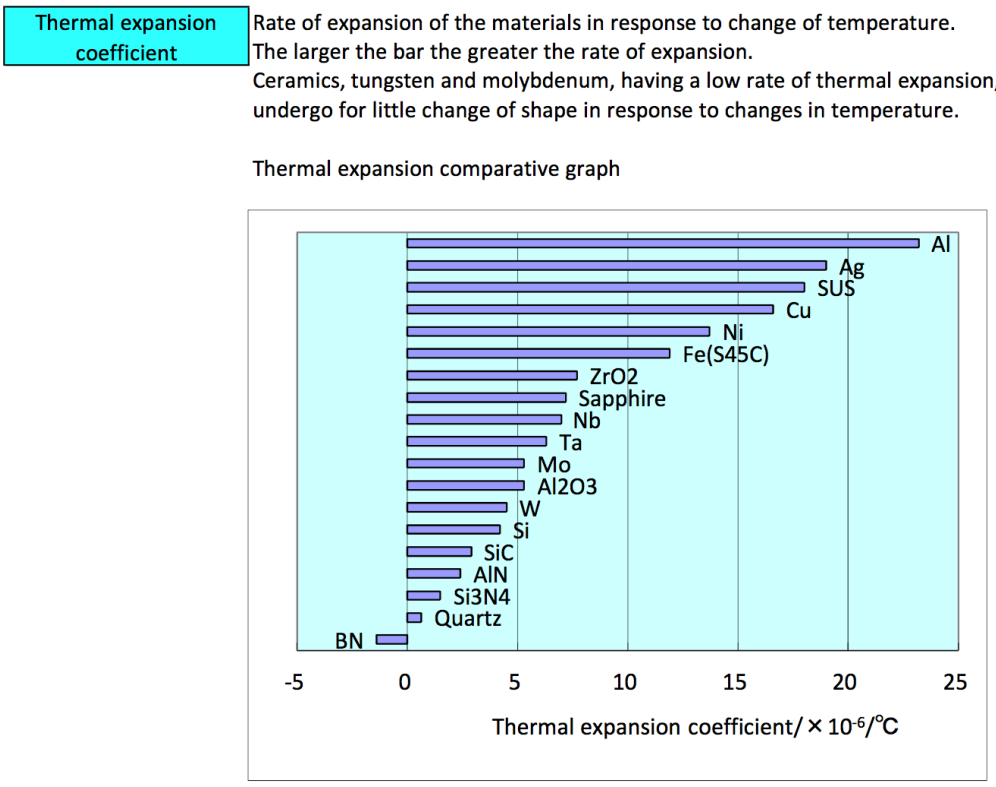

Figure 43: Thermal Expansion Coefficients for Various Materials[52]

This graphic shows that aluminum has the highest coefficient in the group of materials studied with copper as the next highest. While the other materials under consideration are not displayed here, this graphic begins to emphasize the potential benefits of using alloyed metals instead of the pure metals previously under consideration.

Metallic Alloys

[52] "Low Thermal Expansion Materials Guide & Low Thermal Expansion Material Properties." *Top Seiko Co.Ltd.* N.p., n.d. Web. 21 Feb. 2017. <http://top-seiko.com/guide/low-thermal-expansion-materials/>.

In addition to the pure metals studied above, it is important to consider the available alloys that combine many of the positive qualities of each of the individual metals. In the textbook Corrosion: Understanding the Basics, by J.R. Davis, the primary benefits of alloys are detailed with particular attention paid to corrosion resistance[53]. The general table from this text is shown in Table 14 below listed in order of increasing corrosivity.

Table 14: Material Selection for Different Corrosive Environments

Water Type	**Minimum Alloy Selection**
Fresh Water	Steel
	Copper
	Aluminum
Corrosive Fresh Water	Copper (admiralty)
Brackish water and seawater (low to moderate velocity)	70Cu-30Ni, 90Cu-10Ni
Pure and polluted seawater (high velocity)	Stainless steel (type 316)
	Ferritic molybdenum stainless steels (Fe-Cr-Mo)
	Titanium

The rows for seawater are pertinent for this analysis, which led to the consideration of copper-nickel alloys as well as stainless steel and titanium. Stainless steel type 316 is commonly used by divers in the ocean to prevent saltwater corrosion, and therefore could be potentially successful in handling RO feedwater. The primary downside to the proposed alloys in this table are the relatively high density values of both copper and nickel, which would lead to a much heavier design compared to a solution such as titanium. This table, however, does not encompass all of the options for alloys, solely the ones recommended by this author. Depending on the method of manufacturing needed for the final design, and the final definition of feedwater parameters, there are other options that may be better. The effects of using certain metals as an alloy is well documented, and the primary results relative to corrosion resistance are shown for one alloy in Figure 44 below taken from Corrosion: Understanding the Basics.

[53] Davis, J. R., and Inc Books24x7. Corrosion: Understanding the Basics. Materials Park, Ohio: ASM International, 2000. Web. 23 Feb. 2017.

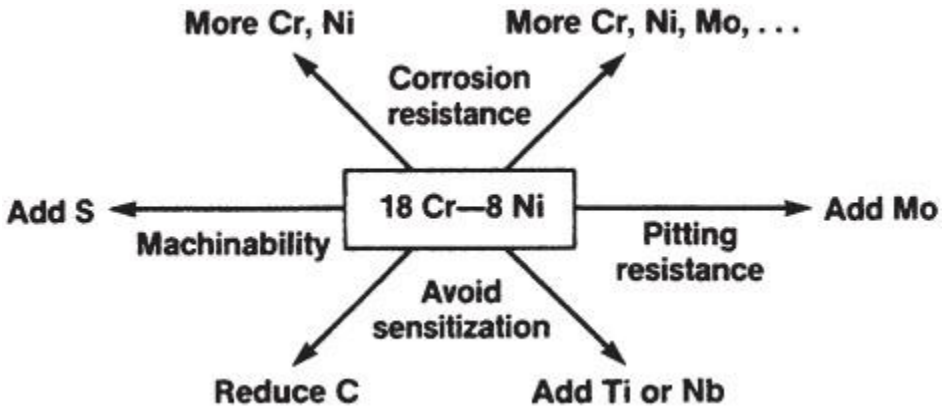

Figure 44: Effects of Material Addition to a Cr-Ni Alloy

7.3.2 Conduit Design

While there are many ways to construct a PV/T system, the one studied in this analysis is a conduit system. This involves conduits which carry the working fluid along the back surface of the PV panel. Other options include a water sheet or a polymer mat.

Cross-Section Shape
Heat transfer is highly dependent on the amount of surface area which is in contact with the two surfaces between which the heat is being transferred. In order to maximize the surface area between the conduit carrying the water and the back of the panel, rectangular conduits would be advantageous over circular ones. The Millennium panel studied in this paper uses circular cross sections, and is compared to the novel PV/T design developed at the Arava and Dead Sea Science Center which has a square cross section.

Size and Number of Conduits
The size of the conduit can also make a large difference in the amount of heat transferred from the panel to the working fluid. As noted in a paper published by Clarkson University and written by R. Shankar Subramanian heat transfer to a fluid flow which is turbulent is much more effective than heat transfer to a fluid flow which is laminar[54]. This is important when considering the relative size of the conduit being used, and the way that each of the conduits is connected.

One of the main factors used to characterize the flow through a pipe is the Reynolds number. The calculation of the Reynolds number is driven primarily by the effective diameter of the pipe and the length of the pipe in the direction of the fluid flow. If the effective diameter of the conduits is increased too much, it will allow a more laminar flow through the tube. Additionally, a larger effective diameter will allow a greater amount of water to pass above the bottom of the conduit, which is the main source of heat transfer to the fluid. With more laminar flow, both of these factors will greatly retard the overall heat transfer to the fluid.

[54] Subramanian, R. Shankar. "Heat transfer to or from a fluid flowing through a tube." web2. clarkson. edu/.../subramanian/.../Convective% 20Heat% 20Transfe r (2008).

A higher number of conduits along the backside of the panel has the potential to add the benefit of increased heat transfer as well as more uniform cooling of the PV panel. The main limiting factors on the number of conduits which can be placed on the back of the panel is the size of the panel and the weight of the system due to the material used.

Insulation
Since the primary goal is to heat the water, the system would benefit from insulation on the backside of the panel to separate the metal conduits from potential heat loss due to convection to the surrounding air. This will help maximize the amount of heat retained in the fluid. In previous iterations of the Arava PV/T system, a spray polyurethane insulation was used, and the Millennium PV/T added another back panel to contain insulation next to the pipes. The spray insulation has lower thermal conductivity than air and therefore, would be more efficient at insulating the heat transfer system.

7.4 Electrical Systems

This section discusses the options for DC/DC conversion, charge controllers, and batteries. This section also explores the potential for a novel protection system to prevent the pumps and the output water from damage or contamination in the event of a system failure.

7.4.1 Power Management

Currently, four PV/T panels are stepped down to 24V to charge the four Absorbed Glass Mat (AGM) batteries, which power the RO system. The charge controlling system in use is an Outback FM80 Charge Controller[55]. This system is ideal because it steps down the voltage as needed, protects the batteries, and has a voltage and current limit much higher than will be needed. However, the system is fairly expensive and bulky, and only allows for one output, which was designed for a battery.

Their potential systems fall under two categories: charge controllers with one output, and charge controllers with two outputs for batteries and the RO system. Running a transient operation is not considered a reliable option. Some studies show that transient operation is possible, but recommend a battery as an alternative even in areas with high irradiance, as weather is not completely predictable or controllable[56]. Basic block diagrams can be found in Figure 45 and Figure 46 below for both single output and dual output systems.

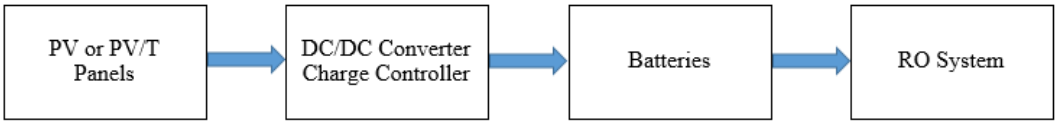

Figure 45: Power Management - Single Output

[55] "Outback Power FLEXmax Series Charge Controllers (FLEXmax 80, FLEXmax 60) Owner's Manual." *Outback Power*. www.outbackpower.com/outback-products/make-the-power/flexmax-series-charge-controllers/item/flexmax-6080
[56] "Solar Performance and Efficiency." *Energy.gov*. 20 August 2013. energy.gov/eere/energybasics/articles/solar-performance-and-efficiency

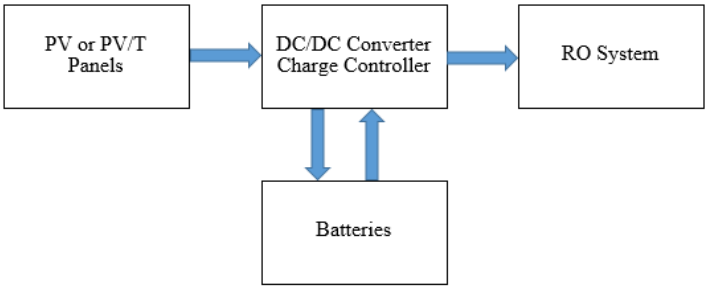

Figure 46: Power Management - Dual Output

For standard charge controllers, potential options are the Outback FM80, the Linear Technology LT8490 High Voltage High Current Buck Boost Charge Controller with Maximum Power Point Tracking[57], the Solar Converters 15 Amp 12/24 Volts MPPT Charge Controller (PT 12/24 – 15)[58], and the BlueSolar MPPT 100/30[59]. For a charge controller with a battery and RO system output, the potential system is the Linear Technology LTC4000-1 High Voltage High Current Controller for Battery Charging with Maximum Power Point Control[60]. The LTC4000-1 would need either the LT3845A High Voltage Synchronous Current Mode Step-Down Controller with Adjustable Operating Frequency[61] or the LTC3789 High Efficiency, Synchronous, 4-Switch Buck-Boost Controller[62]. Table 15 below compares the most important characteristics of these power management systems including cost, input and output voltage and current, capability to step down (buck) and step up (boost) voltage, battery compatibility, size, and casing, which correlates with ease of installation.

[57] "LT8490 High Voltage, High Current Buck-Boost Battery Charge Controller with Maximum Power Point Tracking (MPPT)." *Linear Technology*. cds.linear.com/docs/en/datasheet/8490fa.pdf
[58] "15 Amp 12/24 Volts MPPT Charge Controller – Rev. G." *Solar Converters Inc*. www.solar-electric.com/lib/wind-sun/PT-12-24-15.pdf
[59] "BlueSolar Charge Controller MPPT 100/30 & 100/50." *Victron Energy*. www.victronenergy.com/upload/documents/Datasheet-BlueSolar-charge-controller-MPPT-100-30-&-100-50-EN.pdf
[60] "LTC4000-1 High Voltage High Current Controller for Battery Charging with Maximum Power Point Control." *Linear Technology*. cds.linear.com/docs/en/datasheet/40001fa.pdf
[61] "LT3845A High Voltage Synchronous Current Mode Step-Down Controller with Adjustable Operating Frequency." *Linear Technology*. cds.linear.com/docs/en/datasheet/3845afa.pdf
[62] "LTC3789 High Efficiency, Synchronous, 4-Switch Buck-Boost Controller." *Linear Technology*. cds.linear.com/docs/en/datasheet/3789fc.pdf

Table 15: Power Management Data Comparison – Discussed Characteristics

Type	Cost	Input Voltage	Input Current	Output Voltage	Output Current	Buck/ Boost	Batteries	Size	Casing
Flex Max MP80	High	145V	*	12V, 24V, 36V, 48V, 60V	up to 80A	Yes/*	12V, 24V, 36V, 48V, 60V	41.3 x 14.6 x 11.4cm	yes
LT8490	low	6-80V	up to 20A	1.3V-80V Battery	up to 20A	Yes/ yes	yes, flexible	0.7 x 0.11cm	no
PT 12/24 - 15	moderate	12V, 24V	up to 15A	12V, 24V	15A	Yes/ yes	12V, 24V	18 x 13 x 5cm	no
MPPT 100/30	moderate	up to 100V	up to 30A	12V, 24V	up to 30A	Yes/ yes	12V, 24V	13 x 18.6 x 7cm	Yes
LTC4000 - 1	Low	3V-60V	up to 20A	3V-60V	up to 20A	Yes/ yes	Flexible	0.4 x 0.5cm	no
LT3845A	low	4V-60V	up to 20A	up to 36V	up to 20A	Yes/*	N/A	*	no
LTC3789	low	4V-38V	up to 20A	0.8V-38V	up to 20A	Yes/ yes	N/A	0.4 x 0.5cm	no

*Indicates information was not included in datasheet

Cost

Cost is an important variable to consider. If this system were to be implemented in remote area communities, they may not be able to consider systems that are expensive. Low costs also mean more potential for higher profits for the designer and manufacturer.

The MP80 is the most expensive power management system being considered. It costs about $570 on Amazon[63]. The PT 12/24 – 15 and the MPPT 100/30 are about half of the price of the MP80. All of the Linear Technology IC chips are about $4-$6, however they require some more basic electrical components, and could be estimated to be about $30. In terms of cost, any of the Linear Technology IC chips are a good, low cost choice.

[63] "Outback Flexmax 80 FM80 MPPT 80 AMP Solar Charge Controller." *Amazon*. www.amazon.com/Outback-Flexmax-Solar-Charge-Controller/dp/B008MOITL8

Input and Output Voltage and Current
PV panels have a constantly changing voltage and current output based on the irradiance at that exact moment. During the day, there is generally a higher voltage and current being produced than is necessary, however, as the sun rises and sets there are generally lower amounts of voltage and current being produced. For this constantly changing input, it is necessary to have a power management system that has a wide range of voltage and current inputs that can cover all possible inputs. These inputs are dependent on the capability of the PV panels chosen. Some of the power management systems have only two outputs, 12V and 24V. While it is likely that the voltage needed will be 12V or 24V, if 36V were needed, these options would no longer be available.

The MP80 has a high input voltage of 145V and an output voltage and current range significantly higher than would likely be needed. The LT8490 is compatible with input and output voltages up to 80V and input and output currents up to 20A. The MPPT 100/30 has an input voltage range up to 100V, an output voltage range of 12V or 24V, and an input and output current limit of 30A. All of these specifications for both power management systems should meet the RO system's needs. The PT 12/24 – 15 has an input and output voltage range of 12V or 24V and an input and output current limit of 15A. These specifications exactly meet the current system demands, meaning this is not a great choice for a power management system as there is no room for system fluctuation. The LTC4000-1 if paired with the LT3845A has an input voltage up to 60V, an output voltage up to 36V, and input and output current limits of 20A. This would be sufficient for the RO system as well. If the LTC4000-1 were to be paired with the LTC3789, both the input and output voltages change to 38V. This would be less ideal, as the current PV panel setup can produce more than 38V. For this characteristic, the current system, the MP80, is the best choice because it has the highest input and output voltages and currents, allowing for several different PV panel and output configurations.

Step Down and Step Up Voltage (Buck/Boost Technology)
For the same reasons as stated in the previous section, it is important to have voltage step down (buck) and voltage step up (boost) technology in the power management systems. Buck is especially important since PV panels are generally selected at a higher power rating than is necessary to compensate for efficiency losses due to weather and other external conditions. Boost technology is also important for when there is a disrupt in power and the power being produced is less than what is required. In this case, the LT8490, PT 12/24 – 15, MPPT 100/30, and the LTC4000-1 paired with the LTC3789 are all good choices.

Battery Compatibility
Battery compatibility is important because as a community's needs change, the battery needs may change as well. It also makes it easier to choose a system that is compatible with several different outputs especially if the needed output is yet to be determined.

The MP80 is compatible with 12V, 24V, 36V, 48V, and 60V batteries. The PT 12/24 – 15 and the MPPT 100/30 are both compatible with 12V and 24V batteries. These two systems are only compatible with the system currently in place, or with a system that requires less voltage, which could become a problem if the RO system were to become larger. The LT8490 and the LTC4000-1, regardless of what other IC chip it is paired with, is flexible with the battery output

up to 80V and 60V, respectively. In this case, the MP80 is a good choice because it covers many of the standard battery voltages that may be used. The Linear Technology chips are also a good option because they have a large range of different battery voltages that are compatible, especially if there is not a standard battery voltage being used.

Size
Size can be important if the system may be moving frequently, as some small communities need to do, especially those that are not connected to the electric or water grid. This is also important if the system is being used in a place where having a large system would be inconvenient, such as a military ship. This could also make moving the system more difficult as larger size usually means more weight.

The MP80 is a large system, with its longest side being 41.3cm. This is fairly large and bulky, especially compared to other systems. The PT 12/24 – 15 and the MPPT 100/30 are both about half the size of the MP80 at their longest sides, measuring about 18cm. All of the Linear Technology IC chips measure under a centimeter, and with all the other components that would be necessary are still significantly smaller than the MP80. In this case, any of the Linear Technology IC chips would be ideal, specifically the LT8490 because it does not need a second chip.

Casing/Ease of Installation
Casing and ease of installation are important. Pre-assembled systems are easier to install and are ideal for some communities who may be limited on resources such as money, labor, and technical expertise. Casing is important as this system will be outside and weather protection is necessary.

The MP80 and the MPPT 100/30 both have cases and are ready to install. The PT 12/24 – 15 is ready to install except it needs a casing on the outside for protection. All of the Linear Technology IC chips need to be assembled on a circuit board with the appropriate components as shown in the datasheets, and also would then need to be made a protective casing. In this case, the MP80 and the MPPT 100/30 are the best choices.

7.4.2 Battery

The system is currently using four MegaLight Power 12V 190Ah Deep Cycle Zero Maintenance Absorbed Glass Mat (AGM) batteries[64]. These batteries are safe, low maintenance, and can still perform well when deep cycled. While these are all important characteristics of a battery, they are also very expensive and do not perform well in hot temperatures.

The other potential rechargeable batteries are lead acid, nickel cadmium (NiCd), nickel metal hydride (NiMH), and lithium ion (Li-ion)[65]. These are all commonly used rechargeable batteries for alternative energy systems. Table 16 below compares the most important characteristics of

[64] "12V 190Ah (C_{10}) Deep Cycle AGM Battery ML 220C." *Monbat*. www.monbat.com/en/pages/megalight.html
[65] "BU-107: Comparison Table of Secondary Batteries." *Battery University*. 11 April 2016. batteryuniversity.com/learn/article/secondary_batteries

batteries including operating temperature, self-discharge per month, cycle life, efficiency, maintenance, and overcharge tolerance.

Table 16: Battery Data Comparison – Discussed Characteristics

Type of Battery[66,67,68,69]	Operating Temp (C)	Self - Discharge per Month	Cycle Life (cycles)	Efficiency	Maintenance	Relative Overcharge Tolerance
Lead Acid (Deep Cycle)	-20 to 50	5%	200-300	90%	3-6 month topping charge	High
Nickel Cadmium	-20 to 65	20%	1000	70-90%	Fully discharge every 90 days	Moderate
Nickel Metal Hydride	-20 to 65	30%	300-500	70-90%	Fully discharge every 90 days	Low
Lithium Ion	-20 to 60	Less than 5%	500-2000	99%	None	Low
Absorbed Glass Mat (Dry Cell)	-20 to 49	<2.5% @20C	1000	99%	None	low

Operating Temperature

This system is currently being implemented in the desert, meaning that it can reach very high ambient temperatures upwards of 40°C in the summer. When the system is running and either charging or discharging the battery, this will increase the temperature of the battery, potentially up to 50°C or more. Most batteries will begin to lose efficiency around 40°C, with the optimal operating temperature being 25°C. Having a larger operating temperature range helps significantly, especially since there may not always be a cooling mechanism in place.

The AGM batteries have an upper temperature limit of about 40°C, which makes them not ideal for use in the desert. AGM batteries are known for performing well in very cold temperatures, however this is not applicable in this type of climate. Lead acid batteries have an upper limit of 50°C. NiCd and NiMH both have upper limits of 65°C and Li-ion has an upper limit of 60°C. These three batteries are the best choice for the system in terms of operating temperature because they have an upper limit larger than expected temperatures. It is not likely that the battery

[66] "BU-410: Charging at High and Low Temperatures." *Battery University*. 2 April 2016. batteryuniversity.com/learn/article/charging_at_high_and_low_temperatures

[67] Baroody, Ronald. "Evaluation of rapid electric battery charging techniques." *UNLV Theses, Dissertation, Professional Papers, and Capstones*. University of Nevada, Las Vegas. 2009. digitalscholarship.unlv.edu/cgi/viewcontent.cgi?article=1162&context=thesesdissertations

[68] "BU-201a: Absorbent Glass Mat (AGM)." *Battery University*. 12 July 2016. batteryuniversity.com/learn/article/absorbent_glass_mat_agm

[69] "Which one has a higher life cycle: Gel or AGM batteries?" Civic Solar. www.civicsolar.com/support/installer/questions/which-one-has-higher-life-cycle-gel-or-agm-batteries

temperature could reach 60°C, but if the battery were to reach this temperature, the NiCd, NiMH, and Li-ion batteries would have a significant decrease in efficiency. This temperature could cause permanent damage to the AGM batteries.

Self-Discharge per Month
Self-discharge per month is the amount that the battery would discharge each month if it were not in use. In the desert, there may be times during the summer where there is enough irradiance all day for several days or weeks that the batteries do not need to be used to run the system. In this case, it would be optimal for the batteries to contain their full charge for when they are needed. If the batteries are needed to run the system, this means that there was not enough sunlight and may not be able to charge the batteries if they have discharged significantly. This makes a low self-discharge rate an important characteristic.

The AGM batteries have a very low monthly self-discharge rate at <2.5%, but at a temperature of 20°C. If the temperature is higher than this, which is likely, it is not known how much this would affect the discharge rate. NiCd and NiMH both have very high monthly self-discharge rates of 20% and 30%, respectively. Lead acid has a rate of 5%, and Li-ion has a rate of less than 5%. This makes Li-ion and lead acid the best batteries for this system in terms of self-discharge rate, if the AGM batteries are not considered. It is not possible to completely evaluate this category without knowing how much the AGM batteries' self-discharge rate changes with temperature.

Cycle Life
Cycle life is the amount of times that the battery can be charged and discharged before the battery's capacity reaches below 80% of its original capacity. This is an important characteristic as batteries can be expensive and needing to replace them all of the time can become costly. For this system, the amount of times the battery is charged and discharged is heavily dependent on weather. During summer months in the desert when the batteries may not be needed, they may not be charged or discharged at all, but may be used almost constantly if there is a cloudy week.

AGM batteries have a cycle life of about 1000 cycles. Based on the data in the table, this is about an average cycle life for the options presented. Lead acid has a very low life cycle of 200-300 cycles, and NiMH has a life cycle of about 300-500 cycles. Both of these are fairly low and not the best selection based on this category. NiCd has a high life cycle of 1000 cycles, and Li-ion has a life cycle of 500-2000 cycles. In this case, AGM, Li-ion, and NiCd are the best choices. In order to decide between the three, it would be dependent on the specific battery selected. The capacity of the battery will determine how long the battery can power the system before needing to be charged, which will determine how many times it may be charged and discharged.

Efficiency
If the efficiency of the battery is low, the system is already not getting the most out of the batteries as it could. This means money is being wasted on energy that cannot be used or is being converted to heat. Efficiency also decreases as the battery heats, so having a high efficiency to begin with is important. All efficiencies are assumed in optimal operating temperatures of 25°C.

AGM batteries have a high efficiency of 99%, as well as Li-ion. Lead acid has an efficiency of 90%, and the NiCd and NiMH batteries have an efficiency of 70-90%. The NiCd and NiMH are

not recommended; in terms of battery efficiency, 70% is low. The AGM batteries that are being used currently in the system are a good option, as well as Li-ion. Knowing that batteries' efficiency decreases with heat, and knowing that AGM batteries do not have a high upper limit for operating temperature, Li-ion batteries are the best choice.

Maintenance
Many batteries need to be topped off if they are stored for a long period of time. Some batteries need to be stored at a certain charge, and some need to be discharged after being stored for a while. This becomes an issue with systems that would ideally be self-sufficient.

The AGM batteries require no maintenance, as well as the Li-ion batteries. The lead acid batteries need to be topped off every three to six months. Both the NiCd and NiMH batteries need to be fully discharged every 90 days. In this case, the AGM batteries are the best choice, comparable to the Li-ion batteries.

Overcharge Tolerance
Overcharging a battery can have a serious impact its performance. Although, the system is likely to have a charge controller, which are fairly inexpensive and easy to obtain and can mitigate this issue. However, overcharge is still a serious concern and can have a huge impact on the performance of the battery.
AGM batteries have a very low tolerance to overcharge, meaning that overcharging could seriously damage them, and a charge controller is necessary. This is also true for Li-ion and NiMH batteries. NiCd batteries have a moderate tolerance to overcharge, and a charge controller would still be recommended. Lead acid batteries have a very high tolerance to overcharge. While they may not suffer permanent damage, a charge controller should still be considered. They are also much cheaper than many batteries, which means that it is probably worth the investment instead of having to replace the batteries.

7.4.3 Novel Breaker System

One major component that was not included in the current system is a breaker system. A breaker system would disconnect the power from the pumps when the current being drawn by the pumps is at an unsafe level. A high current could be due to a clogged filter or obstruction in the system, which would wear down the pumps significantly and decrease their lifespan. A low current is not as damaging to the pumps, but could mean that a filter has broken. This would mean that particles that should not be passing through are making it to the clean drinking water. The novel system shown below in Figure 47 would protect against both of these issues. It has a breaker for when the current gets too high, and a current controlled relay for when the current gets too low.

The system works to protect the pumps in two ways. First, if the current is too high it will trip the current controlled breaker in series with the pumps to an open state, which will cause an open circuit and result in no power to the pumps. Second, two wires are put in the side of the pipe near the permeate output. The supply voltage is run through a small section of the water output stream, using the salinity level in the water as a variable conductor to measure the output quality. If the filter were to break, the salinity of the water would increase along with the conductivity. This would increase the current going across the two wires and also the current going across the

inductor. When the current reaches a certain value, it will be enough to create a magnetic field to pull the switch from the closed state to the open state. This would create an open circuit and therefore disconnect the power from the pumps.

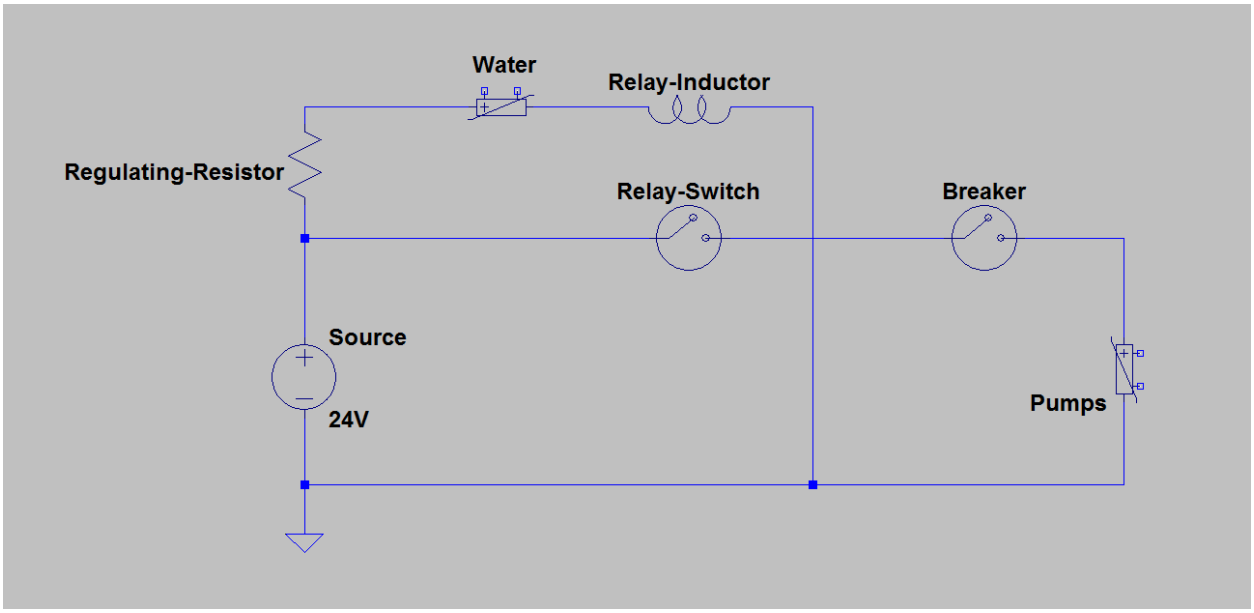

Figure 47: Novel Breaker System Schematic

In the diagram, the variable resistor labeled "Water" is representative of the varying resistance of the water. The inductor labeled "Relay-Inductor" and the switch labeled "Relay-Switch" are representative of the relay. The pumps are also represented as a variable resistor due to the changing current draw. According to Lenntech[70], the maximum conductivity allowed in drinking water is 0.05S/m. Using Equations 12, 13, and 14 below derived from Ohm's Law, it is possible to calculate the conductivity of the water that would trigger the relay and the distance needed between two wires.

$$R_{reg} = \frac{V_{source}}{I_{trig}} - \frac{1}{G_{water}} \quad [13]$$

$$G_{water} = g_{water} * L \quad [14]$$

$$g_{water} = conductivity\ per\ unit\ length\ [\frac{S}{m}] \quad [15]$$

The regulating resistor should be calculated using the supply voltage, trigger current, chosen water quality, and distance between the wires. For this chosen relay, an arbitrary value for the regulating resistor was chosen to be 1000Ω. Based on the trigger current of 7.5mA from the SSR Series Solid State Relay from Fotek[71] and the supply voltage of 24V from the current system, conductivity was calculated to be 0.4545mS. Using the maximum conductivity from Lenntech, the distance between the two wires was calculated to be 9mm long.

[70] "Water Conductivity." *Lenntech*, www.lenntech.com/applications/ultrapure/conductivity/water-conductivity.htm
[71] "SSR Series Solid State Relay." *Fotek*, cdn.sparkfun.com/datasheets/Components/General/SSR40DA.pdf

7.5 PV System

This section explores the parameters that characterize a PV panel and also discusses the effects of localized cooling.

Panel Configuration
There are several options for the PV panel for the PV/T RO system. The current panels being used for the system are the Millennium MSS – MIL – 250W – MO2 PV/T panels[72]. The benefit of this panel is that it has a thermal component already built in. For the purpose of this analysis, only the electrical specifications are being considered and the built-in cooling system is being disregarded. While the thermal cooling system is a benefit, the panel only has a 15.27% efficiency without it.

The other potential PV panels are the Suniva OPT275-60-4-100[73], the Astronergy 300W CHSM6612P[74], the Panasonic VBHN330SA16[75], and the Canadian Solar CS6K-275[76]. The table below compares the most important characteristics of PV panels including: rated power output, size, module efficiency, cost, and power temperature coefficient. These characteristics are compared in Table 17 below.

Table 17: PV Panel Data Comparison – Discussed Characteristics

Type	Power (W)	Voltage (Voc) (V)	Current (Isc) (A)	Front Facing Area (m^2)	Efficiency	Cost (USD)	Power Temperature Coefficient (%/°C)
Millennium (MSS - MIL - 250W - MO2)	250	37.6	8.17	1.584	15.27%	405	-0.37
Suniva (OPT275-60-4-100)	275	38.7	9.43	1.584	16.73%	300	-0.42
Astronergy (300W CHSM6612P)	300	45.16	8.91	1.881	15.5%	255	-0.408
Panasonic (VBHN330SA16)	330	69.7	6.07	1.760	19.07%	455	-0.3
Canadian Solar (CS6K-275)	275	38.3	9.31	1.683	16.8%	235	-0.41

[72] "Millennium Electric: MSS-MIL-PVT-250W-MO2 Data Sheet." *Millennium Solar*.
[73] "Suniva OPT285-60-4-100 Silver Mono Solar Panel." *Wholesale Solar*. www.wholesalesolar.com/1524436/suniva/solar-panels/suniva-opt285-60-4-100-silver-mono-solar-panel
[74] "Astronergy CHSM6612P-305 Solar Panel." *Wholesale Solar*. www.wholesalesolar.com/1977305/astronergy/solar-panels/astronergy-chsm6612p-305-solar-panel
[75] "Panasonic 325 watt Module 96 Cell HIT – Black Solar Panel." *Wholesale Solar*. www.wholesalesolar.com/1941900/panasonic/solar-panels/panasonic-325-watt-module-96-cell-hit-black-solar-panel
[76] "Canadian Solar CS6K-280M-T4 Black Frame White Backsheet Mono Solar Panel." *Wholesale Solar*. www.wholesalesolar.com/1930004/canadian-solar/solar-panels/canadian-solar-cs6k-280m-t4-black-frame-white-backsheet-mono-solar-panel

Rated Power Output
The rated power output is the most important characteristic of a PV panel. Depending on the size of the system, several panels may need to be used. It is recommended that a panel, or panel array, is chosen to have a higher output than is needed for the system. Even if a power management system that can boost voltage is in place, it is still recommended to have the total rated power of the PV system to be higher than needed. For this specification, the Panasonic panel would be the best choice.

Size
The size of the panel is important if the system may be moving frequently, as some small communities need to do. This could also become important if the system is being used in a place where having a large system would be inconvenient, such as a military ship. Larger size could also mean more weight, which would make moving the system more difficult. Additionally, PV panels need open space so that there is less chance of an obstruction, and this could mean taking up more space that may not be easily available. In this case, the Millennium panel or the Suniva panel is the best option.

Efficiency
Module efficiency is the percentage of electrical power that is produced when the panel is placed unobstructed in $1000W/m^2$ of sunlight. Most PV panels have efficiencies in the range of 15%-20%. The best panel is the Panasonic panel with an efficiency of 19.07%.

Cost
If this system were to be implemented in remote communities where they may not be connected to the electric or water grid, they may not be able to consider systems that are very expensive. Low costs also mean more potential for higher profits for the designer and manufacturer. At $235, the Canadian Solar panel is the best option.

Power Temperature Coefficient
The power temperature coefficient is the percent of the power output lost when the panel temperature increases. This is important, especially in hot climates where it is likely that ambient temperature will become higher than the optimal operating temperature. The smaller the power temperature coefficient, the less loss in power. In this case, the Panasonic panel is the best choice and would be least affected by an increase in temperature.

7.6 Integrated System Design

Each of the component systems were analyzed to provide suggestions for an optimized system for energy efficiency. For the RO membrane, the final recommendations suggest the use of a single extra low energy brackish water membrane model M-B2540AXLE from Applied Membranes Inc. This would be used in conjunction with pump scheme #2 which be $1/16^{th}$ the cost, use almost $1/3^{rd}$ less energy, and require 1/2 the input voltage compared to the current design. The specific energy consumption of clean water production would go from 6.67 kWh/m^3 under the current system, to 2.33 kWh/m^3 with the suggested system. This would be coupled with a thermal system made of copper with a working fluid of pure water which runs through an additional heat exchanger to warm the RO feedwater. The recommended panels would be the Canadian Solar panel which was under consideration. The Canadian Solar has the lowest cost and one of the highest Isc ratings. Two of these panels would cost only slightly more than one of the Panasonic panels, and would be suitable for both the 24V/15A and 12V/12A set ups. This would be used with Li-ion batteries due to the characteristics discussed in the previous section. Finally, for the power management system, the suggested system is a two output system using the LTC4000-1 and the LT3845A. The LTC4000-1 chip is using PowerPath technology to determine whether or not the power should be drawn from the PV panels directly or from the batteries. Combining these recommendations would be an effective method for designing a second iteration of the current system studied at the Arava and Dead Sea Science Center.

8 Conclusions

The purpose of this project was to analyze the current PV/T RO system and provide recommendations for improved energy efficiency. The RO experiments were conducted to study the effect of the feedwater temperature on membrane pressure and permeate quality and were deemed inconclusive. Data collection on PV panels demonstrated the correlation between the solar irradiance, to the power output and panel temperature. Additionally, the irradiance and temperature experiments confirmed that temperature gradients and shading on PV panels decrease electrical efficiency. Experiments using the novel PV/T system developed at the Arava and Dead Sea Science Center demonstrated that a 2°C increase in water temperature could be accomplished in 8.46 m of the conduit in the winter. Heat transfer calculations were completed to determine the temperature of the PV panel at any given irradiance and ambient temperature throughout a day using MATLAB. The panel temperature model additionally calculated the heat flux leaving the back of the PV panel for the same input parameters. The estimated heat transfer to the working fluid in the novel PV/T system was calculated in the fluid flow simulation using ANSYS-Fluent. Experiments were conducted in order to collect data to compare to these values. Specific suggestions were made for a more energy efficient PV/T RO system which produces permeate at a flow rate of 1L/min. Tables included in this analysis allow users determine the best components for their needs.

9 Works Cited

"12V 190Ah (C_{10}) Deep Cycle AGM Battery ML 220C." *Monbat*. www.monbat.com/en/pages/megalight.html

"12V Submersible Deep DC Solar Well Water Pump, Solar, battery, alternate energy", eBay, 23 Feb. 2017, www.ebay.com/itm/12V-Submersible-Deep-DC-Solar-Well-Water-Pump-Solar-battery-alternate-energy-/191776770021

"130PSI 6L/Min Water High Pressure Diaphragm Self Priming Pump DC12V 70W FL-3308", *eBay*, 23 Feb. 2017, www.ebay.com/itm/130PSI-6L-Min-Water-High-Pressure-Diaphragm-Self-Priming-Pump-DC12V-70W-FL-3308/131861277842?_trksid=p2047675.c100005.m1851&_trkparms=aid%3D222007%26algo%3DSIC.MBE%26ao%3D2%26asc%3D41395%26meid%3De013ff18c0564ae29d55952427780f53%26pid%3D100005%26rk%3D6%26rkt%3D6%26mehot%3Dpp%26sd%3D131556382165

"15 Amp 12/24 Volts MPPT Charge Controller – Rev. G." *Solar Converters Inc*. www.solar-electric.com/lib/wind-sun/PT-12-24-15.pdf

"About Reverse Osmosis Systems", *APS Water*, 23 Feb. 2017, www.apswater.com/article/39/About+Reverse+Osmosis+Systems

Alex Gusarov, e-mail message to authors, 18 January 2017.

"Astronergy CHSM6612P-305 Solar Panel." *Wholesale Solar*. www.wholesalesolar.com/1977305/astronergy/solar-panels/astronergy-chsm6612p-305-solar-panel

Baroody, Ronald. "Evaluation of rapid electric battery charging techniques." *UNLV Theses, Dissertation, Professional Papers, and Capstones*. University of Nevada, Las Vegas. 2009. digitalscholarship.unlv.edu/cgi/viewcontent.cgi?article=1162&context=thesesdissertations

"Basics of Reverse Osmosis." (n.d.). Retrieved February 23, 2017, from http://puretecwater.com/downloads/basics-of-reverse-osmosis.pdf

"BlueSolar Charge Controller MPPT 100/30 & 100/50." *Victron Energy*. www.victronenergy.com/upload/documents/Datasheet-BlueSolar-charge-controller-MPPT-100-30-&-100-50-EN.pdf

"Brackish Water (FRP Wrapped) Membranes." *Applied Membranes Inc.* Retrieved February 23, 2017, from http://www.appliedmembranes.com/brackish-water-frp-wrapped-membranes.html

"BU-107: Comparison Table of Secondary Batteries." *Battery University*. 11 April 2016. batteryuniversity.com/learn/article/secondary_batteries

"BU-201a: Absorbent Glass Mat (AGM)." *Battery University*. 12 July 2016. batteryuniversity.com/learn/article/absorbent_glass_mat_agm

"BU-410: Charging at High and Low Temperatures." *Battery University*. 2 April 2016. batteryuniversity.com/learn/article/charging_at_high_and_low_temperatures

“Canadian Solar CS6K-280M-T4 Black Frame White Backsheet Mono Solar Panel.” *Wholesale Solar*. www.wholesalesolar.com/1930004/canadian-solar/solar-panels/canadian-solar-cs6k-280m-t4-black-frame-white-backsheet-mono-solar-panel

"Centrifugal Pumps", *EngineeringToolbox*, 22 Feb. 2017, www.engineeringtoolbox.com/centrifugal-pumps-d_54.html

“Commercial/Industrial Thin Film Reverse Osmosis Membranes.” *Applied Membranes Inc.* Retrieved February 23, 2017, from http://www.appliedmembranes.com/commercial-industrial-thin-film-reverse-osmosis-membranes.html

Contreras, Alfredo S. B. "An energy recovery device for small-scale seawater reverse osmosis desalination" Loughborough University, 2009

Davis, J. R., and Inc Books24x7. Corrosion: Understanding the Basics. Materials Park, Ohio: ASM International, 2000. Web. 23 Feb. 2017.

"Desalination Products Catalog", *Energy Recovery Inc*., 22 Feb. 2017, http://www.energyrecovery.com/wp-content/uploads/2014/12/0916_ER_desalProducts_brochure_interactive_v3.pdf

"DOW FILMTEC™ Membranes DOW FILMTEC Seawater RO Elements for Marine Systems", *DOW*, 22 Feb. 2017, http://msdssearch.dow.com/PublishedLiteratureDOWCOM/dh_082d/0901b8038082d595.pdf?filepath=liquidseps/pdfs/noreg/609-00377.pdf&fromPage=GetDoc

"Estuaries", *National Oceanic and Atmospheric Administration*, 22 Feb 2017, http://oceanservice.noaa.gov/education/kits/estuaries/estuaries01_whatis.html

“Extra-Low Energy (XLE) RO Membranes.” *Applied Membranes Inc.* Retrieved February 23, 2017, from http://www.appliedmembranes.com/extra-low-energy-xle-ro-membranes.html

“Extra-Low Energy Brackish RO Membrane Elements.” *Applied Membranes Inc*. Retrieved February 23, 2017, from http://www.appliedmembranes.com/extra-low-energy-brackish-ro-membrane-elements.html

"Factors Affecting RO Membrane Performance", *Water Treatment Guide*, 23 Feb. 2017, www.watertreatmentguide.com/factors_affecting_membrane_performance.htm

"Flojet R8600344A Pump - 22.7 l/m", *Spraytech*, 23 Feb 2017, www.spraytech.uk.com/flojet-r8600344a-pump---227-lm-635-p.asp

F. P. Incropera, D. P. DeWitt, T. L. Bergman, and A. S. Lavine, “Fundamentals of Heat and Mass Transfer”, 6th ed. (Wiley, 2007).

"GT IRRI-GATOR Self-Priming Centrifugal Pumps - 60 HZ", Goulds Water Technology, 23 Feb. 2017, documentlibrary.xylemappliedwater.com/wp-content/blogs.dir/22/files/2012/07/BGT-R3.pdf

“Hydronautics Seawater SWC Series Membranes.” *Applied Membranes Inc.* Retrieved February 23, 2017, from www.appliedmembranes.com/hydranautics-seawater-swc-series-membranes.html

"InvestmentMine." *Metals Pricing*. N.p., 22 Feb. 2017. Web. 22 Feb. 2017. <http://www.infomine.com/investment/metal-prices/>.

Jones, A. D., and C. P. Underwood. "A thermal model for photovoltaic systems." *Solar energy* 70.4 (2001): 349-359.

Lachish, Uri "Optimizing the Efficiency of Reverse Osmosis Seawater Desalination" 22 Feb. 2017, http://urila.tripod.com/Seawater.htm

“LT3845A High Voltage Synchronous Current Mode Step-Down Controller with Adjustable Operating Frequency.” *Linear Technology*. cds.linear.com/docs/en/datasheet/3845afa.pdf

“LT8490 High Voltage, High Current Buck-Boost Battery Charge Controller with Maximum Power Point Tracking (MPPT).” *Linear Technology*. cds.linear.com/docs/en/datasheet/8490fa.pdf

“LTC3789 High Efficiency, Synchronous, 4-Switch Buck-Boost Controller.” *Linear Technology*. cds.linear.com/docs/en/datasheet/3789fc.pdf

“LTC4000-1 High Voltage High Current Controller for Battery Charging with Maximum Power Point Control.” *Linear Technology*. cds.linear.com/docs/en/datasheet/40001fa.pdf

"Low Thermal Expansion Materials Guide & Low Thermal Expansion Material Properties." *Top Seiko Co.Ltd*. N.p., n.d. Web. 21 Feb. 2017. <http://top-seiko.com/guide/low-thermal-expansion-materials/>.

“Millennium Electric: MSS-MIL-PVT-250W-MO2 Data Sheet.” *Millennium Solar*.

Miranda & Thomson, "Theory, Testing and Modelling of a Clark pump", 17 Sept. 2000, Centre for Renewable Energy Systems Technology, Angela Marmont Renewable Energy Laboratory, Loughborough University of Technology, Leicestershire, UK

“Module Circuit Design.” *PVEducation.org*. www.pveducation.org/pvcdrom/modules/module-circuit-design

Moharram, K.A. et al. “Enhancing the performance of photovoltaic panels by water cooling.” Ain Shams Engineering Journal. Vol 4. Issue 4. Pgs 869-877. Science Direct. December 2013. www.sciencedirect.com/science/article/pii/S2090447913000403

"Our Technology." *Spectra Watermakers*, 22 Feb. 2017. https://www.spectrawatermakers.com/us/us/explore/our-technology

“Outback Flexmax 80 FM80 MPPT 80 AMP Solar Charge Controller.” *Amazon*. www.amazon.com/Outback-Flexmax-Solar-Charge-Controller/dp/B008MOITL8

“Outback Power FLEXmax Series Charge Controllers (FLEXmax 80, FLEXmax 60) Owner’s Manual.” *Outback Power*. www.outbackpower.com/outback-products/make-the-power/flexmax-series-charge-controllers/item/flexmax-6080

“Panasonic 325 watt Module 96 Cell HIT – Black Solar Panel.” *Wholesale Solar*. www.wholesalesolar.com/1941900/panasonic/solar-panels/panasonic-325-watt-module-96-cell-hit-black-solar-panel

"Positive Displacement Pumps", *EngineeringToolbox*, 22 Feb. 2017, http://www.engineeringtoolbox.com/positive-displacement-pumps-d_414.html

“Pumps in Parallel or Serial”, *EngineeringToolbox*, 22 Feb. 2017, www.engineeringtoolbox.com/pumps-parallel-serial-d_636.html

"Pump Types Guide - Find the right pump for the job", *PumpScout*, 22. Feb 2017, www.pumpscout.com/articles-scout-guide/pump-types-guide-aid100.html

"Reverse Osmosis System Manual PROFILTER-SW-65", *Treatment CFS Ltd*, 23 Feb. 2017

Sathyanarayana P. et al. "Effect of Shading on the Performance of Solar PV Panel." *SDM Institute of Technology.* Scientific and Academic Publishing. 2015. article.sapub.org/10.5923.c.ep.201501.01.html#Ref

"SAVIOR Sunray SOLFLO-SIJ 2.4-900P-180 BT Brush Type Plunger Pump", *Amazon*, 23 Feb. 2017, www.amazon.com/SAVIOR-SOLFLO-SIJ-2-4-900P-180-BT-Plunger/dp/B0171EQTZ2

Schuss, Christian, et al. "Detecting Defects in Photovoltaic Cells and Panels and Evaluating the Impact on Output Performances." *IEEE Transactions on Instrumentation and Measurement* 65.5 (2016): 1108-1119.

"SIJ 2.4-900P-180 BT", *Sun Pumps Inc.*, 23 Feb. 2017, www.sunpumps.com/Products/SIJ%202.4-900P-180%20BT

"Solar Performance and Efficiency." *Energy.gov.* 20 August 2013. energy.gov/eere/energybasics/articles/solar-performance-and-efficiency

"Solar resource maps for Israel and Surrounding Regions." (n.d.). Retrieved February 23, 2017, from http://solargis.com/products/maps-and-gis-data/free/download/israel-and-surrounding-regions

"SSR Series Solid State Relay." *Fotek*, cdn.sparkfun.com/datasheets/Components/General/SSR40DA.pdf

"STP255-20/Wd, STP250-20/Wd, STP245-20/Wd" *Suntech Power* Feb 23, 2017, http://www.elektropartners.nl/local_resources/file/zonnepanelen/STP250.pdf

Subramanian, R. Shankar. "Heat transfer to or from a fluid flowing through a tube." web2. clarkson. edu/.../subramanian/.../Convective% 20Heat% 20Transfe r (2008).

"Suniva OPT285-60-4-100 Silver Mono Solar Panel." *Wholesale Solar*. www.wholesalesolar.com/1524436/suniva/solar-panels/suniva-opt285-60-4-100-silver-mono-solar-panel

"Sunpumps High Pressure Plunger Pump Model SIJ 2.4-900P-180 BT", *Sun Pumps*, 23 Feb. 2017, www.sunpumps.com/Photo/589?d=2/19/20175:17:15AM

"What is Reverse Osmosis?", *Puretec Industrial Water*, 23 Feb. 2017, puretecwater.com/reverse-osmosis/what-is-reverse-osmosis

"When to use a Positive Displacement Pump", *Pump School*, 23 Feb. 2017, www.pumpschool.com/intro/pd%20vs%20centrif.pdf

"Which one has a higher life cycle: Gel or AGM batteries?" Civic Solar. www.civicsolar.com/support/installer/questions/which-one-has-higher-life-cycle-gel-or-agm-batteries

"Thermal conductivity." *HyperPhysics*. N.p., n.d. Web. 22 Feb. 2017. http://hyperphysics.phy-astr.gsu.edu/hbase/Tables/thrcn.html.

Thomson, Murray, Marcos S. Miranda, and David Infield. "A small-scale seawater reverse-osmosis system with excellent energy efficiency over a wide operating range." *Desalination* 153.1-3 (2003): 229-236.

"Ultra Quiet Mini DC 12V Lift 5M 800L/H Brushless Motor Submersible Water Pump." *eBay*, 19 Feb. 2017, www.ebay.com/itm/Ultra-Quiet-Mini-DC-12V-Lift-5M-800L-H-Brushless-Motor-Submersible-Water-Pump-/121988963251

"Water Conductivity." *Lenntech*, www.lenntech.com/applications/ultrapure/conductivity/water-conductivity.htm

Yechieli, Y. (n.d.). "Evolution of brackish groundater in a typical arid region: Northern Arava Rift Valley, southern Israel." Retrieved February 23, 2017, from http://www.sciencedirect.com/science/article/pii/088329279290026Y

10 Appendices

Appendix A: Experimental Procedure for Effect of Temperature on RO Processes Experiment

Introduction:

The purpose of this protocol is to analyze the effects of temperature of the Reverse Osmosis (RO) process on the permeate. Temperatures of 15, 25, and 30 degrees C are independent variables being tested. Data was recorded on the feedwater flow rate, pressure, and temperature, permeate flow rate, brine flow rate, and the pressure difference between the pumps. The temperature of the water can affect the quality and amount of permeate alongside the lowering the osmotic pressure of the feedwater. It is important to see exactly how temperature affects each of these variables and its overall impact on the reverse osmosis process.

Equipment:

- Extension Cords
- System Data recorder
- Pump
- Thermocouples (3)
- 12 Input Thermocouple reader
- Computer
- Voltage Control System
- Salinometer
- Water heating/cooling device/system
- Water storage tanks
- Salt
- Water Heater
- Filters (3)
- Pressure Gague
- Flow rate sensors (4)
- Desalination system

Procedure:

1. Attach the extension cord to the power source in order to power the data recorder as well as the permeate pressure sensor.
2. Setup thermocouple reader. Attach the thermocouple wire from the system, then two additional thermocouples that will be placed into the water tank.
3. Check to make sure the connections with the reader are good (ie readings on both thermocouples in the tank match). Remove and reattach/jiggle around the connection until they are correct.
4. Check the temperature of the water, heat or cool to the corresponding temperature for the experiment.
5. Once the water has reached the proper temperature, place the intake hose, permeate hose, brine hose, and the air release hose into the salt water tank.

6. Set the output voltage of the system to 24V using the voltage control system.
7. Turn off the high pressure pump and open the valve of the air release hose. Turn on the system and run until the pump is making a steady, standard noise.
8. Close the air release hose valve and turn the high pressure pump back on. Adjust pressure to 55 psi using the valve located below the gauges. Listen to the clark pump for any odd noises.
9. Run the system for 30 minutes to normalize the permeate production.
10. Take a sample of the feedwater, permeate, and brine at the start of the test. Take again every ten minutes until 30 minutes have passed.
11. Heat or cool the samples to 20-25 degrees celsius and read their salt% (ppt) and millisiemens
12. At the same time samples are being taken, record data from the flowmeters on the front of the system alongside the current being used from the system as detailed on the voltage control system.
13. After the fourth set of data is recorded at the 30 minute mark, attach the laptop to the data recorder via ethernet cable and download data.

Information Outputs and Expected Results

Manual Measurements:

- Temperature: This is also taken at the beginning of the experiment. Temperature is important because it affects the efficiency of the system. Membranes perform better in warmer temperatures, but have a temperature limit of 40-45 degrees Celsius.
- Salinity: This is taken in the form of mass percentage in parts per thousand. This is important because the higher the salt content of the water, the higher its osmotic pressure is. In order for the RO system to work, pressure must be above the osmotic pressure.
- Voltage: Voltage is set at the beginning of the experiment to a constant value of 24V. The system requires 24V +/-10% (2.4V) to operate. The voltage controls the pumps of the system.
- Automatic Sensors and Analog Gauges:
- Feedwater flow rate: This is recorded as the water enters the system. It is necessary for efficiency calculations of the system when compared to the permeate flow rate. 1L/pulse
- Feedwater thermocouples (4): The first displays temperature of feedwater on the front of the system. It is important that this value was kept at 35 degrees. Recording this data allows us to pinpoint any inaccurate recordings if the temperature rises/falls at any time. The second records temperature at that same point in the system. The third and fourth both record the temperature in the feedwater tank.
- Pressure difference Sensor: This is measured at the RO membrane output of brine. This is important as pressure must be above a specific level dependent on the salinity of the water in order for the RO membrane to work.
- Permeate Flow rate (2): This is recorded as the permeate leaves the RO system to enter a storage tank, or in this case, returned to the saltwater tank to be mixed with the brine (1L/450 pulses).
- Brine flow rate gauge: This is taken after the brine exits the RO membrane before going through the Clark pump and shown on an analog gauge on the front of the system.

Example Tables

Time	Permeate (mL/min)	Feed (L/min)	Brine Pressure (mbar)	Voltage (mV)	Current High Pressure Pump (mA)	Current Feed Pump (mA)

	Feedwater				Permeate				Brine				Flow				Temperature	
Time	Vol (mL)	Temp (C)	mS	Salt % (ppt)	Vol (mL)	Temp (C)	mS	Salt% (ppt)	Vol (mL)	Temp (C)	mS	Salt % (ppt)	Permeate (L/min)	Concentrate (L/min)	Feed (L/min)	Pumps Pressure (psi)	System (C)	Thermo-couple (C)

Expected Results:
A ten percent recovery rate was expected, a 1:10 ratio of permeate to feedwater respectively. This proves that the system is in proper working order. Less brine pressure is also expected as membranes are more efficient at higher temperatures.

Appendix B: Experimental Procedure for Effect of PV Panel Coverage on Power Output Experiment

Introduction

This experiment tested the photovoltaic panels with and without partial panel coverage simulated by putting a towel on the panel. For all conditions, the power produced by the panel was measured to determine the electrical efficiency. To measure irradiance for each test performed, weather data was collected from the Arava Institute Weather Station.
The practical application for this system is obstructions that may limit the power output of the panel. There may be a cloud blocking the light or a person may walk by, both of which could momentarily reduce the power enough that it is too low for the RO system. This would not only shut down the system so it cannot produce potable water, but also may be damaging to the equipment. It is important to understand how much of an effect this may have, so that photovoltaic panels can be properly sized for an RO system to ensure sufficient power and protection of the equipment.

Equipment

- PV Panel
- Towel
- EKO MP-170 I-V Checker
- Arava Institute Weather Station

Procedure

1. Take a measurement with the I-V checker with the panel uncovered and record the time
2. Cover part of the panel with a towel and allow panel to adjust for 2 minutes
3. Repeat step 1 for each test
4. Record the ambient sunlight, air temperature, and wind speed from the Arava Institute Weather Station

Expected Results

Overall, the PV was expected to have a higher electrical efficiency when there is more sunlight and with less of the panel covered. Covering small parts of the panel will reduce the efficiency by a higher percentage than that of the panel which is covered. Cloud coverage will decrease the power output by at least half.

Appendix C: Experimental Procedure for Effect of Localized Cooling and Heating on PV Panel Power Output Experiment

Introduction

These experiments tested the photovoltaic (PV) panels when there was a temperature gradient due to localized heating or cooling. Two PV panels were used, one as a control panel and one as a test panel. To do this, ice packs and a space heater were used to simulate cold and hot spots on the test panel. For all conditions, the power output of the system and front face temperatures were taken as well as thermal images of the panels. Weather data was taken from the Arava Institute Weather Station. Weather data includes, but is not limited to, amount of ambient sunlight (irradiance), ambient air temperature, and wind speed.
These data are important to consider as they change irregularly and have a significant impact on the performance of the PVT system. To measure them for each test performed, the weather station available at Arava Institute was used. The amount of ambient sunlight is important because if there is not enough sunlight there may not be enough electrical power to drive the RO system. Ambient air temperature is very important to the performance of the PV panels as it has been proven that PV panels have a higher electrical efficiency when kept cool. Because this system will likely be used in the desert, the ambient air temperature in the summer may be high enough to have a significant impact on the PV panels. Wind speed can have two effects on the PV panels. First, wind can naturally cool the panels, which increases the electrical efficiency. Second, higher wind speeds can cause too much dust and debris to cover the panel and block sunlight.

Equipment

- 2 PV Panels
- Mastech MS6520A Infrared (IR) Thermometer
- UFPA Thermal Camera
- Ice packs
- Space Heater
- EKO MP-170 I-V Checker
- Arava Institute Weather Station

Procedure

1. Take a measurement with the I-V checker with the panel at current temperatures and record the time
2. Use the IR thermometer to measure the temperature of the panel on the front in several different places where the ice packs and space heater and the thermal camera to take a thermal photo of the panel
3. Add ice packs or a space heater to the back of the panel and allow temperature of panel to adjust for 15 minutes
4. Repeat steps 1 and 2 for each different test with ice packs, space heater, or both.
5. Remove ice packs or space heater and allow panel to return to normal temperature for 15 minutes
6. Repeat steps 1 and 2 before performing a different test
7. Record the ambient sunlight, air temperature, and wind speed from the Arava Institute Weather Station

Expected Results

Overall, the PV panels were expected to have a higher electrical efficiency with the cooling system in place, and a higher thermal efficiency when the cooling system is not in place. In terms of cooling system configurations, localized cooling was expected to not be as effective in cooling the panels since some of the cells would still be hotter and lower the electrical efficiency. It was expected using the space heater will have a similar effect as covering the panels, as overheating them will cause them to act as an open circuit. Higher air temperature will decrease the electrical efficiency, but increase the thermal efficiency. Depending on how high the wind speed and the direction, it could either increase or decrease the electrical or thermal efficiency. It may cool the panel and increase electrical efficiency, but if too much dust is blown onto the panel it may block sunlight, and it is not clear how much that will affect the panel's performance.

Appendix D: Experimental Procedure for PV/T Experiment

Introduction:

The purpose of this experiment is to find both the amount of heat gained by the working fluid in a PV/T system as well as the effect of cooling PV panels on electrical output. Three different solar panels will be studied. A standard photovoltaic panel acts as the control and the remaining two panels have thermal cooling systems. One PV/T is a commercially available product manufactured by Millennium Solar while the other is an experimental panel designed at the Arava and Dead Sea Science Center.

The primary interest in this experiment is to find how much heat is able to be transferred from the PV panel to the working fluid. Additionally, this experiment has the potential to show the detrimental effect of temperature increases on the electrical output of PV panels. Finally, the experiment will serve as a potential validation method for the team's existing simulations. The team is also interested in seeing the potential temperature gradient along the front of the panel due to the different cooling systems.

Equipment:

- PV Panels (3)
- Standard PV
- Millennium PV/T
- Novel PV/T
- MRC WB - 100 Cooling Baths (2)
- T - Type Thermocouples (4)
- Thermal Camera
- SolarEdge PV Power Output Monitoring System
- Laser Temperature Gauge

Procedure:

1. Using a known sized container, find the flowrate of the two cooling baths by timing how long it takes to fill the container. Repeat this and average the results.
2. Hook up the three panels to the monitoring system.
3. Attach a thermocouple at the inlet and outlet of each cooling bath to monitor water temperature
4. Attach the cooling baths to the two thermal systems.
5. Using a known sized container, find the flowrate coming out of the two thermal systems by timing how long it takes to fill the container. Repeat this and average the results.
6. Setup a datalogger to collect temperatures from the thermocouples every 30 seconds for the duration of the experiment
7. Take a thermal image of each of the three panels as a base value
8. Turn on the cooling baths, continue to take thermal images every 10 minutes.
9. Take temperature readings with the IR thermometer every 10 minutes, offset by 5 minutes from the times where thermal images are taken.
10. Continue to take readings for a total of 2 hours of operation.

Independent Variables:

- PV Type

- Standard, Millennium, and Experimental
- Flow Rate
- The two baths have different flowrates
- Irradiation
- Cooling bath output temperature

Dependent Variables:

- Temperature of the panel
- Electrical output
- Cooling bath input temperature

Expected Results:

This experiment was expected to show that the experimental panel is the most efficient in electricity generation of the three due to its thermal system. There are more pipes along the back of the panel with a larger contact area with the back of the panel. Because of this, it was also expected the experimental panel to put out water at a higher temperature than the Millennium panel.

Appendix E: Panel Temperature Model MATLAB Program Code

WPI ISRAEL MQP C-2017

author: Jonathan Friedman jsfriedman@wpi.edu

```
clear;
```

file input operations

```
[file,path] = uigetfile('*.*','Select the weather data file'); %selecting first file

if (file ~= 0) %checking for null pointer
    filename = sprintf('%s%s', path, file); %assigns file and path if input is not null
else
    disp('Error, no file selected'); %if input is null, displays error message
    return
end

[num,txt,raw] = xlsread(filename); % load Excel sheet
fclose('all');
```

console inputs

```
date_str = input('Input the date in the form of MM/DD/YYYY: ','s');
time_str = input('Input the start time in the form of H:MM ','s');
ampm_str = input('AM or PM ','s');
timedate_str = [date_str,' ', time_str, ':00 ', ampm_str];
time_length = input('How many hours do you want to calculate for? '); %multiply the number of
hours by 10 to find the number of time intervals to calculate, weather station data is every 10
minutes
interval_num = time_length * 6; % 6 intervals per hour, gives the total number of data readings
from the weather station
generate = input('Would you like to export the calculated data to a csv? (y/n) ','s');
```

list building

Pre-allocating the storage arrays for the data to be pulled from excel or to be calculated

```
rad_list = zeros(interval_num,1);
ambient_list = zeros(interval_num,1);
flux_results = zeros(interval_num,1);

% find the starting row in the excel file for the given date
for j=1:size(txt,1)
    if isequal( txt(j,1), cellstr(timedate_str))
        index = j;
        break;
    end
end

% build the rad_list & ambient_list & from num
for k=1:interval_num
```

```
    rad_list(k,1) = num(index+(k-1),7); % radiation is column 7
    ambient_list(k,1) = num(index+(k-1),5) + 273; % converting from Celcius to Kelvin,
tempterature is column 5
end

% time in seconds
t = 1:1:time_length*3600;

% takes the panel temperature as an initial guess
T_module_initial = ambient_list(1,1);
Overall_Results = [];
```

main loop

```
for n = 1:interval_num
    T_module = TempSolver(T_module_initial,rad_list(n,1),ambient_list(n,1)); % Calls TempSolver
to solve for 10 minutes worth of panel temperatures
    flux_results(n,1) = real(FluxSolver(T_module_initial, rad_list(n,1),ambient_list(n,1))); %
Calls FluxSolver to solve for the heatflux at that point in time
    Overall_Results = [Overall_Results T_module]; % appends newest values to overall running list
    T_module_initial = T_module(end); % sets the next input temperature to the last calculated
temperature
end


Overall_Results = real(Overall_Results);
hourly_averages = zeros(time_length,1);
for q=1:time_length
    location = (q-1)*3600;
    if q == 1
        location = 1;
    end
    hourly_averages(q,1) = mean(Overall_Results(location:location+3600));
end
```

graphing

```
yyaxis left
plot(t,Overall_Results,'black');
ylabel('Temperature (K)');
hold on
yyaxis right
plot([1:(size(t,2)/interval_num):size(t,2)],rad_list,'r--');
%plot([1:(size(t,2)/interval_num):size(t,2)],flux_results,'blue');
%uncomment this line if you would like to plot just the heat flux
ylabel('Solar Irradiance (W/m^2)');
xlabel('Time Elapsed (hours)');
ax = gca;
ax.XTick = [0:3600:time_length*3600]; % make a linspace based on starting and ending times
ax.XTickLabel =
({'0','1','2','3','4','5','6','7','8','9','10','11','12','13','14','15','16','17','18','19','20',
'21','22','23','24'});
```

```
ax.YAxis(1).Color = 'black';
ax.YAxis(2).Color = 'red';
title('Solar Cell Module Temperature and Solar Irradiance vs. Time','FontSize',12);
grid on
```

file writing

```
if strcmp(generate, 'y')
    file_str = input('What do you want to name the file? ','s');
    csvwrite([file_str,'.csv'],Overall_Results');
    csvwrite([file_str,'_hourly_averages','.csv'],hourly_averages);
end
```

Published with MATLAB® R2016a

TempSolver.m

```
function [T_module] = TempSolver(T_mod_initial, phi, T_amb)
%%Layers
        %%glass = Glass
        %%arc = ARC
        %%pv = PV Cells
        %%eva = EVA
        %%rear = Rear Contact
        %%ted = Tedlar

A = 1.44; % m^2
e_sky = 0.95; % value for a clear day
e_module = 0.9; % value for clear day
deltaT = 20; % standard value for a clear day
solar_efficiency = 0.1527; %Found experimentally
E = phi*solar_efficiency;
k1 = 10^6; % constant

%%Absortivity
alpha = 0.7; %%Reference RPI Paper

%%Stefan Boltzmann Constant (W/m2K4(C4))
sigma = 5.67e-8;

%%Forced Convective Heat Transfer Coefficient (W/m2K(C))

h_c_forced = 5.5; % experimentally determined

%%Fill Factor Model Constant (Km2)
C_FF = 1.22;

%%Thicc-ness (m)
Tglass = 0.003;
Tarc = 100e-9;
Tpv = 225e-6;
Teva = 500e-6;
Trear = 10e-6;
Tted = 0.0001;

%%Density (kg/m3)
Dglass = 3000;
Darc = 2400;
Dpv = 2330;
Deva = 960;
Drear = 2700;
Dted = 1200;

%%Specific Heat Capacity (J/kgC)
SHCglass = 500;
SHCarc = 691;
SHCpv = 677;
SHCeva = 2090;
```

```
SHCrear = 900;
SHCted = 1250;

%%Calculate Heat Capacity per layer (J/C)
%%Glass
Cglass = A*Tglass*Dglass*SHCglass;
%%ARC
Carc = A*Tarc*Darc*SHCarc;
%%PV Cells
Cpv = A*Tpv*Dpv*SHCpv;
%%EVA
Ceva = A*Teva*Deva*SHCeva;
%%Rear Contact
Crear = A*Trear*Drear*SHCrear;
%%Tedlar
Cted = A*Tted*Dted*SHCted;

%%Total Heat Capacity (J/C)
C_module = Cglass+Carc+Cpv+Ceva+Crear+Cted;

t = 1:1:600; % seconds for 10 minutes
y0 = T_mod_initial; % initial value for solar panel temp (K)
[t,y] = ode45(@rhs, t, y0);
T_module = y';

    function dydt = rhs(t,y)
        dydt = (sigma*A*(e_sky*(T_amb - deltaT)^4 - e_module*y^4)+ alpha*phi*A -
((C_FF*E*log(k1*E))/y) - (h_c_forced + (1.31*(y - T_amb)^(1/3)))*A*(y - T_amb))/C_module;
    end

end
```

Published with MATLAB® R2016a

FluxSolver.m

```
function [heat_flux] = FluxSolver(T, phi, T_amb)
%%Layers
        %%glass = Glass
        %%arc = ARC
        %%pv = PV Cells
        %%eva = EVA
        %%rear = Rear Contact
        %%ted = Tedlar




A = 1.44; % m^2
e_sky = 0.95; % value for a clear day
e_module = 0.9; % value for clear day
deltaT = 20; % standard value for a clear day
solar_efficiency = 0.18; %Found experimentally
E = phi*solar_efficiency;
k1 = 10^6; % constant

%%Absortivity
alpha = 0.7; %%Reference RPI Paper

%%Stefan Boltzmann Constant (W/m2K4(C4))
sigma = 5.67e-8;

h_c_forced = 5.5;

%%Fill Factor Model Constant (Km2)
C_FF = 1.22;

%%Thicc-ness (m)
Tglass = 0.003;
Tarc = 100e-9;
Tpv = 225e-6;
Teva = 500e-6;
Trear = 10e-6;
Tted = 0.0001;

thicc = Tglass + Tarc + Tpv + Teva + Trear + Tted;
%%Thermal Conductivity (W/mK)
TCglass = 1.8;
TCarc = 32;
TCpv = 148;
TCeva = 0.35;
TCrear = 237;
TCted = 0.2;

K_panel =(TCglass^-1 + TCarc-1 + TCpv^-1 + TCeva^-1 + TCrear-1 + TCted^-1)^-1;

%%Density (kg/m3)
```

```
Dglass = 3000;
Darc = 2400;
Dpv = 2330;
Deva = 960;
Drear = 2700;
Dted = 1200;

%%Specific Heat Capacity (J/kgC)
SHCglass = 500;
SHCarc = 691;
SHCpv = 677;
SHCeva = 2090;
SHCrear = 900;
SHCted = 1250;

%%Calculate Heat Capacity per layer (J/C)
%%Glass
Cglass = A*Tglass*Dglass*SHCglass;
%%ARC
Carc = A*Tarc*Darc*SHCarc;
%%PV Cells
Cpv = A*Tpv*Dpv*SHCpv;
%%EVA
Ceva = A*Teva*Deva*SHCeva;
%%Rear Contact
Crear = A*Trear*Drear*SHCrear;
%%Tedlar
Cted = A*Tted*Dted*SHCted;

%%Total Heat Capacity (J/C)
C_module = Cglass+Carc+Cpv+Ceva+Crear+Cted;
heat_flux = K_panel*(T-T_amb)/(thicc/2); % simple conduction through the panel
```

Published with MATLAB® R2016a

Appendix F: Data Collection from Effect of Temperature on RO Processes Experiment

Table 18: All Data Collected from the Microcontroller for the Duration of the Effect of Temperature on RO Processes Experiment

Time	Permeate (mL/min)	Feed (L/min)	Brine Pressure (mbar)	Voltage (mV)	Current High Pressure Pump (mA)	Current Feed Pump (mA)	Feedwater Pressure (bar)	Power (W)
10:05	1000	9	26923	5	11498	7483	26.923	455.544
10:06	1000	10	26663	5	11164	7480	26.663	447.456
10:07	993	10	26442	4	11001	7484	26.442	443.64
10:08	1000	10	26294	4	11251	7460	26.294	449.064
10:09	993	10	26329	4	11560	7489	26.329	457.176
10:10	1000	10	26585	4	11507	7443	26.585	454.8
10:11	1000	9	26751	4	11139	7450	26.751	446.136
10:12	1000	10	26544	4	11023	7463	26.544	443.664
10:13	993	10	26369	4	11041	7483	26.369	444.576
10:14	1000	10	26387	4	11190	7458	26.387	447.552
10:15	1000	10	26613	4	11526	7463	26.613	455.736
10:16	993	9	26612	4	11549	7456	26.612	456.12
10:17	1000	10	26256	5	11439	7454	26.256	453.432
10:18	993	10	26086	4	11108	7441	26.086	445.176
10:19	1000	10	26119	4	11070	7443	26.119	444.312
10:20	993	10	25643	4	11048	7362	25.643	441.84
10:21	1000	9	25933	4	11633	7483	25.933	458.784
10:22	993	10	26373	4	11633	7476	26.373	458.616
10:23	1000	10	26226	4	11619	7450	26.226	457.656
10:24	1000	10	26337	5	11436	7483	26.337	454.056
10:25	1000	10	26275	5	11107	7484	26.275	446.184
10:26	1000	10	26245	5	11055	7484	26.245	444.936
10:27	993	9	26091	5	11084	7487	26.091	445.704
10:28	993	10	26145	5	11412	7498	26.145	453.84
10:29	1000	10	26172	5	11582	7498	26.172	457.92
10:30	993	10	26148	4	11636	7451	26.148	458.088
10:31	993	10	26221	4	11141	7450	26.221	446.184
10:32	993	10	25894	4	11085	7471	25.894	445.344
10:33	993	9	26037	5	11143	7474	26.037	446.808
10:34	1000	10	25925	4	11598	7467	25.925	457.56
10:35	1000	10	26111	4	11567	7505	26.111	457.728
11:55	1000	10	21021	3	10904	7181	21.021	434.04
11:56	1000	9	21238	4	11014	7166	21.238	436.32

11:57	986	10	21168	4	11437	7166	21.168	446.472
11:58	993	10	21324	4	10995	7163	21.324	435.792
11:59	986	10	21262	3	10989	7170	21.262	435.816
12:00	993	10	21094	4	10979	7212	21.094	436.584
12:01	993	9	20924	4	11383	7205	20.924	446.112
12:02	993	10	21054	3	11654	7201	21.054	452.52
12:03	993	10	21240	3	11427	7163	21.24	446.16
12:04	986	10	21216	3	10980	7131	21.216	434.664
12:05	993	10	20983	3	10971	7172	20.983	435.432
12:06	1000	9	21063	3	11176	7170	21.063	440.304
12:07	986	10	21238	3	11656	7188	21.238	452.256
12:08	993	10	21300	3	11727	7194	21.3	454.104
12:09	993	10	21221	4	11613	7179	21.221	451.008
12:10	993	10	21032	4	11103	7205	21.032	439.392
12:11	993	9	21019	4	11073	7225	21.019	439.152
12:12	993	10	21212	4	11065	7244	21.212	439.416
12:13	993	10	21359	4	11121	7236	21.359	440.568
12:14	993	10	21080	4	11661	7243	21.08	453.696
12:15	993	10	20983	4	11689	7205	20.983	453.456
12:16	993	9	21186	4	11719	7183	21.186	453.648
12:17	993	10	21237	4	11154	7216	21.237	440.88
12:18	993	10	21114	4	11096	7214	21.114	439.44
12:19	993	10	20925	4	11059	7194	20.925	438.072
12:20	993	9	20846	3	11080	7188	20.846	438.432
12:21	993	10	21091	3	11527	7214	21.091	449.784
12:22	1000	10	21178	4	11632	7198	21.178	451.92
12:23	1000	10	20901	4	11654	7140	20.901	451.056
12:24	993	10	20942	4	11736	7170	20.942	453.744
12:25	1000	9	21148	3	11317	7127	21.148	442.656
13:35	993	10	17760	2	10997	6838	17.76	428.04
13:36	993	10	17594	2	10970	6834	17.594	427.296
13:37	993	9	17750	2	11081	6834	17.75	429.96
13:38	993	10	17709	2	11598	6847	17.709	442.68
13:39	993	10	17610	2	11575	6794	17.61	440.856
13:40	993	10	17600	2	11219	6803	17.6	432.528
13:41	993	10	17606	2	10965	6776	17.606	425.784
13:42	993	10	17623	2	11001	6786	17.623	426.888
13:43	993	9	17509	2	11240	6751	17.509	431.784
13:44	993	10	17636	2	11611	6808	17.636	442.056

13:45	993	10	17448	2	11449	6799	17.448	437.952
13:46	986	10	17711	2	11034	6808	17.711	428.208
13:47	993	10	17579	2	11033	6803	17.579	428.064
13:48	993	10	17723	2	11003	6799	17.723	427.248
13:49	993	9	17634	2	11435	6799	17.634	437.616
13:50	993	10	17665	2	11729	6803	17.665	444.768
13:51	993	10	17516	2	11563	6764	17.516	439.848
13:52	993	10	17722	2	11062	6816	17.722	429.072
13:53	993	10	17650	2	10999	6760	17.65	426.216
13:54	1000	10	17700	2	11049	6755	17.7	427.296
13:55	986	10	17784	2	11552	6794	17.784	440.304
13:56	993	9	17683	2	11650	6799	17.683	442.776
13:57	993	10	17775	2	11232	6781	17.775	432.312
13:58	993	10	17665	2	10998	6825	17.665	427.752
13:59	993	10	17768	2	11020	6777	17.768	427.128
14:00	1000	10	17724	2	11280	6790	17.724	433.68
14:01	993	10	17767	2	11785	6816	17.767	446.424
14:02	993	9	17797	3	11651	6816	17.797	443.208
14:03	993	10	17709	3	11414	6848	17.709	438.288
14:04	993	10	17690	2	10978	6821	17.69	427.176
14:05	993	10	17757	2	10993	6838	17.757	427.944

Appendix G: Data Collection from Effect of PV Panel Coverage on Power Output Experiment

Table 19: Effect of PV Panel Coverage on Power Output Experiment Data

Test #	Time	Covering	Voc (V)	Isc (A)	Pm (W)	Vpm (V)	Ipm (A)	Efficiency (%)	Avg Rad (W/m^2)	Pin (W)	Efficiency (Calc) (%)
1	10:44	none (full sun)	20.56	9.99	117.85	15.01	7.85	11.78	692.7	620.56	18.99
2	10:51	top half	17.97	0.08	1.01	15.76	0.06	0.10	748.7	670.73	0.15
3	10:54	bottom half	18.06	0.08	1.07	16.23	0.07	0.11	748.7	670.73	0.16
4	10:58	left half	18.16	0.07	1.29	10.84	0.07	0.13	853.0	764.17	0.17
5	11:09	left column	18.71	0.01	0.21	10.65	0.01	0.02	934.0	836.73	0.025
6	11:11	top row	19.56	0.09	1.28	17.73	0.07	0.13	934.0	836.73	0.15
7	11:15	bottom left corner	20.00	1.45	28.98	7.53	1.45	2.90	696.0	623.52	4.65
8	11:19	bottom half, top left corner	18.06	0.06	0.85	16.35	0.05	0.09	696.0	623.52	0.14
9	11:24	top left corner	20.44	3.26	30.91	7.27	3.26	3.09	696.0	623.52	4.96
10	11:25	none (full sun)	20.44	11.47	128.78	15.11	8.52	12.88	554.6	496.84	25.92
11	11:27	non (cloudy)	20.00	4.00	58.20	15.67	3.71	5.82	554.6	496.84	11.71

Figure 48: Appendix G – Top Half

Figure 49: Appendix G – Bottom Half

Figure 50: Appendix G - Left Half

Figure 51: Appendix G - Left Column

Figure 52: Appendix G - Top Row

Figure 53: Appendix G – Bottom Corner

Figure 54: Appendix G – Bottom Half, Top Corner

Figure 55: Appendix G – Top Corner

Appendix H: Thermal Images from Effect of Localized Cooling and Heating on PV Panel Power Output Experiment

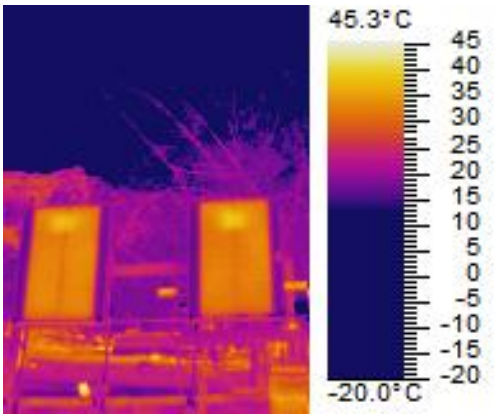

Figure 56: Appendix H – Both Panels Unchanged

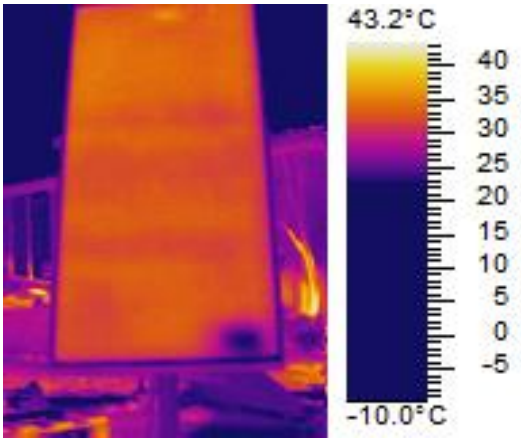

Figure 57: Appendix H – Bottom Corner Only Cooled

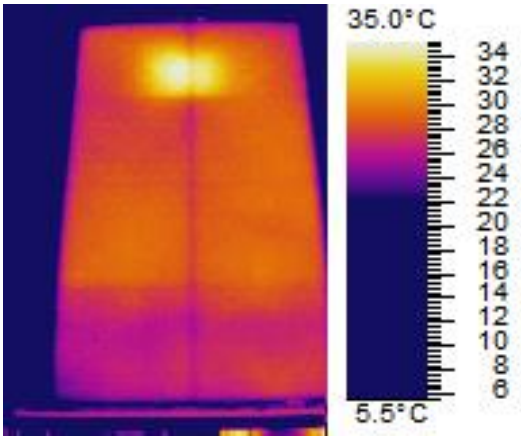

Figure 58: Appendix H – Bottom Row Only Cooled with Ice Packs

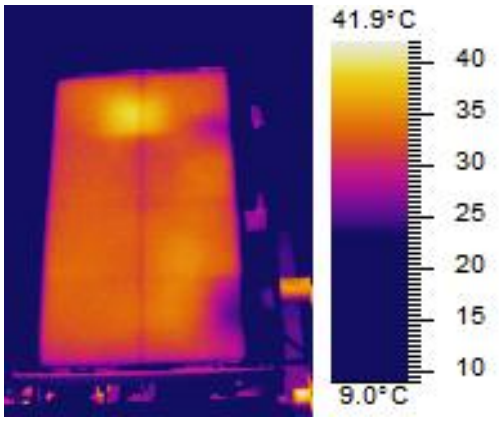

Figure 59: Appendix H – Side of Panel Cooled Only

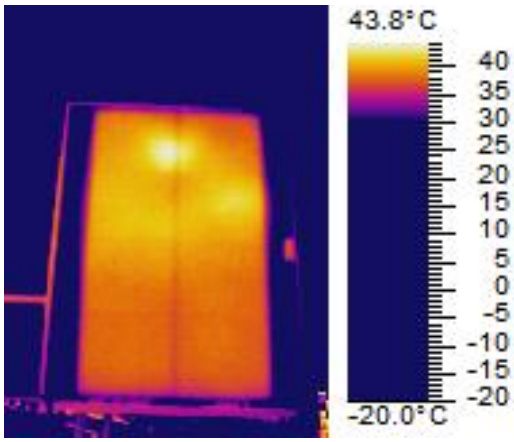

Figure 60: Appendix H – Top Half of Panel Heated

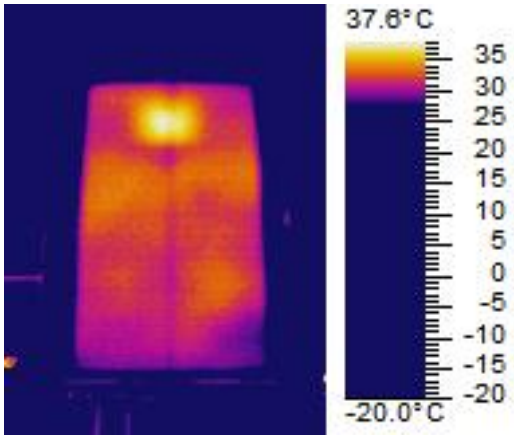

Figure 61: Appendix H – Top Half of Panel Heated and Bottom Row Cooled

Appendix I: Data collection from Effect of Localized Cooling and Heating on PV Panel Power Output Experiment

Table 20: Effect of Localized Cooling and Heating on PV Panel Power Output Experiment Data

Test #	Panel	Time	Heat/ Cool	Config	Voc (V)	Isc (A)	Pm (W)	Vpm (V)	Ipm (A)	Efficiency (Meas) (%)	Panel Temp.	Avg Rad (W/m2)	Air Temp. (C)	Wind Speed (m/s)	Pin (W)	Efficiency (Calc) (%)
45	left	9:23	none	none	4.68	13.89	12.03	3.64	3.31	1.20	32.9	623.8	18.33	3.632	125.56	9.5800
46	right	9:24	none	none	4.69	14.48	12.28	3.66	3.36	1.23	32.8	623.8	18.33	3.632	124.38	9.8700
47	left	9:53	none	none	4.65	17.15	14.21	3.69	3.85	1.42	JB - 33.0 M - 30.0 B - 33.3	707.9	19.48	3.152	142.49	9.9700
48	right	9:54	cool	bottom right	4.66	16.76	5.16	4.51	1.14	0.52	JB - 39.3 M - 33.7 B - 28.5	707.9	19.48	3.152	141.15	3.6600
50	left	10:14	none	none	4.59	29.97	5.75	4.40	1.31	0.58	JB - 43.5 M - 41.0 B - 41.0	759.7	19.59	2.104	152.92	3.7600
51	right	10:15	none	none	4.60	7.58	6.02	4.44	1.36	0.60	JB - 44.4 M - 40.4 B - 40.4	759.7	19.59	2.104	151.47	3.9700
52	left	10:36	none	none	4.61	19.06	6.39	4.26	1.50	0.64	JB - 44.0 M - 42.1 B - 41.9	820.0	20.59	4.061	165.06	3.8700
53	right	10:38	cool	bottom row	4.62	19.38	15.97	3.65	4.38	1.60	JB - 44.4 M - 41.1 B - 39.1	820.0	20.59	4.061	163.50	9.7700
56	left	11:07	none	none	4.56	10.19	4.70	4.45	1.06	0.47	JB - 46.7 M - 43.3 B - 43.3	863.0	21.81	3.707	173.71	2.7100

57	right	11:09	none	none	4.58	7.68	3.44	4.54	0.76	0.34	JB - 46.0 M - 44.5 B - 43.9	863.0	21.81	3.707	172.08	2.0000
58	left	11:30	none	none	4.55	7.97	5.26	4.37	1.20	0.53	JB - 48.5 M - 45.6 R - 43.7	878.0	22.5	3.584	176.73	2.9800
59	right	11:32	cool	right side	4.58	21.57	4.83	4.49	1.08	0.48	JB - 46.1 M - 42.3 R - 40.6	878.0	22.5	3.584	175.07	2.7600
61	left	13:20	none	none	4.51	19.29	4.30	4.41	0.98	0.43	JB - 48.5 M - 45.4 B - 45.4	793.8	24.5	3.369	159.78	2.6900
63	right	13:23	none	none	4.55	16.60	4.80	4.45	1.08	0.48	JB - 48.8 M - 45.7 B - 44.1	793.8	24.5	3.369	158.28	3.0300
64	left	13:43	none	none	4.52	1.54	3.86	4.43	0.87	0.39	JB - 51.2 T - 46.1 B - 46.9	747.2	24.23	3.735	150.40	2.5700
68	right	13:48	heat	top half	4.45	0.89	3.43	4.41	0.78	0.34	JB - 52.2 T - 47.6 B - 46.2	737.0	24.14	0.885	146.95	2.3300
69	left	14:05	none	none	4.55	1.29	4.64	4.42	1.05	0.46	JB - 45.9 M - 44.5 B - 42.9	690.9	24.26	2.115	139.07	3.3400
72	right	14:07	none	none	4.57	1.11	5.09	4.44	1.11	0.51	JB - 48.9 M - 44.3 B - 42.2	690.9	24.26	2.115	137.76	3.6900
73	left	14:30	none	none	4.52	5.07	6.10	4.21	1.47	0.62	JB - 48.2 M - 42.7 B - 42.7	632.0	24.32	0.322	127.21	4.8000

74	right	14:31	both	top half heat, bottom row cool	4.52	5.90	3.11	4.48	0.69	0.31	JB - 48.6 M - 46.3 B - 42.1	632.0	24.32	0.322	126.01	2.4700
75	left	14:50	none	none	4.55	21.76	4.51	4.41	1.02	0.45	JB - 43.7 M - 41.4 B - 40.4	571.6	24.24	0.281	115.06	3.9200
76	right	14:52	none	none	4.57	1.68	3.63	4.47	0.81	0.36	JB - 46.4 M - 41.1 B - 36.9	571.6	24.24	0.281	113.97	3.1900

Figure 62: Appendix I – Set Up

Figure 66: Appendix I – Top Half Heating Only

Figure 63: Appendix I – Bottom Corner Only Cooled

Figure 67: Appendix I – Top Half Heating Bottom Row Cooled

Figure 64: Appendix I – Bottom Row Only Cooled

Figure 65: Appendix I – Right Side Only Cooled

Appendix J: Data Collection from the front of the PV panels from the PV/T Experiment

Front Panel temperatures measured with an IR thermometer, where M stands for the Millennium panel, PV stands for the control panel, and A stands for the novel PV/T system developed with the Arava and Dead Sea Science Center.

Table 21: PV/T Experiment Data

Front Panel Temp. (C)	M - Top	M - Mid	M - Bot.	PV - Top	PV - Mid.	PV - Bot.	A - Top	A - Mid.	A - Bot.
10:55	47.8	50.2	48.3	42.9	42.9	43.1	43.2	46.3	42.4
11:05	45.6	49.4	46.7	42.2	42.1	44	41.9	45.9	41.7
11:15	44.7	47.8	49.5	42.5	42.6	44.2	40.4	45	43.7
11:25	44.3	47.8	47.7	44.1	44.2	45.5	41.2	45.4	42.9
11:35	44	46.9	45.5	41.8	41.9	43.1	40	44.8	41.1
11:45	42.1	46.2	46	41	42.4	43.8	40	45	41.4
11:55	43.6	46.8	45.8	43.9	45.1	45.3	40.7	45.4	41.3
12:05	42.7	46.3	45.3	43	44.2	44.4	40.7	45.4	41.9
12:15	41.9	45.6	44.3	42.1	43.2	43.3	39.3	43.9	39.7
12:25	41.1	44	43.9	39.9	41	42.9	37.6	43.7	38.8
12:35	41.3	44.4	44.3	39.3	40.8	42.3	38.7	44.4	41.3
12:45	42.2	45.9	44.9	42.5	42.7	44.2	39	44	39.9
12:55	41.4	45	44	40.8	42.1	43.1	38.9	44	39.8

Appendix K: Thermal Images from the PV/T experiment

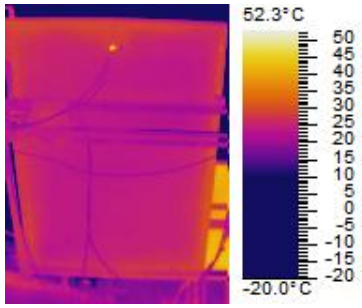

Figure 68: Appendix K - 11:00 Back of Millennium Panel

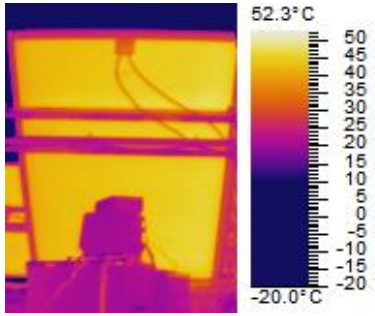

Figure 69: Appendix K - 11:00 Back of SUNTECH

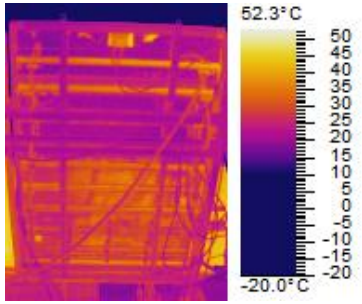

Figure 70: Appendix K - 11:00 Back of Novel PV/T

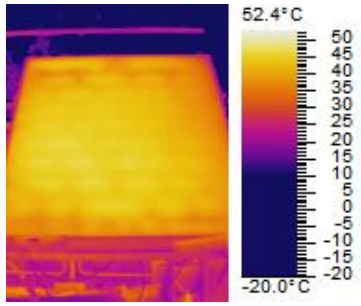

Figure 71: Appendix K - 11:00 Front of Millennium

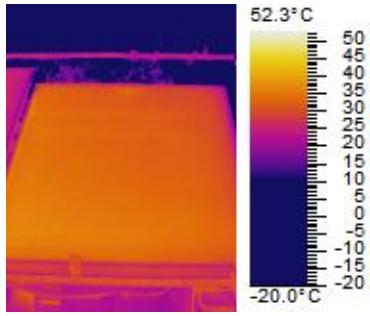

Figure 72: Appendix K - 11:00 Front of SUNTECH

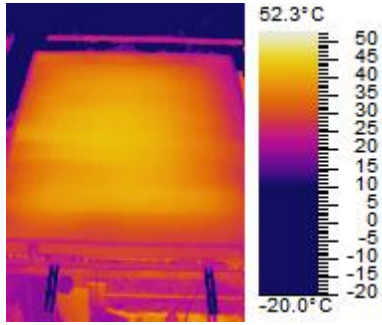

Figure 73: Appendix K - 11:00 Front of Novel PV/T

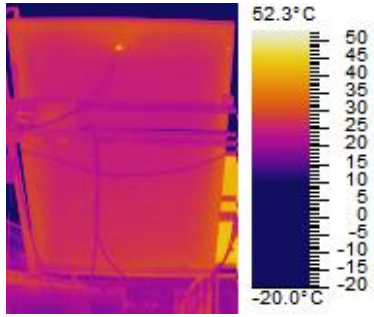

Figure 74: Appendix K - 11:10 Back of Millennium

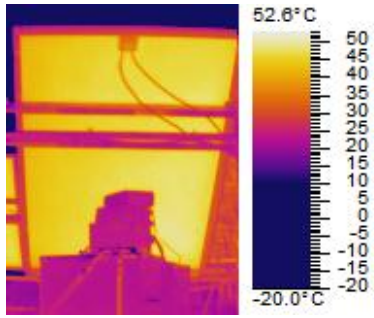

Figure 75: Appendix K - 11:10 Back of SUNTECH

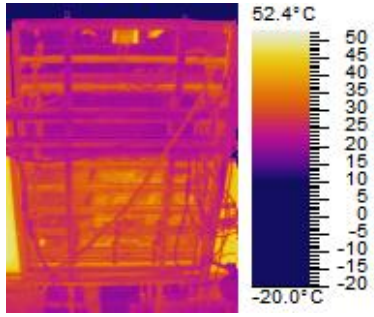

Figure 76: Appendix K - 11:10 Back of Novel PV/T

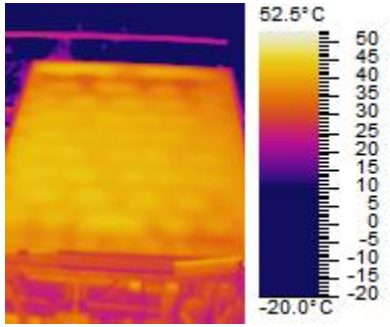

Figure 77: Appendix K - 11:10 Front of Millennium

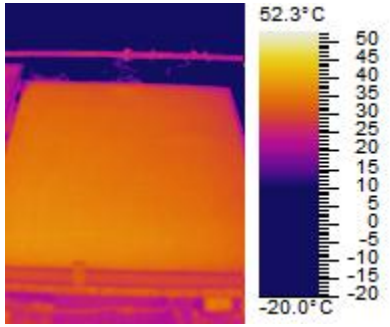

Figure 78: Appendix K - 11:10 Front of SUNTECH

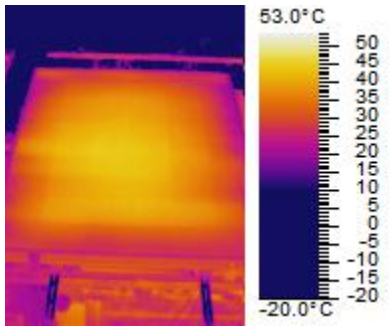

Figure 79: Appendix K - 11:10 Front of Novel PV/T

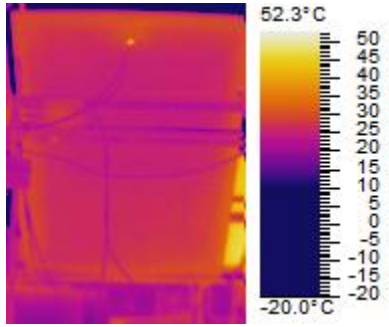

Figure 80: Appendix K - 11:20 Back of Millennium

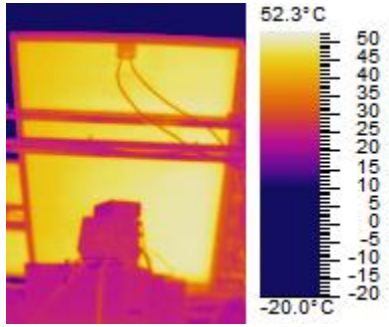

Figure 81: Appendix K - 11:20 Back of SUNTECH

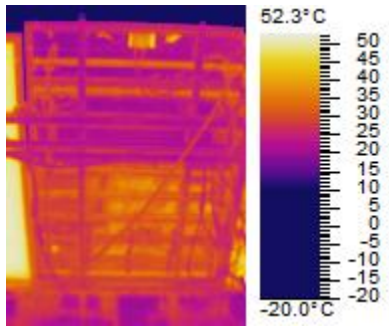

Figure 82: Appendix K - 11:20 Back of Novel PV/T

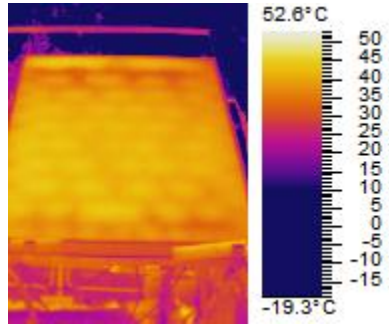

Figure 83: Appendix K - 11:20 Front of Millennium

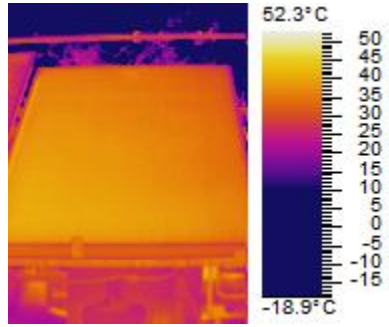

Figure 84: Appendix K - 11:20 Front of SUNTECH

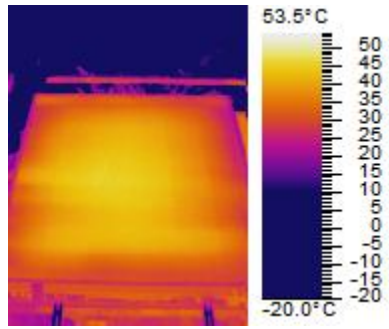

Figure 85: Appendix K - 11:20 Front of Novel PV/T

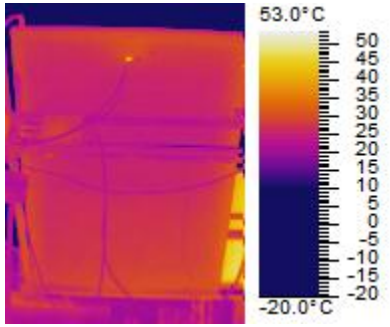

Figure 86: Appendix K - 11:30 Back of Millennium

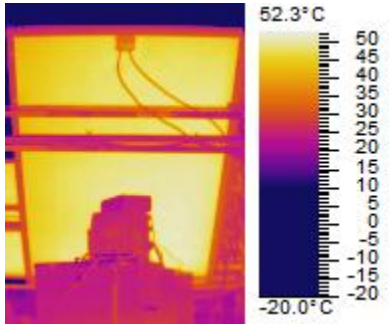

Figure 87: Appendix K - 11:30 Back of SUNTECH

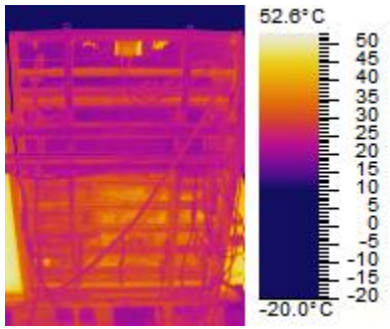

Figure 88: Appendix K - 11:30 Back of Novel PV/T

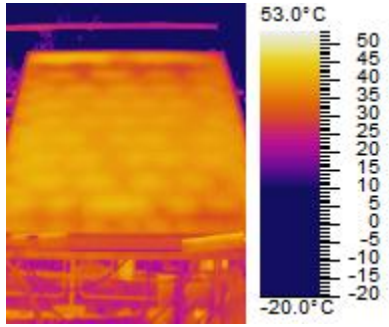

Figure 89: Appendix K - 11:30 Front of Millennium

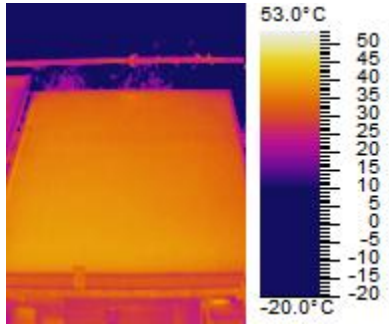

Figure 90: Appendix K - 11:30 Front of SUNTECH

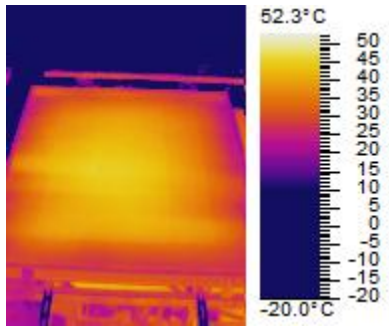

Figure 91: Appendix K – 11:30 Front of Novel PV/T

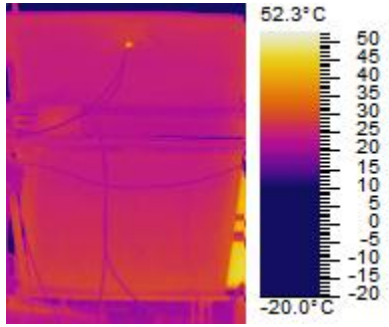

Figure 92: Appendix K - 11:40 Back of Millennium

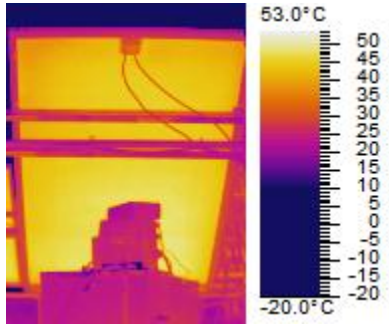

Figure 93: Appendix K - 11:40 Back of SUNTECH

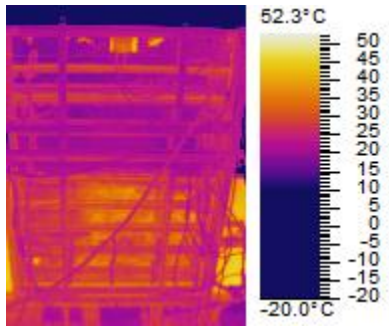

Figure 94: Appendix K - 11:40 Back of Novel PV/T

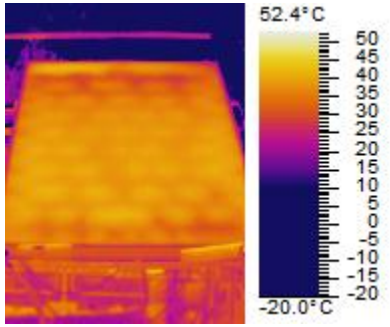

Figure 95: Appendix K - 11:40 Front of MIllennium

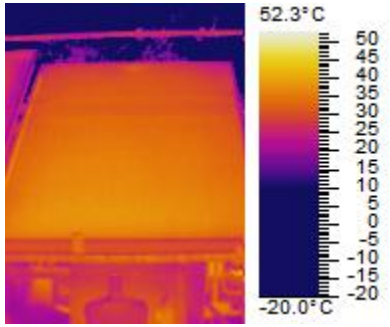

Figure 96: Appendix K - 11:40 Front of SUNTECH

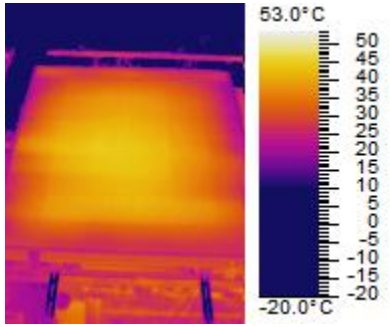

Figure 97: Appendix K - 11:40 Front of Novel PV/T

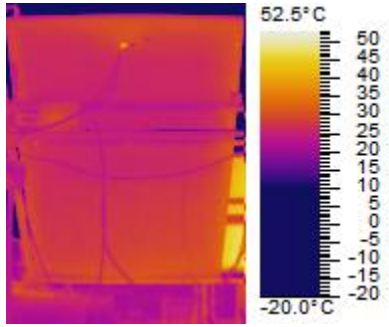

Figure 98: Appendix K - 11:50 Back of Millennium

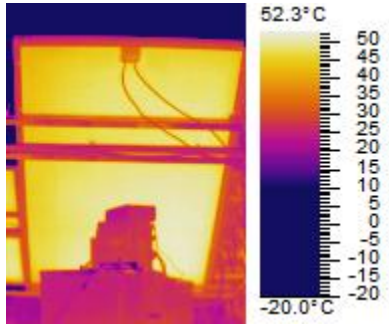

Figure 99: Appendix K - 11:50 Back of SUNTECH

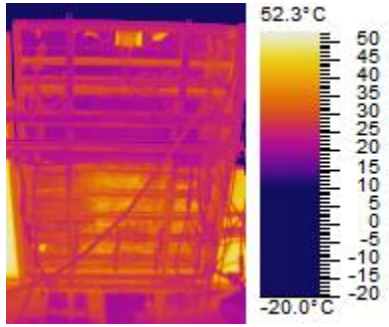

Figure 100: Appendix K - 11:50 Back of Novel PV/T

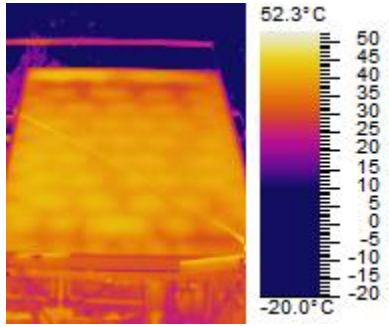

Figure 101: Appendix K - 11:50 Front of Millennium

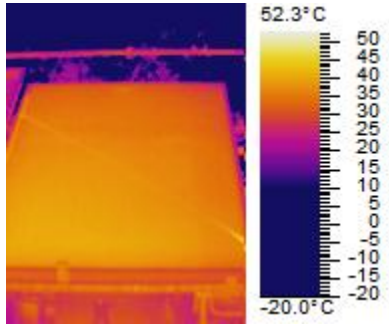

Figure 102: Appendix K - 11:50 Front of SUNTECH

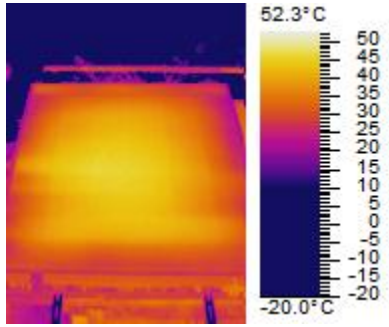

Figure 103: Appendix K - 11:50 Front of Novel PV/T

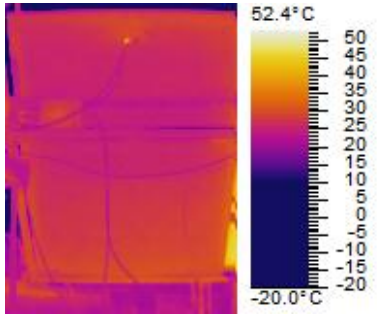

Figure 104: Appendix K - 12:00 Back of Millennium

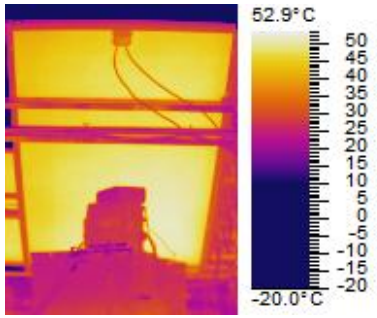

Figure 105: Appendix K - 12:00 Back of SUNTECH

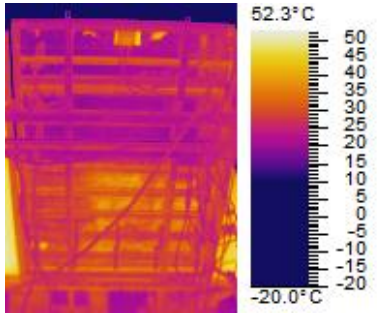

Figure 106: Appendix K - 12:00 Back of Novel PV/T

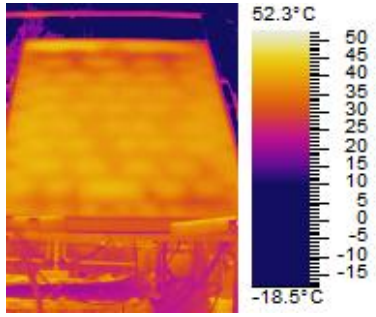

Figure 107: Appendix K - 12:00 Front of Millennium

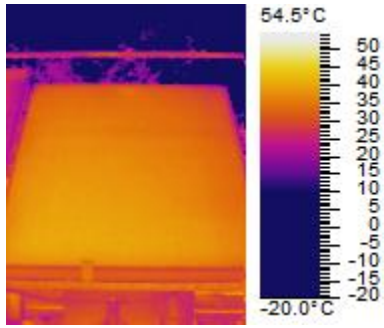

Figure 108: Appendix K - 12:00 Front of SUNTECH

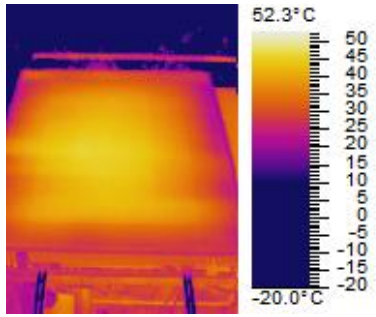

Figure 109: Appendix K - 12:00 Front of Novel PV/T

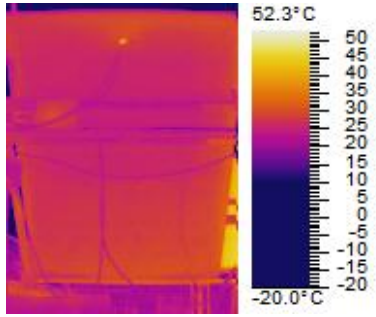

Figure 110: Appendix K - 12:10 Back of Millennium

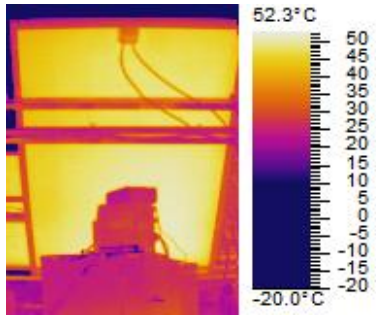

Figure 111: Appendix K - 12:10 Back of SUNTECH

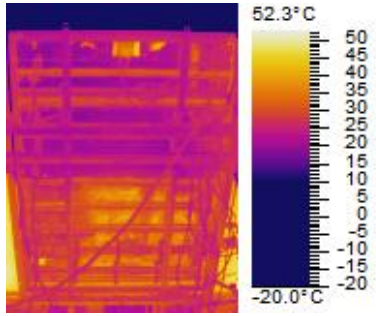

Figure 112: Appendix K - 12:10 Back of Novel PV/T

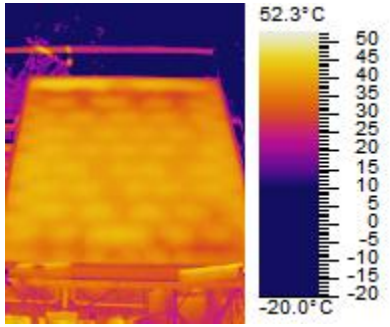

Figure 113: Appendix K - 12:10 Front of Millennium

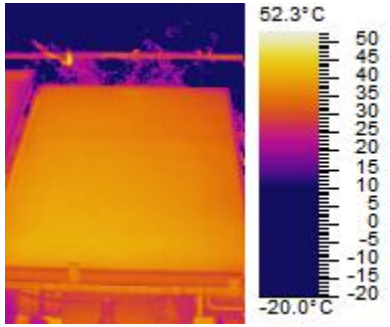

Figure 114: Appendix K - 12:10 Front of SUNTECH

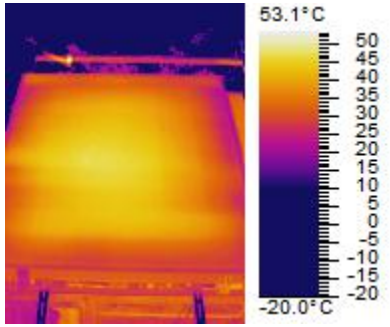

Figure 115: Appendix K - 12:10 Front of Novel PV/T

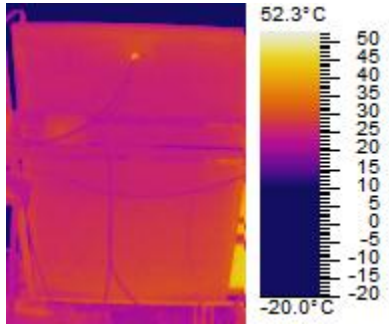

Figure 116: Appendix K - 12:20 Back of Millennium

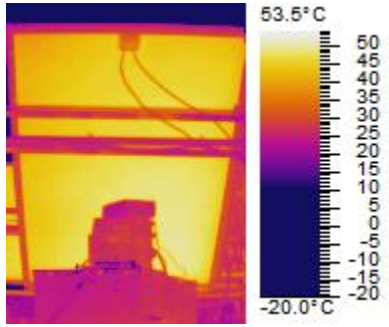

Figure 117: Appendix K - 12:20 Back of SUNTECH

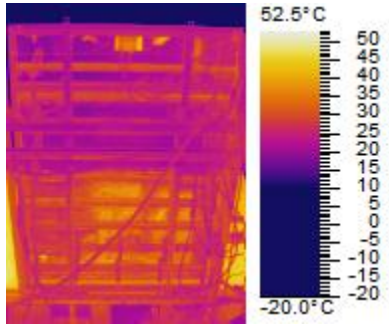

Figure 118: Appendix K - 12:20 Back of Novel PV/T

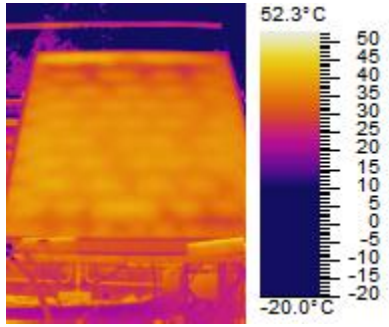

Figure 119: Appendix K - 12:20 Front of Millennium

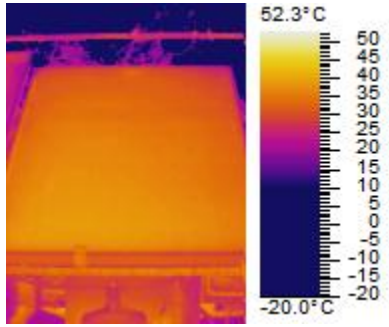

Figure 120: Appendix K - 12:20 Front of SUNTECH

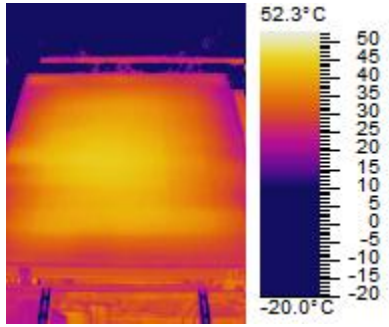

Figure 121: Appendix K - 12:20 Front of Novel PV/T

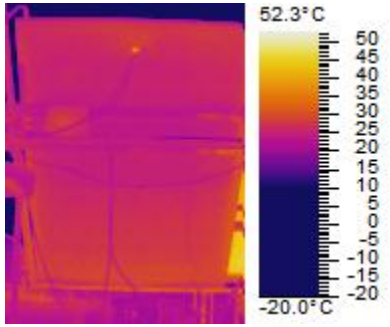

Figure 122: Appendix K - 12:30 Back of Millennium

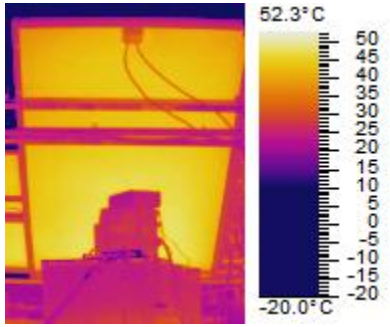

Figure 123: Appendix K - 12:30 Back of SUNTECH

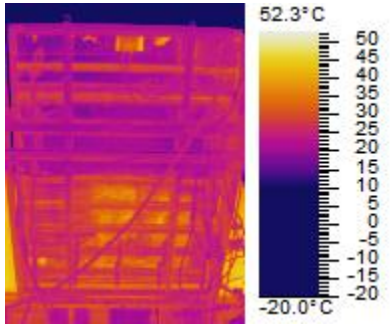

Figure 124: Appendix K - 12:30 Back of Novel PV/T

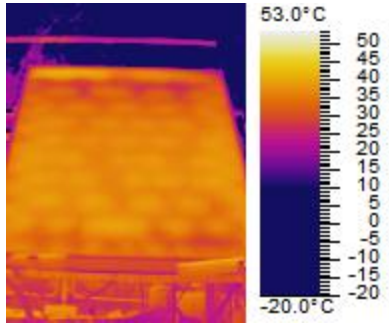

Figure 125: Appendix K - 12:30 Front of Millennium

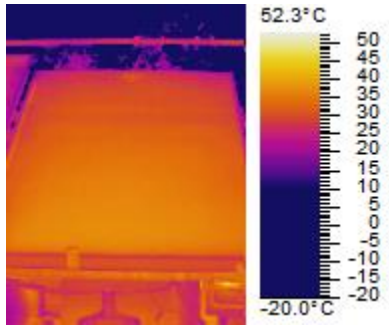

Figure 126: Appendix K - 12:30 Front of SUNTECH

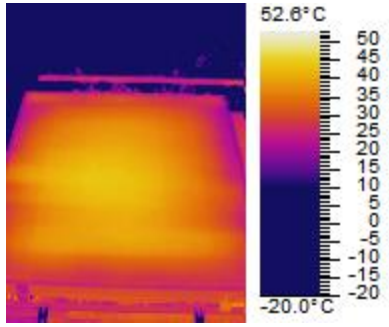

Figure 127: Appendix K - 12:30 Front of Novel PV/T

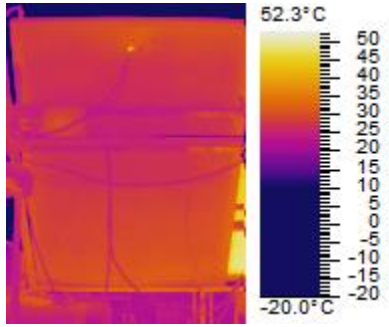

Figure 128: Appendix K - 12:40 Back of Millennium

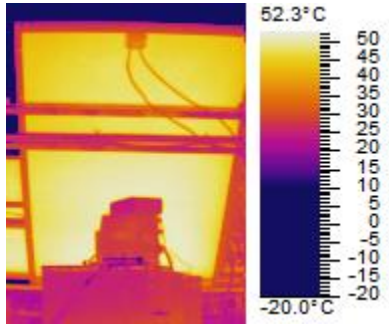

Figure 129: Appendix K - 12:40 Back of SUNTECH

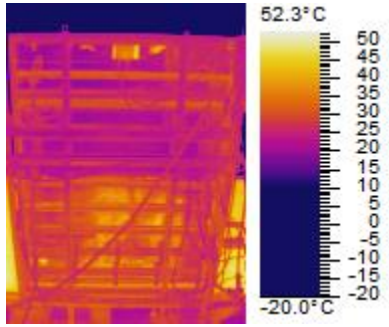

Figure 130: Appendix K - 12:40 Back of Novel PV/T

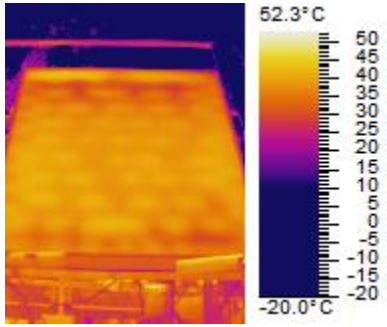

Figure 131: Appendix K - 12:40 Front of Millennium

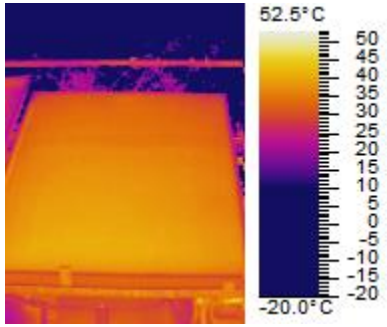

Figure 132: Appendix K - 12:40 Front of SUNTECH

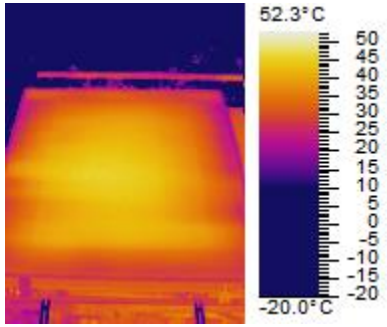

Figure 133: Appendix K - 12:40 Front of Novel PV/T

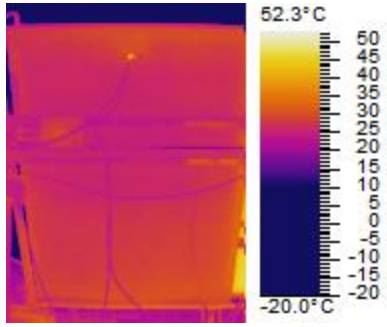

Figure 134: Appendix K - 12:50 Back of Millennium

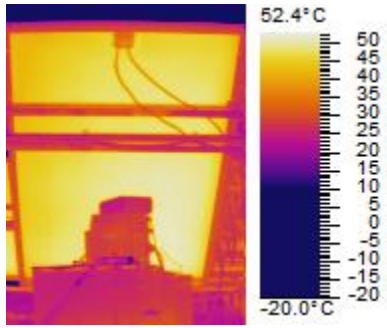

Figure 135: Appendix K - 12:50 Back of SUNTECH

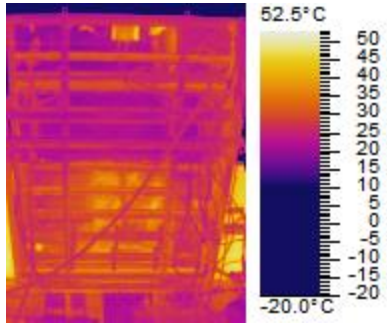

Figure 136: Appendix K - 12:50 Back of Novel PV/T

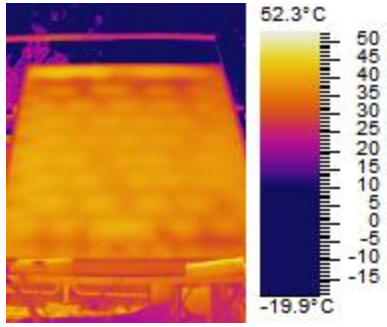

Figure 137: Appendix K - 12:50 Front of Millennium

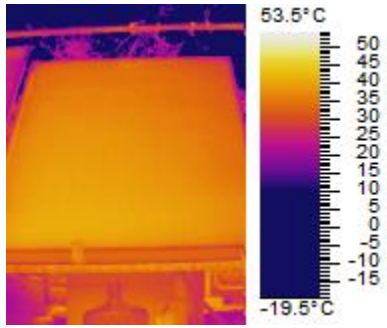

Figure 138: Appendix K - 12:50 Front of SUNTECH

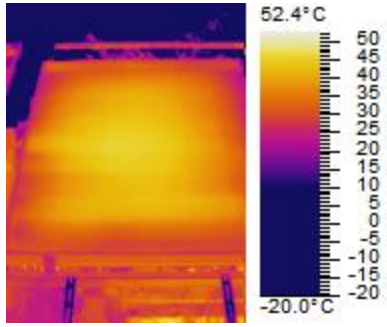

Figure 139: Appendix K - 12:50 Front of Novel PV/T

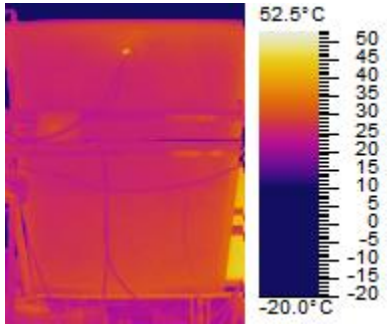

Figure 140: Appendix K - 1:00 Back of Millennium

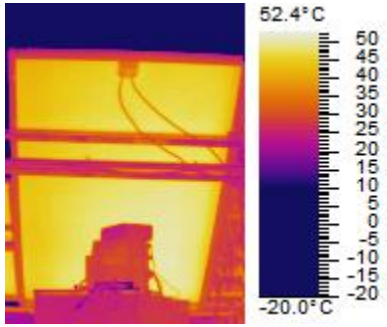

Figure 141: Appendix K - 1:00 Back of SUNTECH

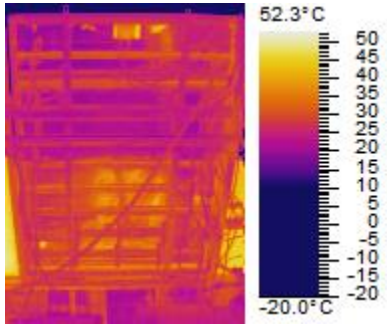

Figure 142: Appendix K - 1:00 Back of Novel PV/T

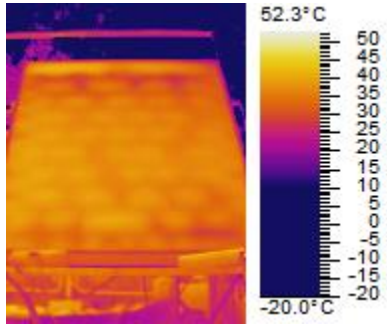

Figure 143: Appendix K - 1:00 Front of Millennium

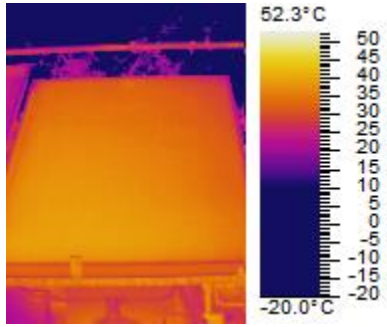

Figure 144: Appendix K - 1:00 Front of SUNTECH

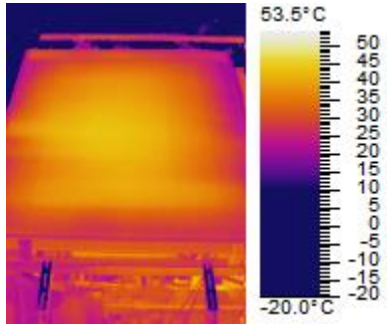

Figure 145: Appendix K - 1:00 Front of Novel PV/T

Appendix L: Data collection from Thermocouples from the PV/T Experiment

TC 1 is the input to the novel PV/T system, TC 2 is the output from the novel PV/T system. TC 6 is the output from the Millennium PV/T system, and TC 8 is the output from the Millennium PV/T system.

Table 22: PV/T Experiment Thermocouple Data

Time	TC 1	TC 2	TC 6	TC 8
11:00:27	27.4	26.9	34.1	19.6
11:10:27	31	31.7	34.1	20.3
11:20:27	28.3	31.5	31.8	20.8
11:30:27	26	29.2	30.2	21.6
11:40:57	26.1	28	28.6	21.3
11:50:27	26.2	28.5	27.4	22.1
12:00:27	26.2	28.6	26.7	22.2
12:10:27	26.5	28.7	26.3	22.6
12:20:27	26.4	28.5	25.8	22.7
12:30:57	26.4	28.1	25.7	22.5
12:40:27	26.1	28.4	25.7	22.7
12:50:27	26.3	28.8	25.8	23.1
13:00:27	26.5	28.6	25.8	23.5

Cooling Bath 1 feeds the Millennium PV/T system, and Cooling Bath 2 feeds the novel PV/T system.

Table 23: PV/T Experiment Cooling Bath Data

Cooling Bath (CB) Temp.	CB1 - Millennium Panel	CB2 - Arava Panel
11:00	31.9	26.6
11:10	34.2	30.3
11:20	31.7	27.5
11:30	29.9	25
11:40	28.3	24.9
11:50	26.9	24.8
12:00	26.2	25
12:10	25.6	25
12:20	25	24.9
12:30	25	24.9
12:40	25	24.7
12:50	25	24.8
13:00	25	25

Appendix M: Data Collection from the Back of the Novel PV/T from the PV/T Experiment

Top refers to the top most section of the Aluminum plate which was measure, Mid refers to the middle section of the Aluminum plate measured, and Bot. represents the bottommost section which was measured. 1, 2, and 3 represent the 3 heights in each section which was measures with 1 being closest to the top, and 3 being closest to the bottom.

Table 24: PV/T Experiment Novel PV/T Temperatures

Arava Back Plate Temp (C)	A - Top 1	A - Top 2	A - Top 3	A - Mid 1	A - Mid 2	A - Mid 3	A - Bot 1	A - Bot 2	A - Bot 3
11:03	32.6	26.8	26.9	29.1	24.7	26	24.6	23.2	29.1
11:13	30.3	25.3	28.8	28.7	26.1	28.2	23.6	22.2	30.1
11:23	30.6	25	28.5	25.3	25.3	28.6	22	25.3	31.6
11:33	28.7	25.9	25.9	26	24.7	27.7	18.6	34.1	29.4
11:43	28.2	24.3	22.3	24.4	26.7	26.8	18.6	33.1	33.1
11:53	31.6	29.2	29.2	29	30	29.9	21.1	21.3	32.6
12:03	29.7	25.9	19.9	27.4	27.2	21.8	20.6	30.3	27.7
12:13	32.2	29.5	28.3	28.2	28.1	22.4	20.2	33.2	28.6
12:23	29.5	25.9	27.7	26.4	26.2	27.3	30.1	36.6	32.3
12:33	30.1	27	23.3	26.9	25.8	26.2	19.1	35.1	31.7
12:43	28	27.8	26.6	26.7	26.8	27.7	27.9	39.5	30.4
12:53	28	27.5	27.4	27.2	28.6	28.6	28.6	33.5	37.3
13:03	30.4	28.5	27.2	27.3	28.5	28.4	22	22	28.8

Appendix N: Power Output Data Collected from PV/T Experiment

Table 25: Weather Conditions and Power Output for Three Panels

	Temp_Avg (C)	Rad_Avg (W/m^2)	Novel PV/T Power Output (W)	Millennium Power Output (W)	PV Power Output (W)
11:00	19.72	831	226.63	225.58	223.28
11:10	19.71	847	228.2	226.24	227.4
11:20	20.89	855	231.96	230.97	230.71
11:30	20.56	863	232.05	231.35	232.63
11:40	21.2	869	235.66	232.8	232.8
11:50	22.24	869	235.91	229.37	233.64
12:00	22.43	866	235.01	232.1	233.49
12:10	22.06	863	231.54	228.82	233.72
12:20	22.08	858	232.96	228.94	233.88
12:30	22.52	851	232.47	232.54	232.31
12:40	22.6	841	228.43	224.53	228.43
12:50	23.14	828	225.14	223.39	226.32
13:00	23.33	814	222.59	218.53	223.9